

PARAMETER ESTIMATION USING SENSOR FUSION AND MODEL UPDATING

by

KEVIN FRANCOFORTE
B.S. Florida Institute of Technology, 2003

A thesis submitted in partial fulfillment of the requirements
for the degree of Master of Science
in the Department of Civil and Environmental Engineering
in the College of Engineering and Computer Science
at the University of Central Florida
Orlando, Florida

Spring Term
2007

© 2007 Kevin Francoforte

ABSTRACT

Engineers and infrastructure owners have to manage an aging civil infrastructure in the US. Engineers have the opportunity to analyze structures using finite element models (FEM), and often base their engineering decisions on the outcome of the results. Ultimately, the success of these decisions is directly related to the accuracy of the finite element model in representing the real-life structure. Improper assumptions in the model such as member properties or connections, can lead to inaccurate results. A major source of modeling error in many finite element models of existing structures is due to improper representation of the boundary conditions.

In this study, it is aimed to integrate experimental and analytical concepts by means of parameter estimation, whereby the boundary condition parameters of a structure in question are determined. FEM updating is a commonly used method to determine the “as-is” condition of an existing structure. Experimental testing of the structure using static and/or dynamic measurements can be utilized to update the unknown parameters. Optimization programs are used to update the unknown parameters by minimizing the error between the analytical and experimental measurements. Through parameter estimation, unknown parameters of the structure such as stiffness, mass or support conditions can be estimated, or more appropriately, “updated”, so that the updated model provides for a better representation of the actual conditions of the system.

In this study, a densely instrumented laboratory test beam was used to carry-out both analytical and experimental analysis of multiple boundary condition setups. The test beam was instrumented with an array of displacement transducers, tiltmeters and accelerometers. Linear

vertical springs represented the unknown boundary stiffness parameters in the numerical model of the beam. Nine different load cases were performed and static measurements were used to update the spring stiffness, while dynamic measurements and additional load cases were used to verify these updated parameters.

Two different optimization programs were used to update the unknown parameters and then the results were compared. One optimization tool was developed by the author, Spreadsheet Parameter Estimation (SPE), which utilized the Solver function found in the widely available Microsoft Excel software. The other one, comprehensive MATLAB-based PARameter Identification System (PARIS) software, was developed at Tufts University. Optimization results from the two programs are presented and discussed for different boundary condition setups in this thesis. For this purpose, finite element models were updated using the static data and then these models were checked against dynamic measurements for model validation. Model parameter updating provides excellent insight into the behavior of different boundary conditions and their effect on the overall structural behavior of the system. Updated FEM using estimated parameters from both optimization software programs generally shows promising results when compared to the experimental data sets. Although the use of SPE is simple and generally straight-forward, we will see the apparent limitations when dealing with complex, non-linear support conditions. Due to the inherent error associated with experimental measurements and FEM modeling assumptions, PARIS serves as a better suited tool to perform parameter estimation. Results from SPE can be used for quick analysis of structures, and can serve as initial inputs for the more in depth PARIS models. A number of different sensor types and spatial resolution were also investigated for the possible minimum instrumentation to have an acceptable model representation in terms of model and experimental data correlation.

To Karen, for her support, encouragement and most importantly, patience.

ACKNOWLEDGMENTS

The author would first like to thank Dr. F. Necati Catbas for his assistance and guidance with this research study and the work associated with developing this overall thesis; Dr. Masoud Sanayei for his valuable discussions and insight into the parameter estimation process; and his research students at Tufts University, for their support and help with PARIS software programming and general understanding; my committee members, Dr. Bruce Butler, Dr. Kevin Mackie, and Dr. Lei Zhao for their time and valuable feedback; donated steel material from Cato Steel, whom it was a pleasure to work with.

I wish to also thank my colleagues in Dr. Catbas's research team and in the UCF structures laboratory for their advice, contributions, support with instrumentation and testing, and keeping me sane with the light-hearted moments. Their names in no particular order are: Mustafa Gul, Melih Susoy, Ricardo Zaurin, Mike Olka, Zach Haber and Jason Burkett.

I would also like to thank Janine Pardee, P.E. of Duo Associates, Inc. for her enormous insight into the world of structural engineering and the lessons and stories she has shared with me throughout this process. By virtue of her knowledge and guidance, I have become a much better engineer since I started my graduate studies in structural engineering.

Finally I wish to thank my family and friends for their loving support and words of encouragement. They have been a constant source of inspiration and balance for me while I worked on completing my research and thesis. Words cannot express how grateful I am to have them in my life.

TABLE OF CONTENTS

LIST OF FIGURES	x
LIST OF TABLES	xiii
LIST OF ACRONYMS/ABBREVIATIONS	xv
CHAPTER ONE: INTRODUCTION AND LITERATURE REVIEW	1
Background	1
Literature Review	2
Parameter Estimation Theory	4
Static Analysis – Error Functions	7
CHAPTER TWO: OPTIMIZATION	10
Spreadsheet Parameter Estimation (SPE)	10
SPE – Parameter Estimation Procedure	10
SPE – Optimization Setup	14
PARAmeter Identification System Software (PARIS)	18
Finite Element Model Creation	20
Parameter Estimation Data	22
CHAPTER THREE: NUMERICAL STUDIES AND MODEL DESIGN	27
Design Considerations	27
Analytical Model	29
Sensor/Data Validation	31
SPE – Numerical Validation	33
PARIS – Numerical Validation	35

Model Validation Using Dynamic Test Data.....	39
CHAPTER FOUR: EXPERIMENTAL STUDIES – UCF TEST BEAM.....	41
Sensor Instrumentation	41
Displacement Transducers	41
Vibrating Wire Tiltmeters.....	43
CR10X Datalogger.....	44
AM16/32 Multiplexer	45
AVW1 Interface.....	46
Load Case Selection.....	47
Material Testing for Initial Values.....	53
Boundary Condition (BC) Selection.....	59
Experimental Setup.....	62
CHAPTER FIVE: TEST RESULTS AND DISCUSSION	65
Optimization Load Selection	65
Measured DOF Selection.....	69
SPE Statistical Analysis.....	72
BC1 Parameter Estimation Results.....	79
BC3a Parameter Estimation Results	84
BC3b Parameter Estimation Results.....	87
BC5b Parameter Estimation Results.....	92
CHAPTER SIX: CONCLUSIONS AND RECOMMENDATIONS	97
Recommendations.....	99
APPENDIX A: INSTRUMENTATION.....	102

APPENDIX B: SPREADSHEET PARAMETER ESTIMATION (SPE).....	107
APPENDIX C: DATALOGGER SETUP	113
LIST OF REFERENCES	117

LIST OF FIGURES

Figure 1: Direct Structural Analysis Process (Sanayei et al. 2004).....	5
Figure 2: Parameter Estimation Process (Sanayei et al. 2004)	5
Figure 3: SPE Global Stiffness Matrix Showing Spring Referenced Cell.....	13
Figure 4: SPE Global Stiffness Matrix Partition Labels	13
Figure 5: SPE Error Function Vector.....	14
Figure 6: (a) SPE Adjustable Cells (b) SPE Target Cell	15
Figure 7: Solver Parameter Window.....	16
Figure 8: Solver Options Window	17
Figure 9: PARIS Optimization Procedure (Courtesy of Tufts University).....	19
Figure 10: Ksss Test Beam Model.....	21
Figure 11: PRF Element.....	21
Figure 12: Sample PARIS Objective Function Plot	24
Figure 13: Sample PARIS Iteration Path Plot.....	25
Figure 14: Test Beam Sawhorse Support.....	28
Figure 15: (a) Dynamic Test on Sawhorse (b) Frequency Response Function of Sawhorse	29
Figure 16: SAP2000 Test Beam (Extruded View)	30
Figure 17: Test Beam FEM information.....	31
Figure 18: Verification of Optimization Using a Numerical Example.....	35
Figure 19: PARIS Initial and True Section Property Matrices	36
Figure 20: PARIS Global Minimum (4 MDOF).....	37
Figure 21: PARIS Global Minimum (12MDOF).....	38

Figure 22: Impact Hammer Tests on the Beam	40
Figure 23: Displacement Transducer Setup.....	42
Figure 24: Displacement Cable Attachment Method.....	43
Figure 25: Geokon VBWG Tiltmeter	44
Figure 26: Campbell Scientific CR10X Datalogger	45
Figure 27: Campbell Scientific AM16/32 Multiplexer.....	46
Figure 28: Campbell Scientific AVW1 Interface	47
Figure 29: Test Beam Experimental Load Locations	47
Figure 30: LC1_Full Elevation View	48
Figure 31: Load Case(s) LC2_A1...A5	49
Figure 32: AASHTO Standard Truck Load (AASHTO 2004).....	50
Figure 33: Moving Truck Load Cases (a) LC3_A1 (b) LC3_A2 (c) LC3_A3.....	51
Figure 34: Compression Tests of 5 Duro50 Pads Using UTM.....	53
Figure 35: Vertical Stiffness Values for Different Neoprene Pads.....	54
Figure 36: Vertical Stiffness Derivation from Material Tests	55
Figure 37: Mechanical Properties for Neoprene (Courtesy of Moldeddimensions.com).....	57
Figure 38: Sample Material Test Plot for Steel Angle Support.....	59
Figure 39: Pin Supports (BC1)	60
Figure 40: 1 Duro50 Pad Support (BC3a)	61
Figure 41: 5 Duro50 Pad Support (BC3b)	61
Figure 42: (a) 5 Duro70 Pad Support, L-Side (b) 5 Duro50 Pad Support, R-Side	62
Figure 43: Experimental Test Beam Setup	64
Figure 44: Experimental Vs. FEM (PARIS Updated) Displacement Values	65

Figure 45: Load Combination LC2_A1A2A3AA5	66
Figure 46: Load Combination LC2_A1A2A3	67
Figure 47: Load Combination LC2_A3A4A5	68
Figure 48: Load Combination LC2_A1A3A5	69
Figure 49: 12 Measured DOF Setup	70
Figure 50: 7 Measured DOF Setup	71
Figure 51: 4 Measured DOF Setup	72
Figure 52: Measurements & Identified Deflections with Statistical Bounds (BC1_LC3_A2)	73
Figure 53: Measurements & Identified Deflections with Statistical Bounds (BC3a_LC3_A2)...	74
Figure 54: Measurements & Identified Deflections with Statistical Bounds (BC3a_LC3_A2)...	75
Figure 55: Histograms for BC1 Supports K_1 and K_2	77
Figure 56: Histograms for BC3a Supports K_1 and K_2	77
Figure 57: Histograms for BC3a Supports K_1 and K_2	78
Figure 58: Comparison of Updated FEM and Experimental Displacements for BC1_LC1	81
Figure 59: Mode Shape 1 Comparison for Experimental & Updated FEM Data (BC1).....	83
Figure 60: Comparison of Updated FEM and Experimental Displacements for BC3a_LC1.....	85
Figure 61: Mode Shape 1 Comparison for Experimental & Updated FEM Data (BC3a).....	87
Figure 62: Material Test Plot for 5 Duro50 Neoprene Pads Stacked Together	88
Figure 63: Comparison of Updated FEM and Experimental Displacements for BC3b_LC1	90
Figure 64: Mode Shape 1 Comparison for Experimental & Updated FEM Data (BC3b).....	92
Figure 65: Comparison of Updated FEM and Experimental Displacements for BC5b_LC1	94
Figure 66: Mode Shape 1 Comparison for Experimental & Updated FEM Data (BC5b).....	96

LIST OF TABLES

Table 1: Displacement Measurement Data Validation	32
Table 2: Rotation Measurement Data Validation	32
Table 3: Load Case (LC) Descriptions	52
Table 4: Sample Material Test Results for Duro50 Pads.....	58
Table 5: Averaged Stiffness Values for Different Load Levels	58
Table 6: Initial Boundary Condition Cases.....	60
Table 7: W8x13 Beam Dimension Comparison	63
Table 8: SPE Updated Spring Stiffness Values for BC1 Using Single Force Load Sets	76
Table 9: SPE Updated Spring Stiffness Values for BC3a Using Single Force Load Sets.....	76
Table 10: SPE Updated Spring Stiffness Values for BC3b Using Single Force Load Sets	76
Table 11: Comparison of Mean Stiffness Values vs. Material Test Data.....	78
Table 12: Updated Spring Stiffness Values for BC1 w/ Multiple Load & Sensor Cases.....	79
Table 13: Mean Updated Spring Stiffness Values for BC1	80
Table 14: BC1 Model Validation Using Dynamic Data.....	82
Table 15: BC1 MAC Value Comparison.....	82
Table 16: Updated Spring Stiffness Values for BC3a w/ Multiple Load & Sensor Cases.....	84
Table 17: Mean Updated Spring Stiffness Values for BC3a	84
Table 18: BC3a Model Validation Using Dynamic Data	86
Table 19: BC3a MAC Value Comparison	86
Table 20: Updated Spring Stiffness Values for BC3b w/ Multiple Load & Sensor Cases.....	89
Table 21: Mean Updated Spring Stiffness Values for BC3b	89

Table 22: BC3b Model Validation Using Dynamic Data.....	91
Table 23: BC3b MAC Value Comparison.....	91
Table 24: Updated Spring Stiffness Values for BC5b w/ Multiple Load & Sensor Cases.....	93
Table 25: Mean Updated Spring Stiffness Values for BC5b.....	93
Table 26: BC5b Model Validation Using Dynamic Data.....	94
Table 27: BC5b MAC Value Comparison.....	95

LIST OF ACRONYMS/ABBREVIATIONS

AASHTO	American Association of State Highway and Transportation Officials
BC	Boundary Condition
CMIF	Complex Mode Indicator Function
DOF	Degree of freedom
Duro	Durometer
E	Modulus of Elasticity (ksi)
FEA	Finite Element Analysis
FEM	Finite Element Model
FRF	Frequency Response Function
GRG2	Generalized Reduced Gradient Algorithm
I	Second moment of inertia
K ₁	Vertical spring stiffness; left side (kip/in.)
K ₂	Vertical spring stiffness; right side (kip/in)
LC	Load Case
MAC	Modal Assurance Criteria
MATLAB	Matrix Laboratory software
MDOF	Measured Degree of Freedom
MIMO	Multiple-Input Multiple-Output
n	Joint number
NDT	Non-Destructive Testing
PARIS	PARameter Identification System software

rad	Radians
SPE	Spreadsheet Parameter Estimation
UTM	Universal Testing Machine
VBWG	Vibrating Wire Gage
$\{e(k)\}$	Error Function
$\{F_a\}$	Forces in terms of measured DOF
$\{F_b\}$	Forces in terms of unmeasured DOF
$\{F_a\}^m$	Measured force DOF
$\{J(k)\}$	Objective function
$\{U_a\}$	Displacements/rotations in terms of measured DOF
$\{U_b\}$	Displacements/rotations in terms of unmeasured DOF
$\{U_a\}^m$	Measured displacements/rotations DOF
Δ_n	Displacement of i^{th} joint (in.)
ω_n	Frequency of i^{th} mode shape (rad/sec)
Φ_n	i^{th} mode shape
θ_n	Rotation of i^{th} joint (deg.)

CHAPTER ONE: INTRODUCTION AND LITERATURE REVIEW

Background

Engineers often use finite element analysis (FEA) to validate their hand calculations or in more complex structures, confirm their intuitions regarding the overall structural behavior of the system. If the situation arises where an existing structure such as a bridge or building is being refurbished, modified or retrofitted, engineers can consult the finite element model (FEM), add new information regarding the system, run new analyses and observe possible changes to the structure. The reliability of these analyses is directly related to how well the structure is modeled in the software. Experimentally acquired data can be used to calibrate or update finite element models to better represent the actual behavior of an existing structure. It is possible to manually calibrate numerical models using data as well as using fully automated, optimization-based algorithms. These approaches are expected to capture actual behavior by updating critical parameters. Boundary condition modeling is a very critical issue for civil structure modeling and this study focuses on model parameter estimation using sensor data with special emphasis on boundary conditions.

Uncertainty due to boundary condition modeling is one of the major contributors to most of the misrepresentations of a structural model (Catbas et al, 2007). Engineers generally use fixed or pinned connections for boundary conditions at the supports of structures, thereby simplifying the overall model analysis. Reducing or increasing the stiffness of the supports has a great deal of influence of the resulting stiffness of the structure, especially when modeled incorrectly in finite element software. There may be a compromise in safety or integrity of the

structure, if the finite element model (FEM) is unreliable, due to improper modeling of the boundary conditions. Through parameter estimation and model parameter updating, engineers can avoid these pitfalls and have greater confidence in the FEM of the structure in question.

Literature Review

Although the concept of parameter estimation using model updating is not new, the availability and power of today's computers has allowed much improved algorithms and computational efficiency for this area of research. Customized optimization programs or algorithms have been developed for specific structural problems or as commercial software. The focus of this research will deal with the use of a MATLAB-based parameter estimation program, PARIS, along with an Excel-based spreadsheet program, SPE developed as part this thesis work.

Early experiments with parameter estimation focused on using simulated static measurements to solve for unknown stiffness parameters. Sanayei and Saletnik (1996a) used simulated strain measurement data to estimate the unknown element areas and moments of inertia for a two-dimensional truss and frame example. In the companion paper to that study, simulated measurement data with modeling error was then used on the same example to determine the impact of using noisy measurements for parameter estimation (Sanayei and Saletnik 1996b). Liu and Chian (1997) proposed and tested a method for identifying element properties of a truss using static strain data. It was found that using strain gages provided an economical alternative to measuring nodal displacement with expensive displacement transducers.

A heuristic method for determining optimum measurement DOF and load placement was recommended by Sanayei and Saletnik (1996b) before using experimental static displacement and strain measurements to update stiffness parameters of a small 2D frame model (Sanayei et al. 1997).

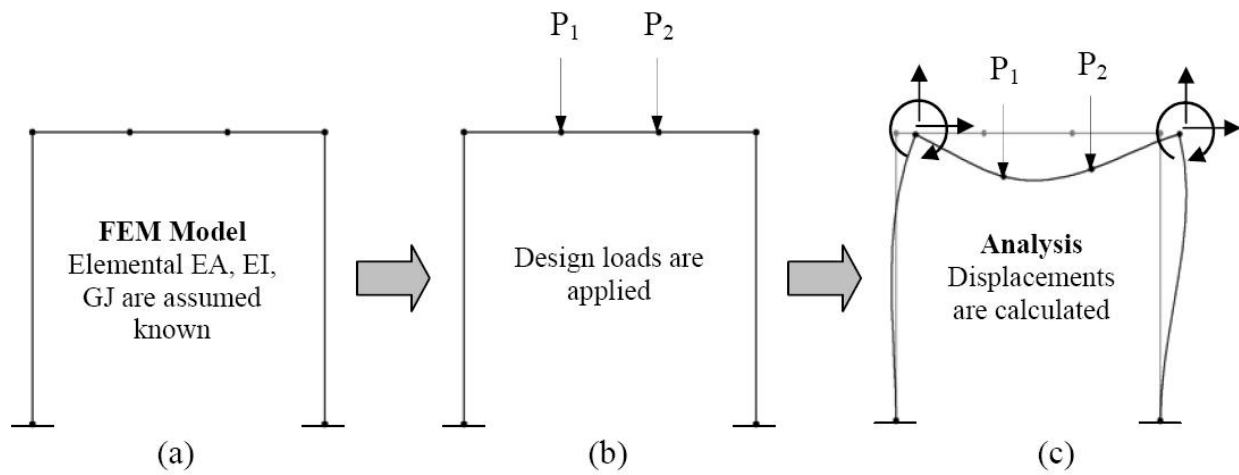
Developments in FEM elements such as the Soil Substructure Superelement (K_{sss}) were used to model the complicated interface below the ground level of an example bridge structure by accounting for the coupling between DOF typically neglected in practical analysis (Sanayei et al. 1999). Also, a proposed partial-restrained frame (PRF) element was used to model the semi-rigid behavior of structural connections and parameter estimation was performed to update unknown vertical and rotational spring properties for the K_{sss} and PRF elements, respectively. Similar studies from Aktan et al. (2001) showed that unknown vertical stiffness parameters of neoprene pads used on a grid structure could be successfully estimated with the aid of material test data for the optimization process.

Parameter estimation is not limited to static or dynamic responses only. Data from both tests can be combined and used as composite data for structural identification. Data sets involving static displacements and eigenmodes were utilized by Oh and Jung (1998), for a two-span continuous beam structure. Aktan et al. (1998) proved that unknown parameters of complex 3D models could be successfully updated and calibrated using an automated optimization process. More recent experimental studies involving complicated grid structures have shown that combinations of all measurement data types (strains, rotations, displacements, mode shapes, etc.) can be combined or stacked in normalized error functions which were minimized to obtain updated parameters, including unknown neoprene pad vertical stiffness (Sanayei et al. 2006).

The significance of modeling error in parameter estimation is evaluated in detail in Sanayei et al. (2001). Parameter estimation results were presented showing the affect of various types of error (modeling, FEM, and parameter estimation) and its impact on the objective function and overall reliability of the studies. In Ventura et al. (2003), commercially available automated parameter estimation software, *FEMtools*, could be used to successfully update unknown structural parameters of a large (48-story) civil structure. The original and updated FEM natural periods and MAC values were compared indicating good correlation between the models.

Parameter Estimation Theory

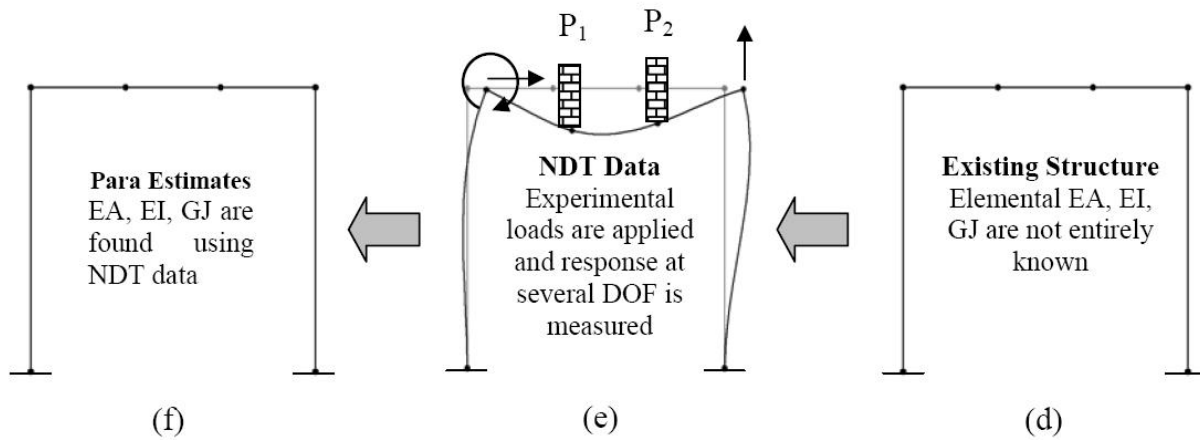
Parameter estimation is the procedure through which the parameters of a structure, whether stiffness, cross sectional area, elastic modulus or moment of inertia, are updated using measured Nondestructive Test (NDT) data. In real-world scenarios, structural member properties may be different from their expected or published values due to variances that arise during fabrication, construction or destructive events such as damage or fatigue problems that occur over the service life of the structure. Using optimization methods, one can minimize the error between the analytical and measured responses, thus updating the unknown parameters using experimental data sets. The updated model can then serve as a starting point, or baseline model for future analysis. Figure 1 and 2 details the parameter estimation process and how it compares with traditional structural analysis (Sanayei et al. 2004).



Direct Structural Analysis

- (a) Analytical model is developed with known material and sectional properties A, I, J, E, and G
- (b) Design load cases are determined and applied to the analytical model
- (c) Displacements are calculated using conventional structural analysis methods

Figure 1: Direct Structural Analysis Process (Sanayei et al. 2004)



Structural Parameter Estimation (Inverse Problem)

- (d) Existing structure for condition assessment. Section properties are not known with high confidence.
- (e) Experimental loads are applied and displacements and rotations are measured (NDT data).
- (f) Geometric Parameter Estimation is performed using NDT data and initial section properties are updated.

Figure 2: Parameter Estimation Process (Sanayei et al. 2004)

For direct structural analysis, the member properties are usually known, loads are applied, and the responses such as displacements or rotations are measured. The reverse is true for parameter estimation in that the section properties (stiffness, mass, etc.) are not that well known. Experimental loads are applied to the structure and the responses (NDT) at a few DOF are measured. Using the NDT data, parameter estimation is performed and the initial unknown parameters are updated.

When we speak of parameter estimation we are searching for the “truth,” i.e. the unknown parameter values which accurately reflect the measured responses of the structure. The problem is that we may not be able to properly identify the unknown parameters because of inherent errors associated with the identification process. The errors that we speak of include unknown measurement errors from the sensors and loads, and modeling errors from the FEM. Other errors arise from improper fabrication of materials. We cannot readily “identify” the actual conditions of the structure, but we can estimate them with great certainty (Sanayei, 2007).

In this study, one of the objectives is to develop and use a simplified approach that can be implemented by practicing engineers for parameter estimation using static measurements. The author mainly focuses on identifying the parameters that define the boundary conditions. The test structure and the boundary conditions can be considered analogous to single span, simply supported bridges such as concrete T-beam bridges (Catbas et al. 2005). As a result, the author was not concerned with updating the element stiffness properties since the error due to incorrect boundary condition modeling will likely govern the success of the finite element model. Linear vertical springs will be used to model the joint stiffness at the boundaries, for a total of two unknown stiffness parameters. To estimate the spring stiffness parameters, static displacement and rotational data were measured on the test beam. Microsoft Excel’s built-in SOLVER

function, utilizing the General Reduced Gradient (GRG2) algorithm, is used to minimize the error between the analytical and experimental data. Results from PARIS based parameter estimation software will also be compared to the Excel data. A brief overview of the optimization programs as well as the error functions are summarized in the following sections.

One contributor of error in this study is directly related to experimental error. The loads were stacked on top of small plates in order to recreate point loading as opposed to a distributed load condition. Since the 38 lb weights were manually stacked at the load points, there is difficulty in maintaining an equal distribution of the weight across the top flange of the beam. Small errors in location may cause the beam to be loaded more towards the front or back of the top flange, causing the beam to rotate or tilt. Also, small errors due to the sensors and equipment are inherent with any experimental study. Calibration of the sensors is required to ensure that measurement error is fully minimized.

Static Analysis – Error Functions

The classical matrix formulation for FEM force-displacement relationship is

$$\{F\} = [K]\{U\} \quad (1)$$

where $\{F\}$ is force vector, $\{U\}$ is vector of displacements and/or rotations and $[K]$ designates the structure stiffness matrix.

Since data over the entire set of degrees of freedom were not measured, the formulation in equation (1) can be partitioned according to measured and unmeasured DOF. Partitioning the force displacement relationship of equation (1) gives

$$\begin{Bmatrix} F_a \\ F_b \end{Bmatrix} = \begin{bmatrix} K_{aa} & K_{ab} \\ K_{ba} & K_{bb} \end{bmatrix} \begin{Bmatrix} U_a \\ U_b \end{Bmatrix} \quad (2)$$

where the subscripts a and b denote “measured DOF” and “unmeasured DOF”, respectively.

By using static condensation, the analytically determined forces, $\{F_a\}$ can be solved in terms of the experimentally measured displacements and rotations, $\{U_a\}^m$ where

$$\{F_a\} = ([K_{aa}] - [K_{ab}][K_{bb}]^{-1}[K_{ba}])\{U_a\} + [K_{ab}][K_{bb}]^{-1}\{F_b\} \quad (3)$$

For this research all of the unmeasured DOF are partitioned to $\{F_b\}$, and part of equation (3) will be equal to a zero vector and cancel the multiplied sub matrices $[K_{ab}]$, $[K_{bb}]^{-1}$. In reality, $\{F_b\}$ may contain forces which are not at measured DOF. For those cases, $\{F_b\}$ will have to be included, by multiplying sub-matrices given in equation (3). The error function is simply the difference between the analytically determined forces, $\{F_a\}$ and the experimental (applied) forces $\{F_a\}^m$, where $\{e(k)\}$ denotes the error as a function of the unknown boundary condition stiffness parameters and is given as

$$\{e(k)\} = ([K_{aa}] - [K_{ab}][K_{bb}]^{-1}[K_{ba}])\{U_a\}^m + [K_{ab}][K_{bb}]^{-1}\{F_b\}^m - \{F_a\}^m \quad (4)$$

Similarly, by taking the inverse of the stiffness matrix $[K]$ in equation 1, the flexibility matrix and force vector can be used to solve for the displacements and rotations, $[U]$. Using the same procedure as outlined in equations (2) through (4), the analytically measured displacements or rotations are solved as

$$\{U_a\} = \left([K_{aa}] - [K_{ab}] [K_{bb}]^{-1} [K_{ba}] \right)^{-1} \left(\{F_a\}^m - [K_{ab}] [K_{bb}]^{-1} \{F_b\}^m \right) \quad (5)$$

The new error function based on the difference between analytically determined and experimentally measured displacements or rotations is

$$\{e(k)\} = \left([K_{aa}] - [K_{ab}] [K_{bb}]^{-1} [K_{ba}] \right)^{-1} \left(\{F_a\}^m - [K_{ab}] [K_{bb}]^{-1} \{F_b\}^m \right) - \{U_a\}^m \quad (6)$$

Since some of the multiplication in equations (4) and (6) involves taking the inverse of some of the sub-matrices, the error functions will be nonlinear functions of the stiffness parameters of the boundary conditions.

CHAPTER TWO: OPTIMIZATION

Once test data is collected and the error functions are defined, an optimization algorithm is required in order to minimize the error between the analytically determined data and the experimental data. An optimization algorithm uses iterative approaches to determine the best or optimal solutions for a given set of equations. For this thesis, two different optimization approaches and software will be utilized and the results of the updated parameters compared.

Spreadsheet Parameter Estimation (SPE)

One of the objectives of this study was to explore development and use of a parameter estimation software that could be utilized by engineers or personnel that are not considered experts in this particular field. The goal was to have a process in place whereby the intended user would require little instruction or training to carry out the parameter estimation analysis. A widely used software common to most, if not all engineering offices, is spreadsheet-based software, particularly Microsoft Excel. This spreadsheet is also customized for a specific problem; that being the test beam structure. No provisions were made to setup a spreadsheet for generic parameter estimation of different structure types.

SPE – Parameter Estimation Procedure

The procedure for parameter estimation using SPE is setup to directly manipulate and analyze equation (1). A specific error function, namely the displacement output error function of equation (6) is used to form the error function vector and ultimately the objective function. This

error function is more robust than that of equation (4) because we are directly comparing displacement and rotations, which we have more inputs for, rather than comparing measured forces, which there were only a few of. By using more known measurements, the difference in the error function vectors is greatly reduced before parameter estimation takes place. Parameter estimation in Excel is rather straight forward when setting up a basic template. All of the necessary matrix manipulation commands are built-in to the program including: “MMULT()” for multiplication of matrices and “MINVERSE()” for taken the inverse of a matrix.

At this time, the user does not directly enter data such as joint location, connectivity, or element type in the spreadsheet to create the FEM. This spreadsheet-based optimization program works in conjunction with one of the new features of SAP2000 version 10, in order to expedite the parameter estimation process. When a SAP200 analysis is performed, the user has the option of extracting the structural stiffness and mass matrices to a separate file, which can be copied into the spreadsheet. The stiffness matrix is modified such that only the global degrees of freedom (DOF) were remaining. Any axial degrees of freedom were neglected and the analysis is limited to 2-D bending only, so the 21x21 DOF stiffness matrix reduces to a 14x14 DOF global stiffness matrix. Since the global stiffness matrix is a function of spring stiffness at the boundaries, locations where those parameters affect the matrix were identified and entered into the necessary cells. These references to the unknown spring stiffness values were the parameters that update the stiffness matrix when the optimization is performed. The user may wish to enter any experimental measurement and load vectors at this point so that later analyses can be made quicker by copying and pasting the vectors into the appropriate areas of the spreadsheet.

Once the global stiffness matrix is entered in the spreadsheet, it is observed that DOFs 1 (K_{11}), and 13 (K_{1313}), were affected by the spring stiffness values in the cells shown in equation (7).

$$[K]_g = \begin{bmatrix} \frac{12EI}{L^3} + k_1 & -\frac{6EI}{L^2} & \cdots & K_{1,13} & K_{1,14} \\ -\frac{6EI}{L^2} & \frac{4EI}{L} & \cdots & \vdots & \vdots \\ \vdots & \vdots & \ddots & \vdots & \vdots \\ \vdots & \vdots & \cdots & \frac{12EI}{L^3} + k_2 & \frac{6EI}{L^2} \\ K_{14,1} & K_{14,2} & \cdots & \frac{6EI}{L^2} & \frac{4EI}{L} \end{bmatrix} \quad (7)$$

This procedure is validated by checking the stiffness matrix for the same structure with “free” end restraints. A new FEM with spring supports of arbitrary value is then run and the resulting stiffness matrix reflects the increase in K_{11} and K_{1313} due to the axial stiffness term of the spring element (Figure 3).

		Spring #	Stiffness	Units
		K ₁	50.00	kip/in
		K ₂	50.00	kip/in

STEP 5	This is the global stiffness matrix for the test beam structure. Cells K ₂₂ and K ₁₂₁₂ will be updated to reflect the change in the boundary condition						
	1	2	3	4	5	6	7
	=((12*29000*39.6)/(24*3))+SG\$158						
[K] ⁱ	11963	191.00	-996.88	11963	0	0	0
	-996.88	-11963	1993.8	0	-996.88	11963	0
	11963	95700	0	382800	-11963	95700	0
	0	0	-996.88	-11963	1993.8	0	-996.88
	0	0	11963	95700	0	382800	-11963
	0	0	0	0	-996.88	-11963	1993.8
	0	0	0	0	11963	95700	0
	0	0	0	0	0	0	-996.88
	0	0	0	0	0	0	11963
	0	0	0	0	0	0	0

Figure 3: SPE Global Stiffness Matrix Showing Spring Referenced Cell

Since not all of the DOF contain sensors to measure data, a transform matrix, [T] is used to partition the global stiffness matrix and the experimental force and displacement/rotation vectors according to measured and unmeasured DOF. The user simply designates the new DOF order (from known to unknown DOF) and enters “1” in the appropriate cells. Further matrix manipulation is needed to partition the global stiffness matrix (note: this process becomes easier once the spreadsheet has been setup the first time). The global stiffness matrix is colored according to the partition labels on the spreadsheet (Figure 4).

$$[K_T]^i = \begin{bmatrix} K_{aa} & K_{ab} \\ K_{ba} & K_{bb} \end{bmatrix}$$

Figure 4: SPE Global Stiffness Matrix Partition Labels

The next calculations use static condensation techniques to solve for the analytically determined forces or displacement and rotations (equations 4 and 6 respectively) in terms of the measured forces or displacements and rotations. With the analytically determined displacement and rotation vector created, an error function vector is generated (Figure 5).

Analytically determined measurements		Experimentally determined measurements		Difference (error)	
$\{U_p\}^i$	-	$\{U_p\}^e$	=	$\{E\}$	KNOWN DOF
-0.00083		-0.00082		-0.00001	2
-0.02733		-0.02983		0.002499008	3
-0.00073		-0.00077		4.15626E-05	4
-0.04144		-0.05024		0.00879703	5
-0.00042		-0.00040		-1.36875E-05	6
-0.04642		-0.05258		0.006155729	7
0.00000	-	0.00007	=	-6.98724E-05	8
-0.04145		-0.04780		0.006354077	9
0.00042		0.00042		-3.89211E-06	10
-0.02733		-0.03254		0.00520545	11
0.00073		0.00079		-5.90444E-05	12
0.00083		0.00084		-1.02206E-05	14

Figure 5: SPE Error Function Vector

SPE – Optimization Setup

For nonlinear problem optimization, Solver uses the Generalized Reduced Gradient (GRG2) algorithm, developed by Leon Lasdon and Allen Waren, of the University of Texas at Austin and Cleveland State University, respectively (Flystra et al. 1998). The Solver works by iteratively solving for the target value, by changing values for the cells that are independent and adjustable. For this research, the target cell represents the objective function and the adjustable cells represent the unknown spring stiffness parameters, K_1 and K_2 (Figure 6).

Spring #	Stiffness	Units
K_1	50.00	kip/in
K_2	50.00	kip/in

(a)

Set the "TARGET CELL", which is the square root of the sum of the squares, from {E}:	
Minimize this cell ("Target Cell")	0.00018901

(b)

Figure 6: (a) SPE Adjustable Cells (b) SPE Target Cell

Since Excel can only designate one cell as the "Target Cell" or objective function, the Euclidean norm of the displacement and rotation error functions is calculated (square root of the sum of the squares) to define the objective function $J(k)$ as

$$J(k) = \sum_i E(k)_i^2 \quad (8)$$

where i represents a displacement or rotation measurement at a specific DOF. The method of least squares is used because it can be shown that equation (8) minimizes the error for noise (measurement, modeling error, etc.) that is assumed to be normally distributed. The square root that is typically found in this equation is omitted because it has no bearing on the affect of the outcome of the minimization process. Equation 8 is much akin to minimizing the length of a vector, given it starts at zero and ends at vector coordinates (u, v, w, x, y, z). The length of the vector L would be solved by taking the square root of the sum of the squares, i.e.

$$|L| = \sqrt{(u^2 + v^2 + w^2 + x^2 + y^2 + z^2)}$$

The Solver menu can be reached by going to the Tools menu and selecting “Solver...” from the list. Once the Solver window is opened, the buttons for the Target value as well as adjustable values are visible (Figure 7).

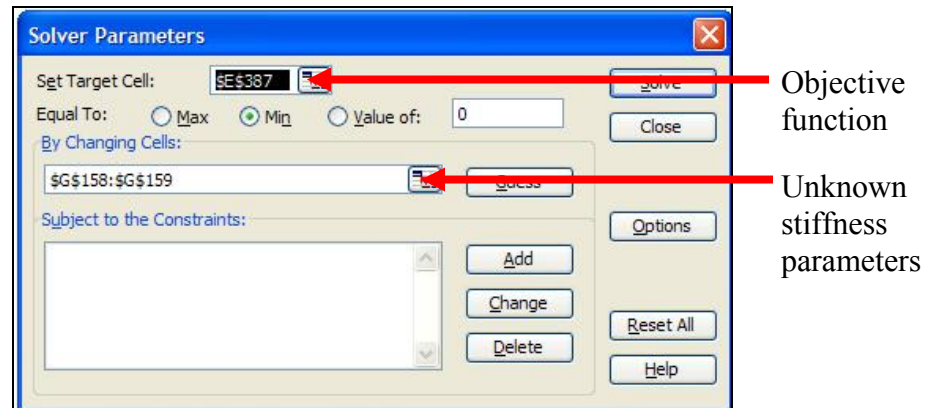


Figure 7: Solver Parameter Window

In order to set the convergence criteria as well as the algorithm settings, the “Options” button is selected. Setting the convergence criteria is the most important option in this window since it is what drives the algorithm to locate the global minimum (Figure 8).

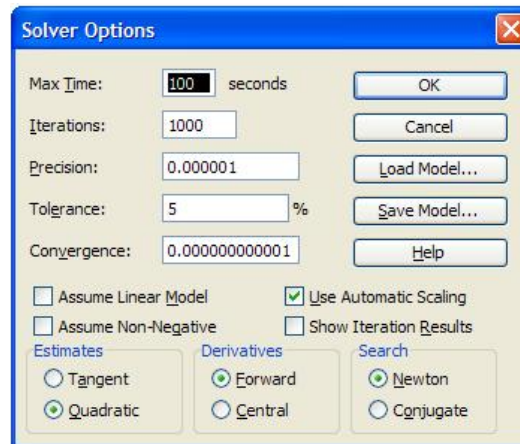


Figure 8: Solver Options Window

For this study, the convergence is set to approximately $1\text{E-}12$ to ensure that the global minimum is located. Automatic scaling is also selected in case the initial guesses have different magnitudes than those of the updated parameters, and Solver is unable to converge to them. Generally speaking, the choice of search method, either Newton or Conjugate, does not appear to have any significant impact on the outcome of the update parameters.

In many problems the best or optimum cell along with any constraints, are functions of the adjustable or “changing” cells. By taking the partial derivative of the function to be optimized, with respect to the unknown parameters a vector called the gradient is formed. The gradient vector measures the rate of change of the objective function, according to each unknown parameter. When Solver begins a numerical analysis, it incrementally changes the adjustable cells (unknown parameters) based on the gradient of the function. For target cells that are minimized, if the partial derivative with respect to one adjustable cell is close to zero while another is a large positive value, Solver will more than likely decrease the changing cell value on the next iteration. Optimality conditions are satisfied when the gradient vector is equal to zero,

since it would indicate that the global minimum is found (i.e. no error in the system). For this condition, the initial parameters would have no effect on the objective function since the global minimum would have already been identified. For our research, since error is present in the system the optimum solution will be located when the gradient vector is at its lowest value or approximately equal to zero (if possible).

Although Solver may find an optimum solution to the problem, there is no guarantee that it is the global solution to the problem. This case arises when the gradient vector is equal to zero, but the values for which the partial derivatives are equal to zero are numerous (many). For those problems in which the function has many local optimum points (maxima or minima), Solver may have difficulties locating the lowest “true” point or “global” solution to the problem. Often, the algorithm will be caught in a local “minima” which is near the starting point based on the initial values, and ultimately converge to that point. In order to avoid the pitfalls of being trapped in a local optimum, users should have a solid understanding of the problem or try multiple starting values with the best initial values.

PARAmeter Identification System Software (PARIS)

PARIS is parameter estimation software developed by Dr. Masoud Sanayei and his graduate students at Tufts University in Medford, MA. PARIS is written in the MATLAB programming language and uses static and/or dynamic measurements to update stiffness and mass parameters of linear-elastic systems. It has been used for research studies in the fields of structural parameter estimation, model updating, and health monitoring. This program can be

configured for both 2D and 3D structural parameter estimation. The following flowchart shows the procedure for carrying out parameter estimation using PARIS:

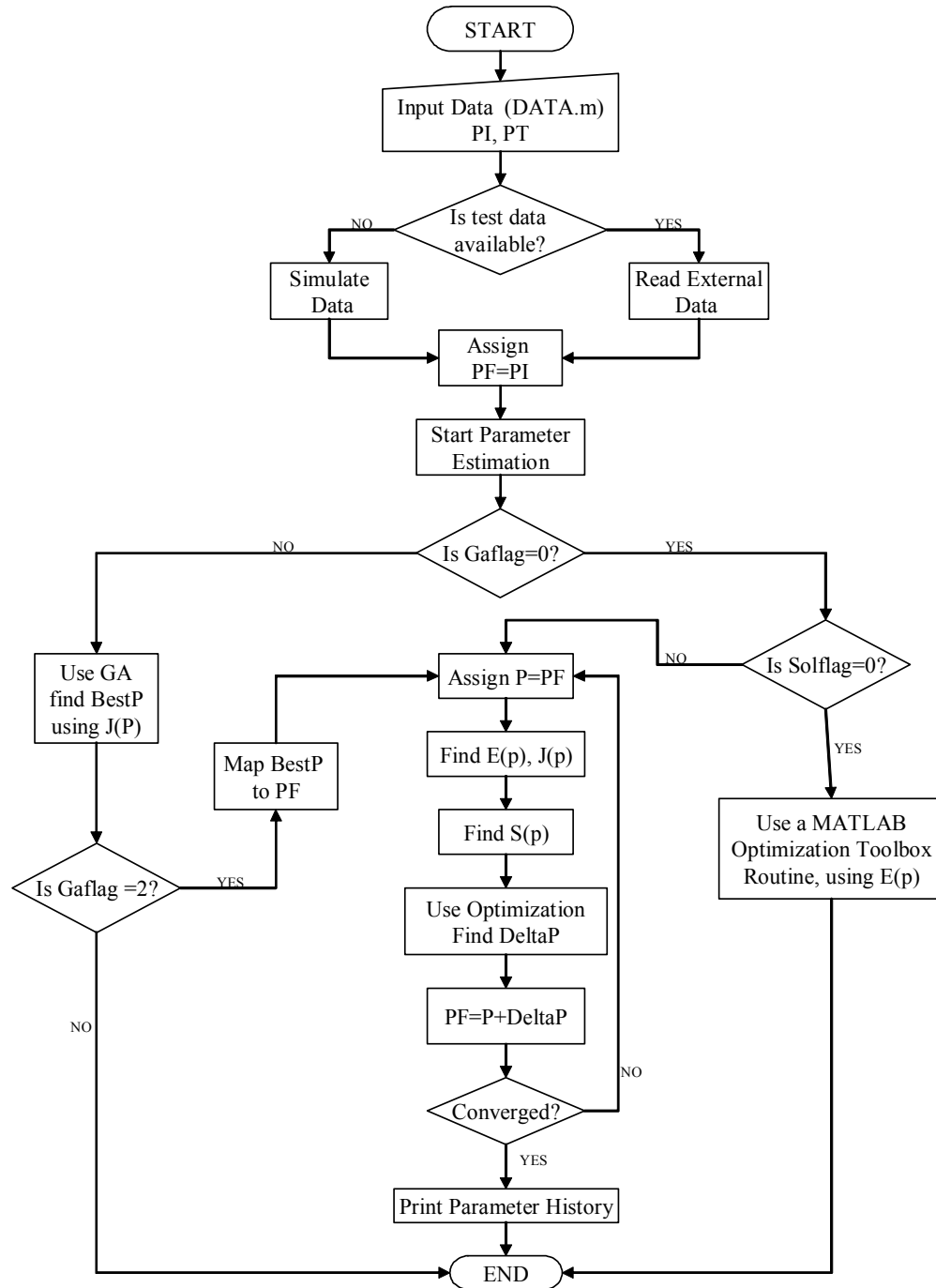


Figure 9: PARIS Optimization Procedure (Courtesy of Tufts University)

Finite Element Model Creation

Upon initialization of the PARIS program, the user defines the structure by entering data into specific matrices. Material data, specifically for steel or concrete, can be entered into a material matrix and is referenced by the element connectivity matrix. Joint data is first entered according to x, y, and z coordinates (required for 3D problems). After joint data is entered, the element connectivity matrix is formed by specifying what elements will be used to model the structure and to which joints they were attached. The following elements can be use to model different structures in PARIS:

1. 2D & 3D Truss Elements
2. 2D & 3D Frame Elements
3. 2D & 3D K_{sss} (Soil-Substructure Superelement)
4. 2D & 3D Partially Restrained Frame element (PRF)

For this research, 2D frame elements were used to model the steel I-beam and K_{sss} elements represent the boundary supports. The K_{sss} element was developed for parameter estimation in order to capture the mass and stiffness properties for the complicated interface below the ground level of a structure (Sanayei, 1999). The K_{sss} element is represented by a single node with three DOF, whereby making it a 3 x 3 stiffness matrix (Figure 10).

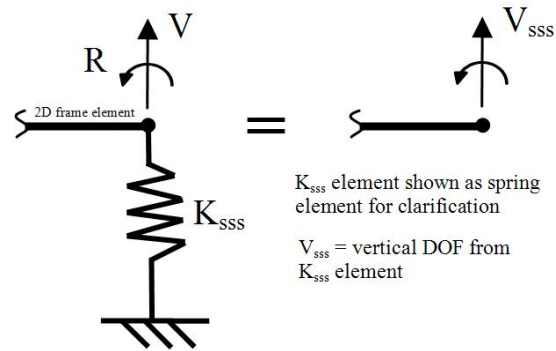


Figure 10: Ksss Test Beam Model

For our case, all horizontal DOF were eliminated since we were assuming all loads were in the vertical direction, and also assuming that there is no rotational capacity of the K_{sss} element since only vertical deflection of the pads was observed during testing. Here it is used to model the vertical flexibility of the supports of the test beam and is shown as a vertical spring on all further drawings or models in this thesis for clarity.

Preliminary models of the test beam involved using 2D PRF elements along with K_{sss} elements, to account for the assumed rotational stiffness of the boundary conditions (Figure 11).

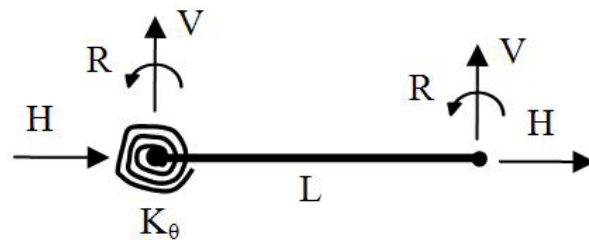


Figure 11: PRF Element

PRF elements are used to model semi-ridged joints, or joints which are neither fully fixed nor fully pinned. One rotational DOF is added to the end of a typical 2D frame element and this DOF is connected by a torsional spring to the rotational DOF at the joint (Sanayei et al. 1999). A 6 x 6 stiffness matrix defines this element, and for $K_\theta = 0$, the joint becomes pinned (moment release) and for $K = \infty$ (rigid), the element becomes a normal frame element.

Next, the structure support information is entered into a boundary condition matrix. Ones or zeros were entered depending upon which joint DOF were to be constrained or not constrained (negative 1 for non-existent DOF). The section properties matrix is the last matrix which is used to define the physical structure by assigning section properties such as mass and stiffness to each element. The first matrix is defined by initial sectional properties of the structure or data which can be determined from blue prints or field measurements. The initial property matrix is used with the experimental (NDT) data that is input into the program. The second matrix is used exclusively with simulated measurement data, in which case the actual member properties are known.

Parameter Estimation Data

With the FEM information completed, the user next selects the settings they want to use for parameter estimation. There were a total of 16 different error functions the user may select for parameter estimation. Static displacement error functions, like those of equations (4) and (6) were used primarily for this research study, but static strain, modal displacement, and modal frequency data-based error functions may also be used, provided they have the appropriate measurement data. The user can opt to use multiple error functions if both static and dynamic

measurement data is available. While not used in the study, readers are encouraged to find more information regarding multi-response error function or error function “stacking” from Sanayei et al. (2006).

Applied forces or moments were entered into a load case matrix detailing the joint location(s), load direction (x, y, z), and load intensity. Single or multiple load force cases may be specified. Due to the programming language of MATLAB, users can setup all of their load case matrices ahead of time and then comment them out of the program (“%”), so that only the case they want to be read is used.

The last part of the parameter estimation data section is to specify which DOF were used by the measurement data file. A measured node matrix is used to define which DOF is measured or not measured according to the experiment. Ones (measured) or zeros (not measured) identify which displacement or rotational DOF collected measurements. Again, the user can enter different DOF combinations depending upon the number of measurements they wish to use and comment out the ones that won’t be read for analysis. Similar matrices were used for measured modal information from dynamic analysis.

Other sections in the code were specific to normalization methods, parameter grouping options, weighting methods, simulated measurement error, modeling errors, and parameter estimation limits and controls. These sections were used limitedly or not at all for this research study and will not be described in detail. The last sections cover convergence control in which the user specifies the limit for both the error and objective functions. This criterion deals with the relative change in the unknown parameters and at convergence the values should be close to or at one. The user specifies a 1 for one of the input flags if actual test data is to be used. The measurement data is placed in a text (.txt) file and referenced by another command. Multiple

files may be kept in this section and turned on or off (by commenting out) for different parameter estimation runs.

Another powerful tool of PARIS is its ability to plot the objective function, $J(k)$ in 3D space for viewing, showing two variables at a time (Figure 12).

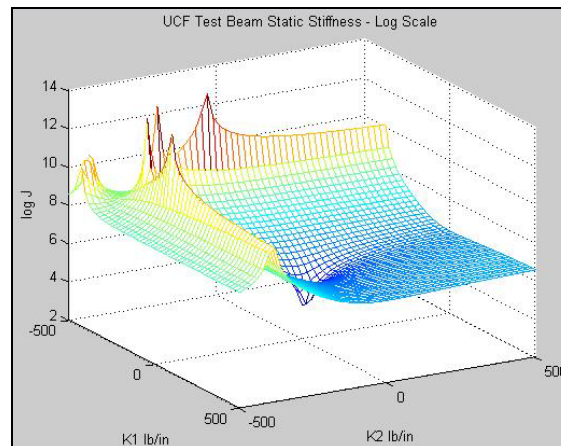


Figure 12: Sample PARIS Objective Function Plot

Objective function plots can provide insight into the behavior of the non-linear function as different initial conditions were tried, sometimes shifting or even changing the objective function, $J(k)$ itself. Objective function plots also let users see a 3D plot of the complex function, indicating regions which may be feasible for initial starting points for the unknown parameters. An objective function surface plot, shown in Figure 12, shows the global minimum for two unknown spring stiffness values. If there is a global minimum or solution to the function, then it will show up on these plots as a well-defined sharp point representing the best solution to the problem.

Another graphic that can be produced is the iteration plot path, showing the plot of the initial values as they converge toward the global minimum of the objective function. This path is usually not well-defined for analyses that converge quickly to the global minimum (represented by a few straight lines). For those functions which are highly prone to many local minima in addition to the global minimum, algorithms that are powerful will show the path of the iterations as it travels around and over the minima, ultimately reaching the global solution. Figure 13 shows the iteration plot path for the objective function shown in Figure 12.

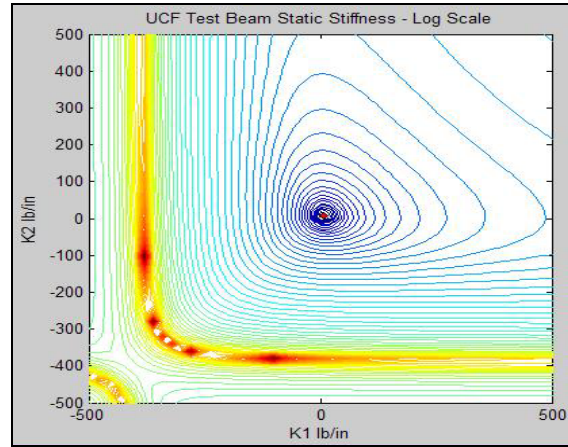


Figure 13: Sample PARIS Iteration Path Plot

While there are 6 different solution techniques or algorithms to choose from, the method of least squares is used primarily for all the analysis in this study. The error functions in equations (4) and (6) are algebraically non-linear functions of the stiffness parameters. Using a Gauss-Newton method (Sanayei et al. 1999), the error function vector is linearized using a first order Taylor series expansion and the change in unknown parameters can be found for each iteration i .

$$\{p_{i+1}\} = \{p_i\} + \{\Delta p\} \quad (9)$$

The objective function, $J(k)$ is minimized once the convergence limit for the relative change in the unknown parameters is reached. For all PARIS analysis, the limits for the relative change in the objective function, $J(k)$, and error function, $\{e(k)\}$ is 1E-12 and 1E-06, respectively.

Once convergence criteria were met, the updated parameters were then input back into the FEM, and the responses were evaluated by the user. PARIS is a powerful analysis tool because of its ability to be customized by the user.

CHAPTER THREE: NUMERICAL STUDIES AND MODEL DESIGN

Design Considerations

Designing and manufacturing a test specimen incorporates many different considerations. Four main criteria governed the choice of a beam for this research study. First of all, any beam selected must be capable of hosting the sensors in terms of surface space for mounting. Secondly, the strain gages, tiltmeters and displacement transducers need to be able to operate in their specified ranges. In other words, the gages can only read data above their minimum values specified in the spec sheets. Thirdly, the modal frequencies needed to be such that at least the first few modes must be easily excited. Last, the loading values have to be predetermined and checked for satisfactory outputs in terms of the values being recorded by sensors. As one can see, this is a simply but iterative process which is summarized below.

- Sensor mounting space
- Measurable data
- Modal frequencies
- Loading values

Considering all the above, it was decided that a W8X13, 12 ft in length would best satisfy all of the above criteria. The approximate 4-inch wide flange of the beam would allow us to place two sensors side by side if required, and the 8-inch depth allows for placement of the tiltmeters we had in our inventory. Since a 12 ft clear span was designed, the beam was actually ordered as 13 ft.

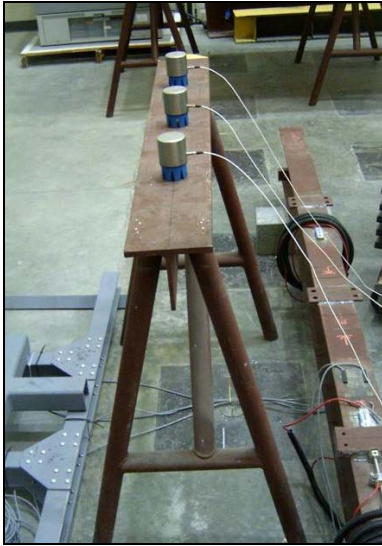
Once the beam type and loads were known, the next step was to design the supports. Two main criteria needed to be satisfied for the supports. Most importantly, no deflections or deformations should be induced. From a practical perspective, the author decided that a height of 3 ft. beneath the beam would be sufficient for working space. It becomes quite cumbersome to install gages and run wiring on a structure supported close to the ground. Based on recommendations from steel manufacturers, heavy WT sections were used as supporting surfaces with pipes used as the legs. The final product (Figure 14) resembles what is commonly known as a “saw horse.”



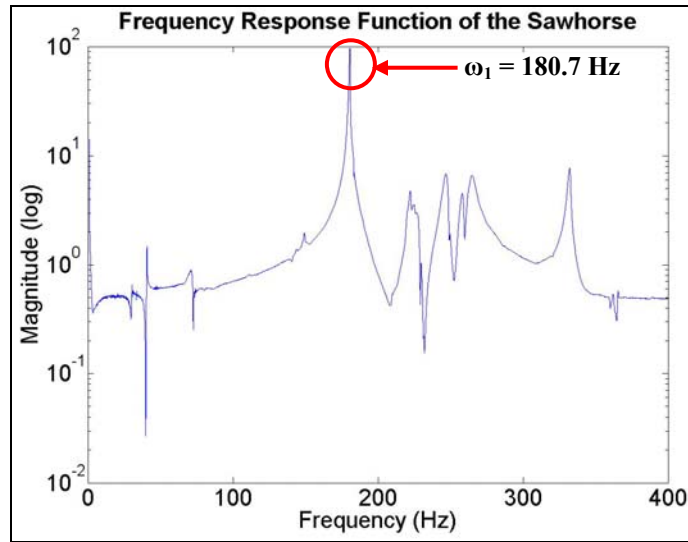
Figure 14: Test Beam Sawhorse Support

Dynamic tests of the supports were also carried out, so that the 1st natural frequency of the sawhorse was verified as being greater than 3 times the 1st natural frequency of the beam. Three

PCB seismic accelerometers were used to capture the time-history data and DAQ Express software was used to plot the frequency response function (modal frequencies) (Figure 15).



(a)



(b)

Figure 15: (a) Dynamic Test on Sawhorse (b) Frequency Response Function of Sawhorse

The first mode was checked to ensure that the sawhorse support was much stiffer than the beam so that there would be no coupling of the 1st modes between them. By assuring that the 1st natural frequency of the support (180.7 Hz) is much greater than the 1st natural frequency of the beam (~40 Hz) then no modal coupling will take place.

Analytical Model

The test beam analytical model was created using SAP2000, a commercially available finite element analysis software, by Computers and Structures, Inc. Discretization of the beam was based primarily on the location of pre-existing sensors. Based on the pre-existing sensor

layout (those which could not be removed without damaging them completely), the beam was discretized into six equal elements, each 24 inches in length (Figure 16).

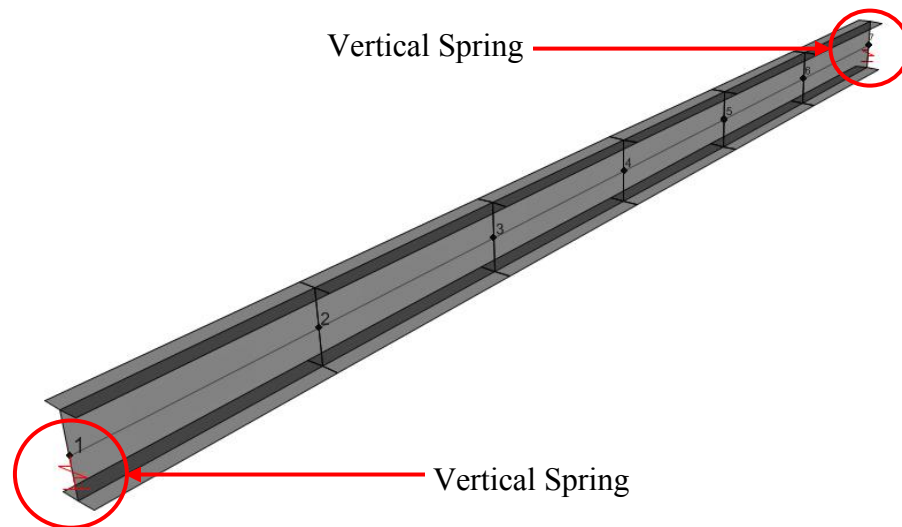


Figure 16: SAP2000 Test Beam (Extruded View)

Frame elements were used to model the behavior of the structure, and the degrees of freedom were limited to a 2-D plane only, restricting any torsion or bending moments not on the principal axis. Sensors were located at the joints of the model, allowing for quick comparison of displacement and rotation measurements. Experimental force locations were restricted to only the measurement degrees of freedom, which occurred at the structural model joints.

For analysis purposes, the assumption was made that any shear and axial deformation would be small when compared to bending deformation, therefore eliminating their contributions from the analysis. Using the property modifiers in SAP2000, the area for the frame elements is set to a large value such that axial deformation is neglected and the shear areas are set to zero to eliminate shear deformations. Member elements were assumed to be homogenous and prismatic,

as well as exhibiting linear-elastic behavior. Due to the complexities of modeling the non-linear behavior of the neoprene pads, this study will focus solely on the linear-elastic region of the materials. Figure 17 shows the FEM joint, element, and DOF labels and locations. The boundary conditions were described by a set of linear vertical springs, allowing for settlement of the joints. Truly fixed or pinned support conditions would have restrained vertical deflection.

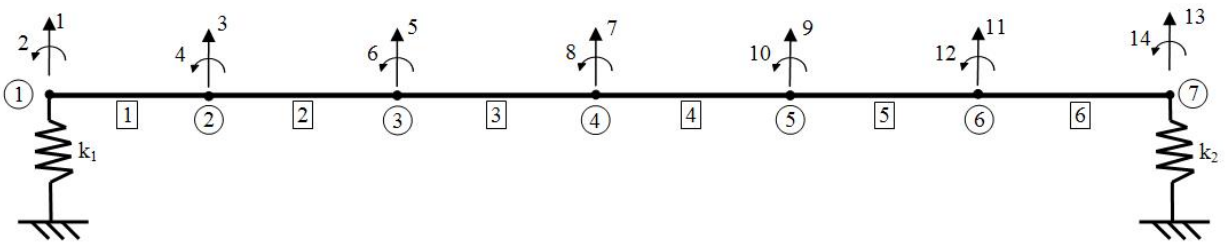


Figure 17: Test Beam FEM information

Sensor/Data Validation

Validation of the experimental data sets must be carried out before using them with the optimization programs. The author must verify that the experimental data was credible and that no significant errors existed. This was also a chance for us to verify that the sensors were working properly by making sure there were no unwanted measurement errors such as spikes and drift. Data validation also provides a starting point for the parameter estimation studies, by letting us know how close the experimental and preliminary analytical model were to one another. The author assumed that a non-calibrated FEM of the test beam with truly pinned supports was going to be stiffer than the physical model, and compared the experimental data for LC1 (1x1x1/8 angle steel supports) to observe the percent difference between them.

A sample load case, two 0.416 kip symmetric point loads, was selected to verify the displacement and rotational measurements for a “pin-pin” boundary condition setup. Three different data sets were used in the comparison: closed-form solution, SAP2000 FEM, and experimental data. The closed-form solution or “exact” solution is derived from structural analysis calculations using the moment-area theorem and was used to show how much error was due to low order FEM approximation. Displacement data is shown in Table 1 and rotational data is shown in Table 2.

Table 1: Displacement Measurement Data Validation

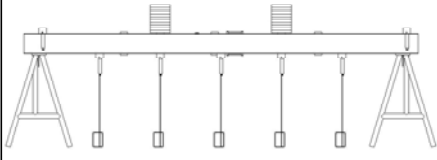
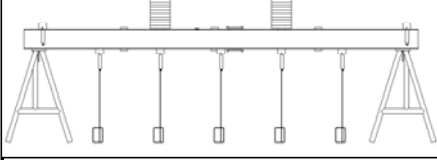
Load Case # (with description)	Beam Location (in.)	Disp. Sensor #	Closed Form (in.)	Pin-Pin SAP2000 (in.)	[% Diff.]	Exp. Δ (in.)	[% Diff.]
LC1	0	Δ_0	0	0	-	-	-
	24	Δ_1	-0.0192	-0.0192	0.1%	-0.027	41.5%
	48	Δ_2	-0.0334	-0.0334	0.1%	-0.042	24.7%
	72	Δ_3	-0.0384	-0.0384	0.1%	-0.046	18.6%
	96	Δ_4	-0.0334	-0.0334	0.1%	-0.041	23.5%
	120	Δ_5	-0.0192	-0.0192	0.1%	-0.026	37.3%
	144	Δ_6	0	0	-	-	-

Table 2: Rotation Measurement Data Validation

Load Case # (with description)	Beam Location (in.)	Rot. Sensor #	Closed Form (rad.)	Pin-Pin SAP2000 (rad.)	[% Diff.]	Exp. θ (rad)	[% Diff.]
LC1	0	θ_1	-0.00083	-0.00083	0.1%	-0.00086	2.6%
	24	θ_2	-0.00073	-0.00073	0.1%	-0.00065	10.9%
	48	θ_3	-0.00042	-0.00042	0%	-0.00040	4.0%
	72	θ_4	0	0	0%	0	0%
	96	θ_5	0.00042	0.00042	0%	0.00043	3.2%
	120	θ_6	0.00073	0.00073	0.1%	0.00067	7.9%
	144	θ_7	0.00083	0.00083	0.1%	0.00087	4.4%

From both tables, the difference in the closed-form solution versus the SAP2000 model is relatively small. This indicated that our FEM was discretized enough as to provide good approximate solutions for both the displacement and rotation measurements. By looking at the displacement results we can see that there is generally a 20-40% difference between the closed form solution and the experimental values. This should raise a red flag since a pinned connection (experimental) should have little or zero deflection at the supports (clearly they were deflecting from Table 1). It was not the goal of this author to verify that actual pin supports were used for part of the experiment. The small steel angles were intended to be used for the experiments and it will later be discussed how assuming them as pin supports is generally incorrect. For the rotational measurements, there is fairly good correlation between the data sets. The preliminary results show that the FEM is a stiffer model than the experimental results indicates. Based on the results of the data verification the author will need to reduce approximately 30% error between the experimental and non-calibrated FEM.

SPE – Numerical Validation

Before using experimental data with the optimization programs for updating the unknown stiffness parameters, the programs must first be validated using error free data (noise free). With zero error present in the system, one should expect to obtain the exact values for the unknown parameters. To test the reliability of the SPE program with no input (measurement) error, two similar finite element models were generated (Figure 18). The first FEM will represent the “experimental” or “actual” test beam setup including applied force(s) at select DOFs, and will consist of linear translational springs for boundary conditions. The values selected for the spring

stiffness will represent the “actual” stiffness values to match or update the second model.

Equation 1 is rearranged to solve for the “measured” displacements and rotations (10).

$$[U_{\text{exp}}] = [K]^{-1} [F_{\text{known}}] \quad (10)$$

After performing an analysis with the first model and obtaining the “known” measurements, $[U_{\text{exp}}]$, we use this vector as our input (NDT) data. The second FEM or “initial” model will be identical to the “actual” FEM with the exception of the spring stiffness values. Different spring stiffness values were input into the model and a new analysis is run. The goal here is to see if the “initial” stiffness matrix will update to produce “known” displacement, based on the matrix using the “actual” displacement and rotation matrix, but using unknown stiffness quantities. The analysis results indicate that SPE identifies the “unknown” parameters correctly in this validation study.

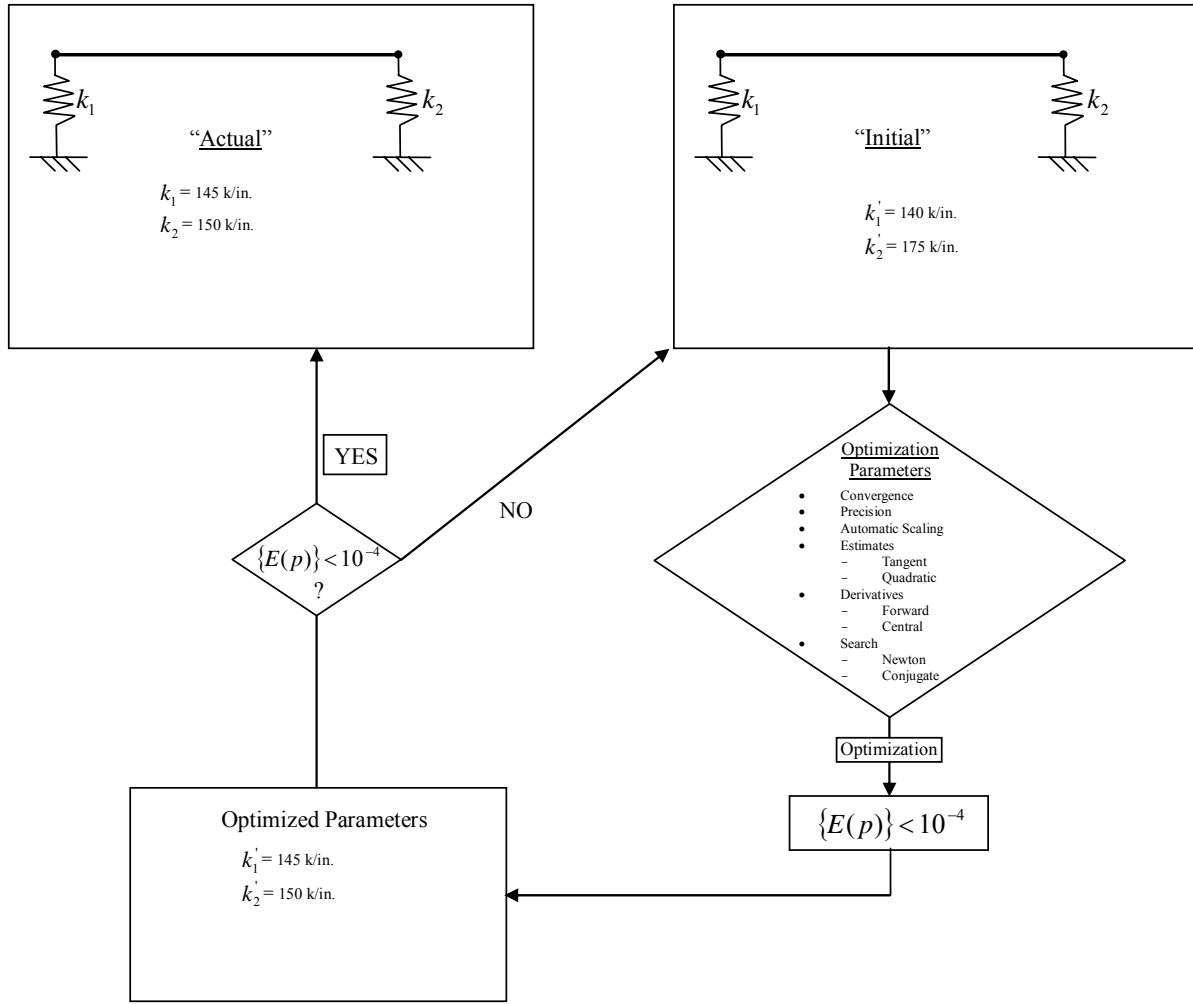


Figure 18: Verification of Optimization Using a Numerical Example

PARIS – Numerical Validation

Like SPE, it is also important to perform validation studies with PARIS using noise or error free measurement data. By using the simple relationship found in equation (10) we can solve for displacement and rotations by assuming we already know the “actual” spring stiffness values and our measured force vector. Using this data, we multiply the inverse of the stiffness matrix with the measured force vector. The resulting displacement/rotation vector is based on the

“known” spring stiffness values. Again the data from this vector is copied to its own text file and used as the input into PARIS. Under the initial section property matrix, initial spring values different from those that were used to obtain the “known” displacement vector, were entered into the correct spots (Figure 19).

```

%8x13 section properties are assumed to be true
%
secprpi=[ 1    200    0    0    240    0    5    0    0    0
          2    3.84   39.6    0    0    0    0    0    0    0
          3    3.84   39.6    0    0    0    0    0    0    0
          4    3.84   39.6    0    0    0    0    0    0    0
          5    3.84   39.6    0    0    0    0    0    0    0
          6    3.84   39.6    0    0    0    0    0    0    0
          7    3.84   39.6    0    0    0    0    0    0    0
          8    200    0    0    290    0    5    0    0    0];

secprpt=[ 1    200    0    0    250    0    10    0    0    0
          2    3.84   39.6    0    0    0    0    0    0    0
          3    3.84   39.6    0    0    0    0    0    0    0
          4    3.84   39.6    0    0    0    0    0    0    0
          5    3.84   39.6    0    0    0    0    0    0    0
          6    3.84   39.6    0    0    0    0    0    0    0
          7    3.84   39.6    0    0    0    0    0    0    0
          8    200    0    0    300    0    3    0    0    0];

```

Figure 19: PARIS Initial and True Section Property Matrices

PARIS is then run, and the updated parameters should be exactly equal to the “known” parameter values we used to get the “actual” displacement vector from.

With little or no measurement error we can expect the objective function plot to look something like Figure 20, where the global minimum is represented by a well-defined sharp point in the function.

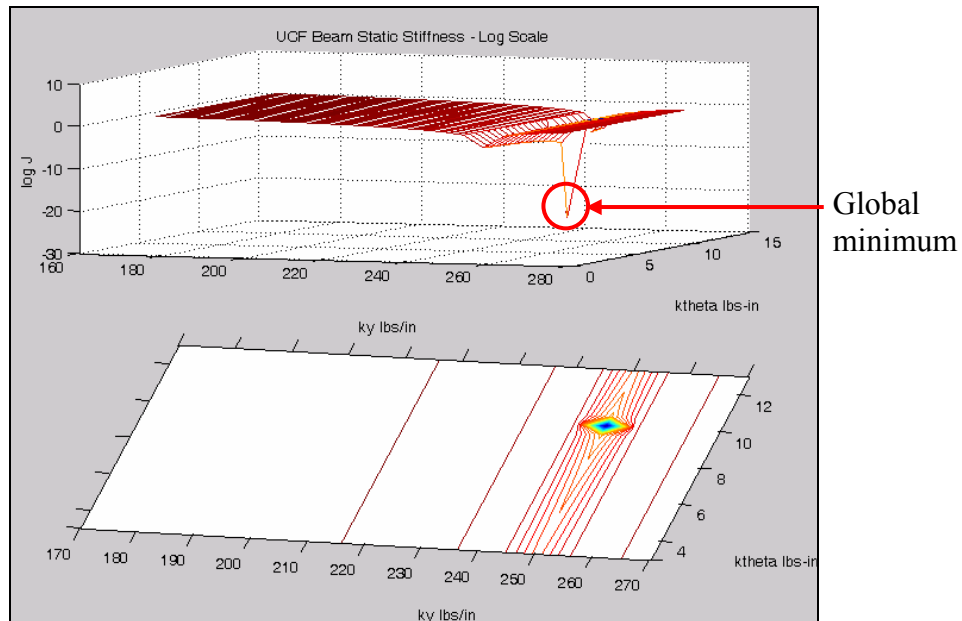


Figure 20: PARIS Global Minimum (4 MDOF)

This plot illustrates the global minimum of the objective function for two variables, using the minimum number of measurements required. An interesting concept of measurement selection for parameter estimation is that adding more known measurements (or “sensors”) to the analysis does not necessarily mean that the objective function plot will become clearer or sharper. As shown in Figure 21, an analysis using more observations (12MDOF) may create a “foggier” objective function surface because all of the measurements are averaged. These additional measurements do not make the plot clearer because of added interference. This interference may be due numerical procedures and in a real life case due to measurement errors associated with additional sensors. When all of the new additional measurements were averaged, the plot becomes smoother but the global minimum is not as clear as it was before, using the minimum number of observations. Due to the fact that this is for validation purposes and there is no

measurement error, the global minimum value will still be the same as the minimum sensor case. However, for actual test data including measurement error, it will be harder to locate the global minimum because of the variability of the averaged measurements.

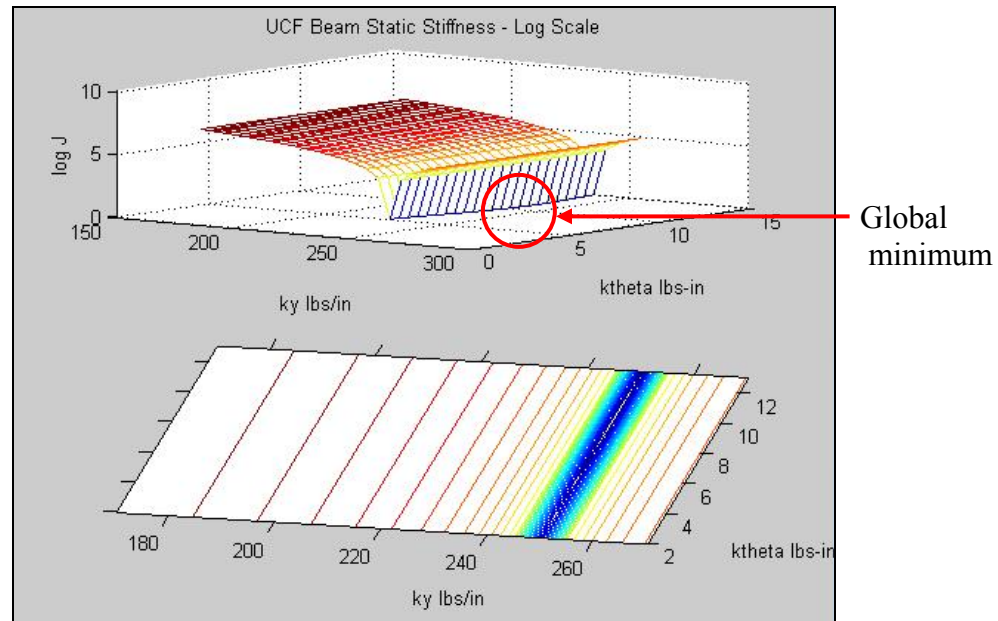


Figure 21: PARIS Global Minimum (12MDOF)

When performing the analysis using PARIS, a few key points must be kept in mind in order to determine if the parameter estimation process was successful. Engineering judgment must be used when making initial value assumptions. By looking at the experimental data, inferences regarding the behavior of the system can be made, leading to better guesses for the parameter estimation process. Convergence plots should be checked to make sure that the iteration steps are not diverging or traveling in the wrong direction. Graphic plot of the objective function can be checked to see if the plot shows a convex curve, representing a clear global minimum instead of a flat plot, which would indicate problems with the measurement locations

locating the global minimum. The norms of the unknown parameter values and the sensitivity matrix can give clues as to how observable the unknown parameters were with regards to the selected measurements and load sets. Norms which were large and close together in value, indicated measurement locations that were highly observable and good for the parameter estimation analysis.

Model Validation Using Dynamic Test Data

A unique aspect of this research study is that the updated finite element models were validated using independent dynamic tests. At this time, the author will not be updating the mass parameters for the dynamic comparison. This may be accomplished by using experimental mode shapes and/or frequencies to update the mass matrix. By looking at the dynamic properties of the updated finite element models, we can use the mode shapes and frequencies as another tool, in addition to using the updated static measurements. Time history data was collected using several PCB seismic accelerometers located at all of the static load points (A1, A2...A5), and at both of the supports. An impact hammer was used to excite the structure and the behavior was captured using the accelerometers (Figure 22).



Figure 22: Impact Hammer Tests on the Beam

The natural frequencies and mode shapes were used for comparison. First, MIMO (Multi-input multi-output) FRFs (Frequency Response Functions) were obtained by using impact tests. Then those FRFs were fed to CMIF (Complex Mode Indicator Function) algorithm to identify the modal parameters, i.e. the natural frequencies and mass normalized mode shapes. Finally, results coming from dynamic tests, static tests and updated FEM were compared. Further details about the methodology and algorithm can be found in Catbas et al. (2004).

The accuracy of the updated parameters was verified not only by comparing the natural frequencies, but by also comparing the mode shapes. Modal Assurance Criteria (MAC) values were used to compare the mode shapes between the updated and experimental FEMs. The first mode is generally the dominating or critical mode and missing it will indicate errors. MAC values from 0.95 to 1.0 indicate a very good (reliable) match between the updated and experimental models.

CHAPTER FOUR: EXPERIMENTAL STUDIES – UCF TEST BEAM

Sensor Instrumentation

For our experimental tests, it is critical that sensors be placed where maximum responses can be measured adequately. Previous strain studies conducted on the test beam included the use of arc-weldable strain gages, and numerous spot-weldable strain gages. The load points for the experiment were based on the 24 in. discretization length of the frame elements in the SAP2000 model. Some of the preexisting sensors were located at the desired load points so a decision was made to keep them rather than removing them from the beam. Removing the spot-weldable strain gages would have proved too costly since, removing the contact shim from beneath the gages would have rendered the sensors useless for future studies. Provisions were made to overcome this situation by using shim plates to elevate the load path above the installed sensors.

Displacement Transducers

Precision measurements were needed for us to be able to record small incremental changes in deflection, and the superior construction of the string potentiometers from Spaceage Control Inc., allowed us to do so (Figure 23). In general, these devices measure displacement via a flexible cable that extracts from and retracts to a spring-loaded drum. They convert mechanical motion into electrical signals that can be measured. An internal spring helps maintain tension on the cable and the threaded drum rotates a precision rotary sensor that produces an electrical output proportional to the cable travel. These displacement transducers were easy to configure,

setup, and make measurements from. Advantages of using these sensors were; ease of installation, cost effectiveness, reliability, and minimal signal conditioning requirements. The locations of these sensors allow us to capture the displacement profile of the beam for a multitude of load cases.

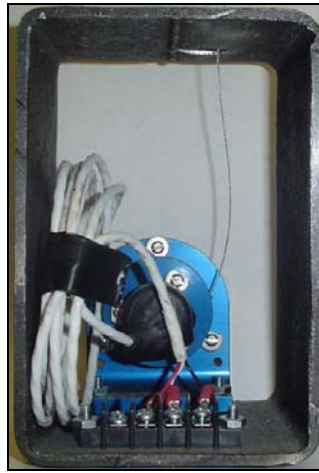


Figure 23: Displacement Transducer Setup

Due to the fact that attaching the cable of the transducer to the lower flange of the beam creates a tension force in the cable, the sensors must be heavy enough to resist that force. Failure to resist the tension force would result in the cable snapping back into the gage, possibly damaging the internal parts, and rendering the sensor useless.

Cato Steel donated some steel HSS 6x4x1/4 tubing to use as housing for the sensor. The steel tubing was cut into equal sections that were wide enough to allow a sensor, additional wire and a terminal strip to rest safely inside. A hole drilled through the top of the housing permitted the cable to pass through while the gage remained screwed into the base, along with the terminal

strip. The terminal strips allow for quick connection between the sensor and the datalogger that will be used to record measurements.

Two options were presented to us when deciding how to attach the cables to the beam for displacement tests. One method was to create a lanyard and wrap additional cable around the upper and lower flanges of the beam, tighten it to prohibit slippage and then clip the transducer cable to the lanyard cable. The other method uses high-strength magnets, designed for holding PCB seismic accelerometers onto steel structures. This method proved to be faster since all we needed to do was to thread the transducer cable through an opening in the base of the magnet, attach a clip to prevent the cable from traveling back through the hole and attach it to the flange of the beam (Figure 24).



Figure 24: Displacement Cable Attachment Method

Vibrating Wire Tiltmeters

These tiltmeters are comprised of a pendulous mass, which is under the force of gravity. As tilt increases or decreases, the mass attempts to rotate beneath the elastic hinge point and the tension in the vibrating wire changes, altering the natural frequency. An electromagnetic coil

plucks the vibrating wire in order to read the natural frequency. Some advantages of using vibrating wire tiltmeters are that they combine high range with high sensitivity, and have excellent long-term stability. Since the sensor outputs readings in units of frequency, there is little attenuation over long cable lengths.

Geokon vibrating wire gage (VBWG) tiltmeters were placed approximately 6 inches from the supports on either side of the beam, where maximum rotation values will be measured (Figure 25). Also, for our loading scenario, the resolution of the gages is high enough to record the small incremental changes that we may see due to loading of the test beam.



Figure 25: Geokon VBWG Tiltmeter

CR10X Datalogger

The CR10X is a rather inexpensive and robust data collection unit, found extensively in environmental and civil monitoring applications (Figure 26). The CR10X datalogger is a rugged unit capable of running in some of the most demanding environments, and in temperatures

ranging from -25°C to +50°C. Our unit has 2 Mbytes of internal storage capacity, allowing for up to 524,288 data values per MByte, where high-resolution data (5 decimal characters) equals 4 bytes and low-resolution data (4 decimal characters) equals 2 bytes. The CR10X is capable of sampling rates from real-time to 64Hz and up to 750Hz using burst measurements over short intervals. Analog inputs allow for 6 differential or 12 single ended measurements, as well as accommodations for resistance measurements (resistive bridge-based), as well as excitation outputs of -2.5V to +2.5V.

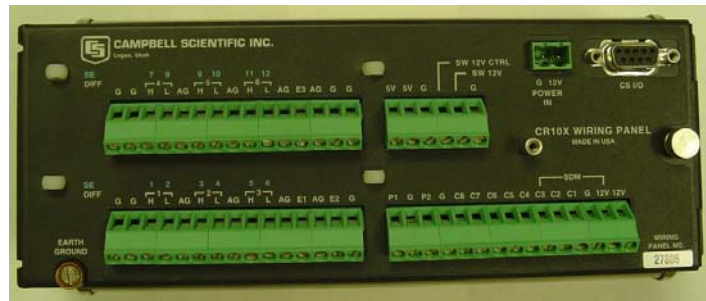


Figure 26: Campbell Scientific CR10X Datalogger

AM16/32 Multiplexer

The main purpose for the multiplexer is to increase the number of sensors that can be measured by the CR10X (Figure 27). It is also used when there are more sensor inputs than the datalogger channels will allow. Because of its relatively inexpensive cost, up to 4 multiplexers can be used with one CR10X datalogger, allowing hundreds of sensors to be run at a time. Two separate modes, “2x32” and “4x16” allows for scanning of 32 sensor input channels, each having 2 lines and for scanning of 16 sensor input channels, each having 4 lines respectively. The

maximum number of sensors that can be multiplexed is limited to: 32 single-ended or differential analog sensors not requiring excitation (thermocouple) or 16 single-ended or differential sensors requiring excitation (full bridge strain gages). In a differential measurement, the voltage on the H input is measured with respect to the voltage on the L input. A single-ended measurement is used to measure voltage at a single-ended input with respect to ground. Although often used in conjunction with the CR10X, the multiplexer is only good for indoor, non-condensing environments. Separate enclosure units can be purchased to protect the system if it is used outdoors. Like the CR10X, the AM16/32 can be used in temperatures ranging from -25°C to $+50^{\circ}\text{C}$.

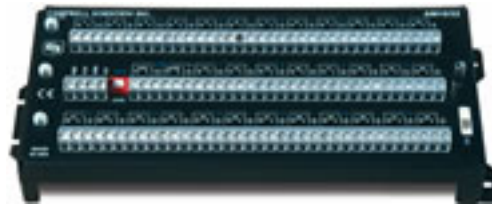


Figure 27: Campbell Scientific AM16/32 Multiplexer

AVW1 Interface

The AVWI provides important signal conditioning that helps to convert the swept frequency excitation from $+2.5\text{V}$ to $+12\text{V}$ (Figure 28). Most of the Geokon VBWG's require a 12V source since a 2.5V source may not be strong enough to pluck the tensioned wire over its frequency range. Due to its nature, the AVW1 also provides transformer isolation and noise reduction for the vibrating wire signal.

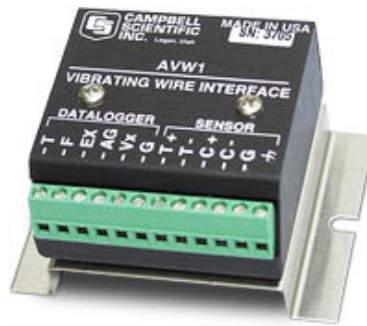


Figure 28: Campbell Scientific AVW1 Interface

Load Case Selection

For the test beam experiments, a total of 13 load cases (LC) were conceived to test different load location and intensities. Four of these load cases deal with varying load intensity which will later prove to have a significant impact on the load case selection process.

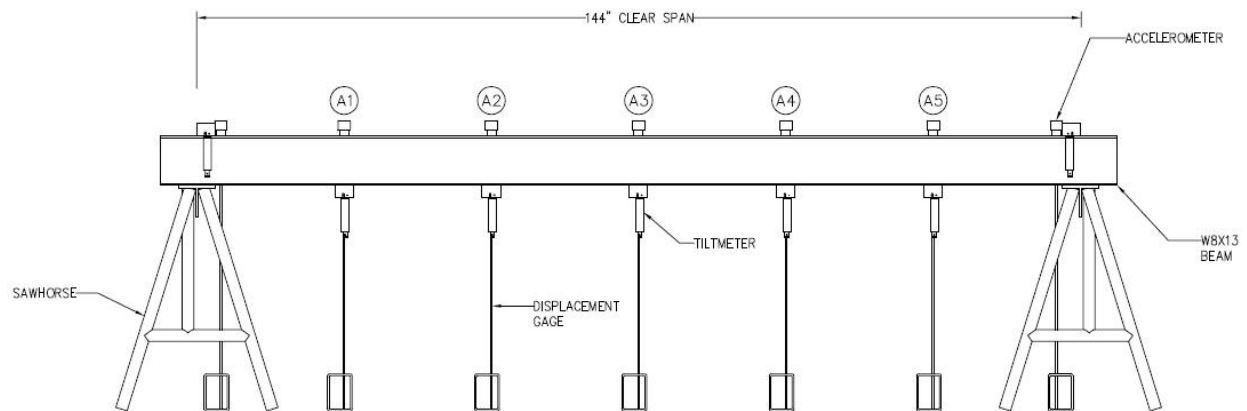


Figure 29: Test Beam Experimental Load Locations

The various load locations shown in Figure 29, are labeled from left to right as A1, A2, A3, A4, and A5. These five locations allow for the loads to be placed at various points along the beam and in several different combinations. The following is a brief explanation of each loading scenario:

1. **LC1_Full** – This load case represents two symmetrically placed point loads at load locations A2 and A4 on the test beam (Figure 30). This load case was chosen because it elicits good responses from the sensors due to the intensity of the loads. By selecting a symmetric load case, the researcher was also able to observe the behavior of the actual load distribution as captured by the instrumentation.

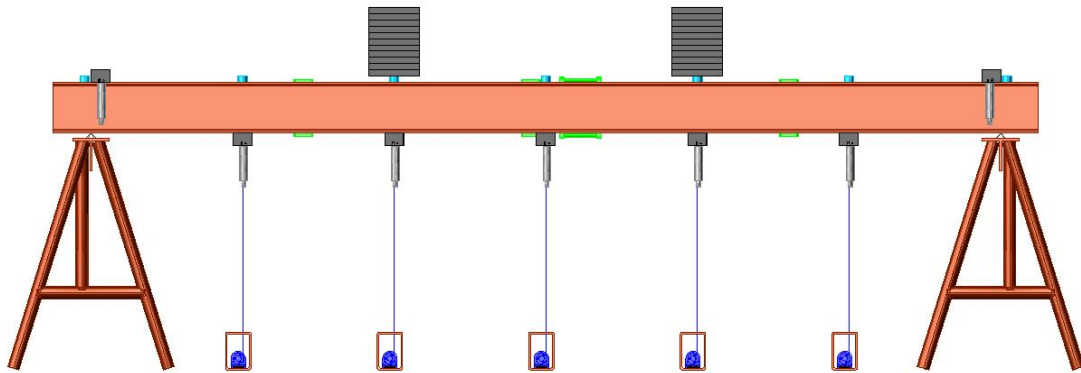


Figure 30: LC1_Full Elevation View

2. **LC2_A1...A5** – This load case is actually five separate (individual) point loads starting at load location A1 and progressing to load location A5. The author wanted to capture the structural behavior of the test beam due to a moving point load across the structure. Each load is applied one at a time and measurement data is collected for

each load location. For parameter estimation, the data from combining these load cases should provide reliable, accurate results. Figure 31 shows the load as it moves to each new load point, represented as a faded-colored stack of weights.

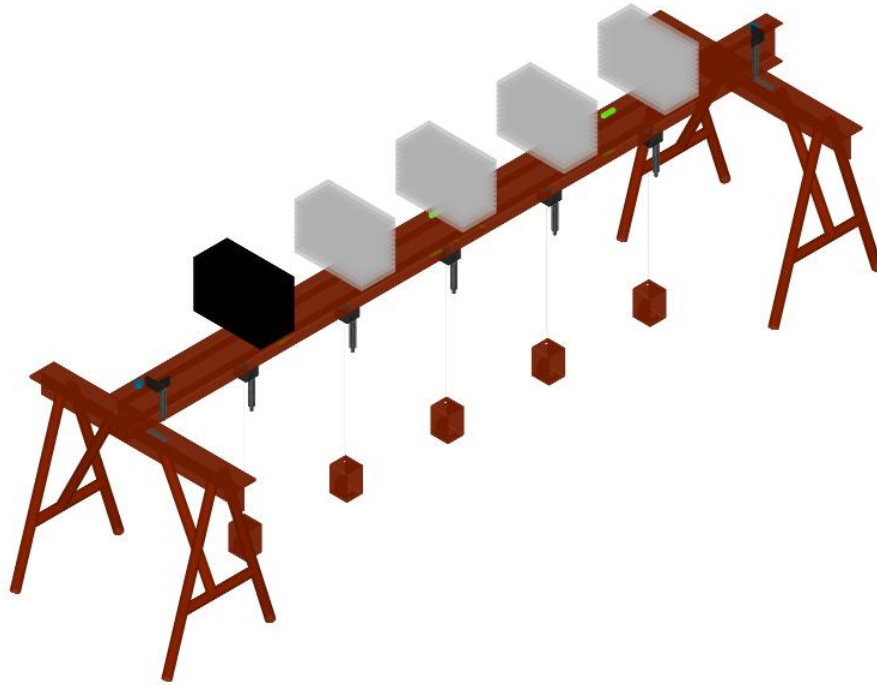


Figure 31: Load Case(s) LC2_A1...A5

3. **LC3_A1...A3** – For the final load case, a series of moving point loads, representing axle loads from a truck was implemented. The load configurations and intensities were based on the 4:4:1 axle loads for the American Association of State Highway and Transportation officials (AASHTO) design truck (Figure 32).

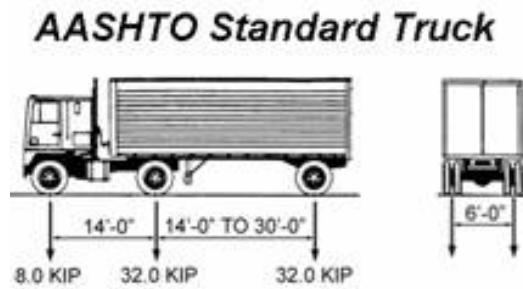
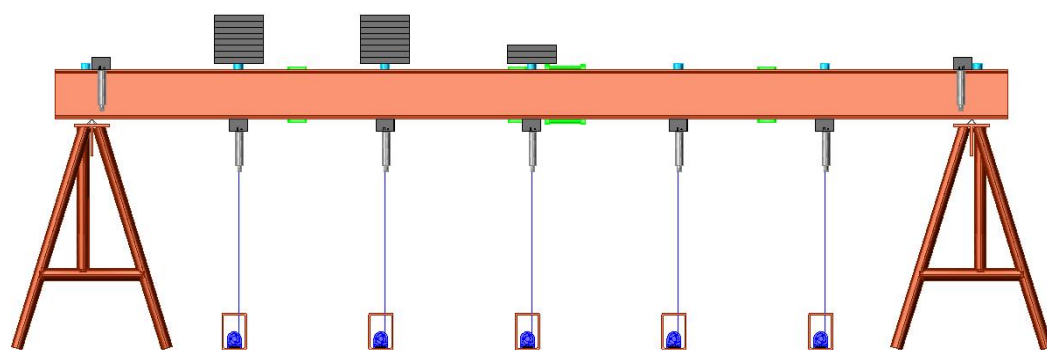
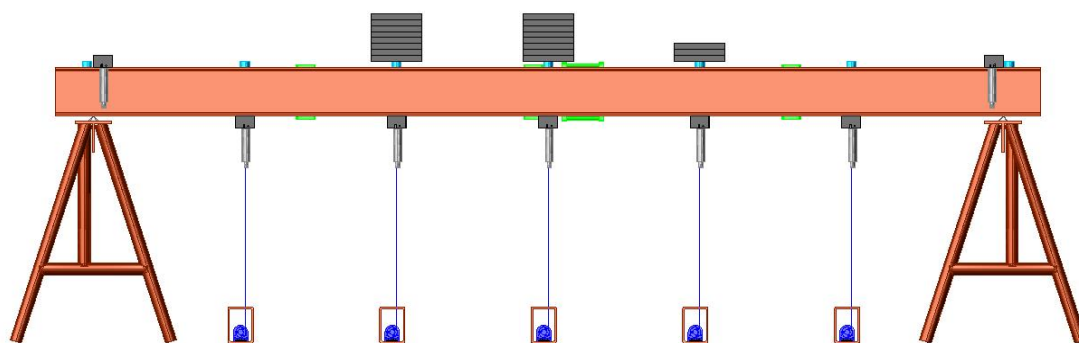


Figure 32: AASHTO Standard Truck Load (AASHTO 2004)

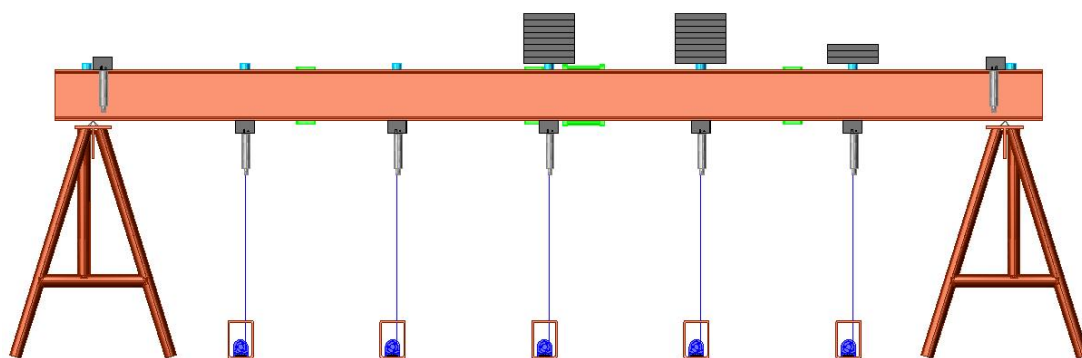
This load case is a slight variation on the previous moving point loads, in that it simulates multiple point loads moving at once (as a group) as well as having significant increased weight (Figure 33). The first two loads were approximately 0.304 kip each, representing the majority of the loads from the truck bed. The load simulating the weight from the front axle is approximately 0.076 kips, or one-quarter the weight of the two rear axles.



(a)



(b)



(c)

Figure 33: Moving Truck Load Cases (a) LC3_A1 (b) LC3_A2 (c) LC3_A3

Table 3 describes each load case and specifies the load intensity (load level) as well.

Table 3: Load Case (LC) Descriptions

Load Case	Load Level	Total # of plates	Load by Location (lbs.)				
			A1	A2	A3	A4	A5
LC1	1/3	8	-	150.2	-	151.7	-
	2/3	14	-	301.5	-	303.0	-
	3/3	22	-	415.5	-	415.9	-
LC2	1	11	416	-	-	-	-
	1	11	-	416	-	-	-
	1/3	4	-	-	152	-	-
	2/3	8	-	-	304	-	-
	3/3	11	-	-	416	-	-
	1	11	-	-	-	416	-
	1	11	-	-	-	-	416
LC3	1	18	304	304	76	-	-
	1	18	-	304	304	76	-
	1	18	-	-	304	304	76

After careful consideration, and initial load testing, the author decided that the intermediate load (1/3, 2/3 load levels) cases were to be eliminated because sufficient amounts of data would be generated with heavier loads, which also provided a better response from the sensors on the test beam. It should be shown that the load placed on the test structure must be great enough to elicit good responses from the sensors collecting the required data. For the actual loads, steel plates weighing approximately 38 lbs. each were manually stacked at the designated load locations.

Material Testing for Initial Values

As stated previously, a major contributor to the success of the optimization procedure is the ability to have good initial values to start with. Without proper understanding of the objective function, multiple initial values, ranging over a widespread area must be utilized to successfully locate the global minimum. This is to ensure that initial guesses do not become trapped in local minima. One method used to determine the initial values or “starting points” for the optimization programs, is to perform material testing on the support pads and steel angles on the Universal Testing Machine (UTM) to obtain vertical stiffness values (Figure 34).



Figure 34: Compression Tests of 5 Duro50 Pads Using UTM

Compression tests on the neoprene pads were performed in order to obtain stiffness values to use as the initial guesses (Figure 35). Compression tests also help to identify the behavior or consistency in material properties for individual pads as well as pads stacked together vertically.

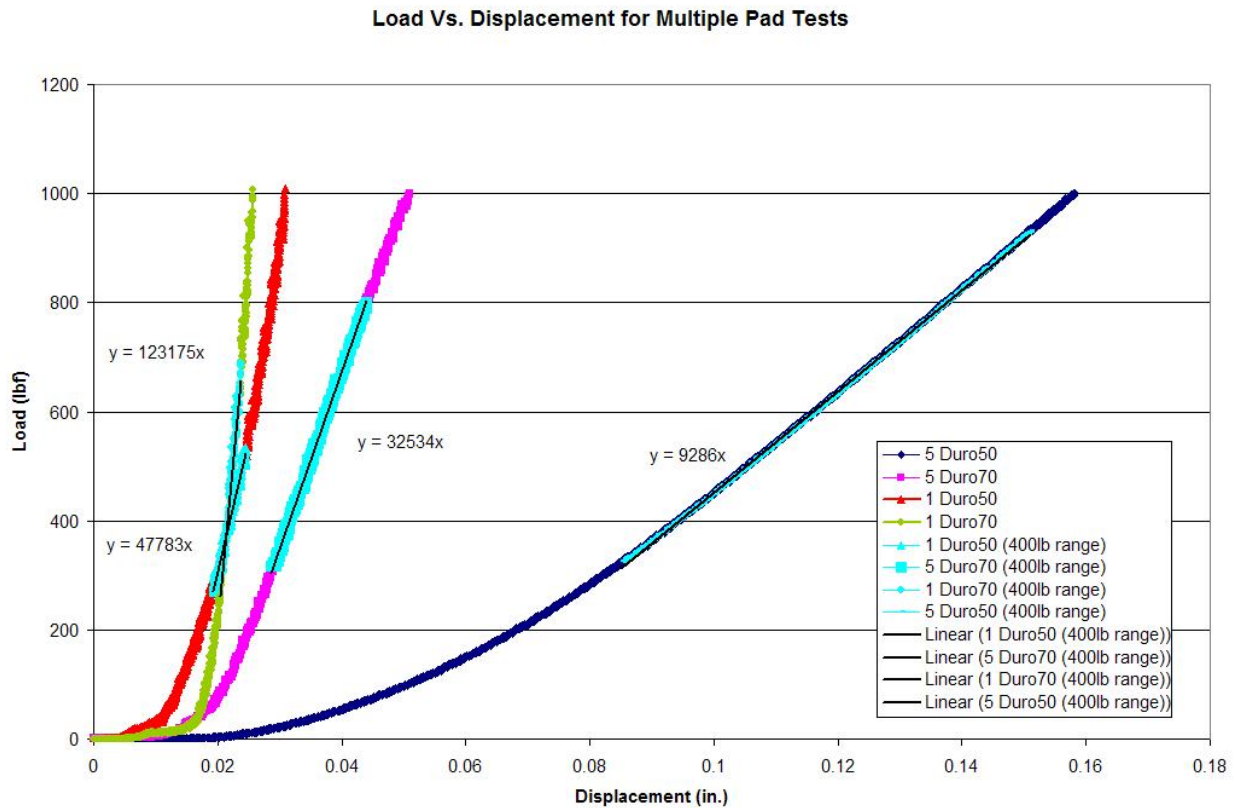


Figure 35: Vertical Stiffness Values for Different Neoprene Pads

All of the pads tested were gradually loaded with 1 kip and then unloaded. Due to the pads nonlinear behavior, load versus deflection curves were plotted for every compression test case; linear regions were identified and highlighted by a linear trend line. This is a rough approximation since the pads exhibit visco-elastic behavior and change stiffness with respect to both time and load. Using basic structural analysis, the reactions that the supports may “experience” for each load case can be estimated. The vertical stiffness values were now approximated by using the estimated reactions with the corresponding linear trend line for that region (Figure 36).

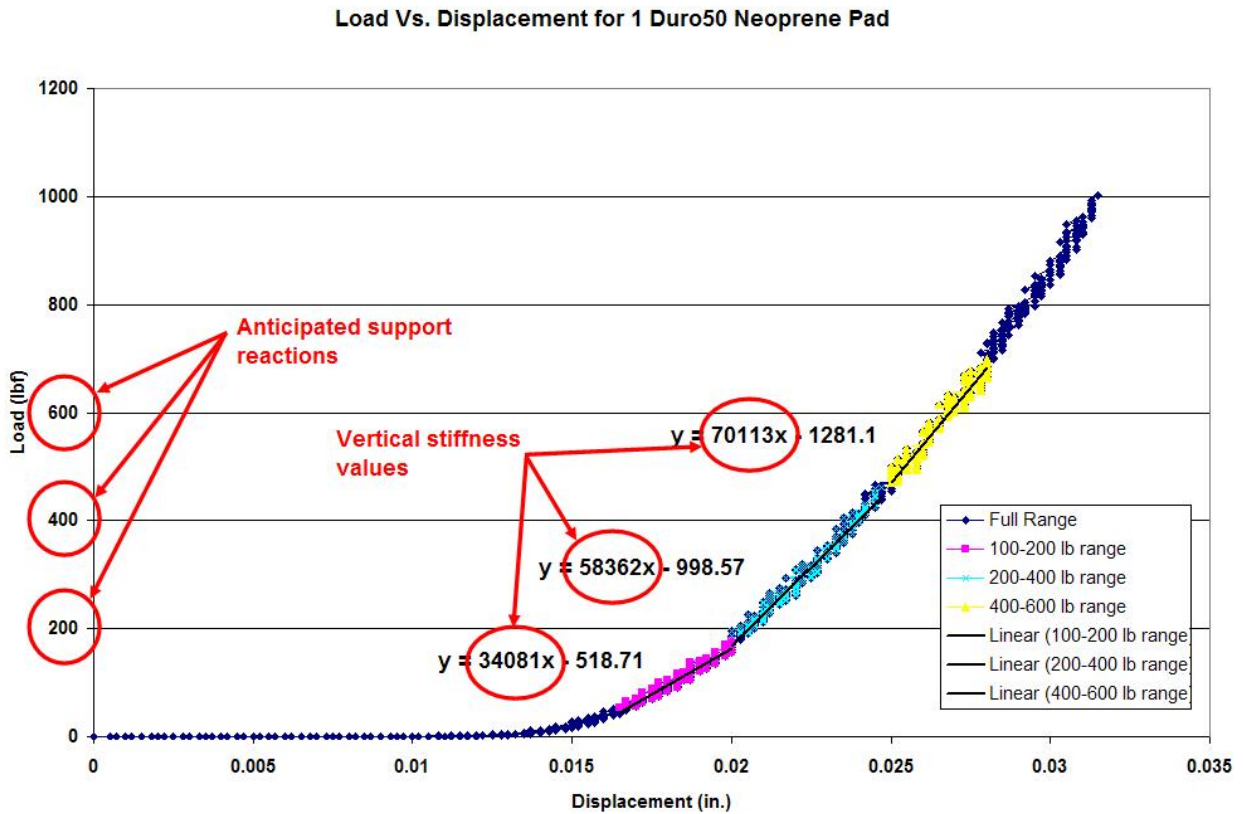


Figure 36: Vertical Stiffness Derivation from Material Tests

With the vertical stiffness values based from the material tests now assumed to be known with a high degree of certainty, we can also check them using the stiffness relationship shown in equation (11). This equation was used to check the nominal value for the pad stiffness and compare with the slope values from material tests. Using the same material test plots, the data is converted to a stress versus strain plot so that the Modulus of Elasticity, E , can be estimated. Estimating E values for non-linear materials is often very hard to accomplish so linear-elastic regions were assumed for the plots. Using the same process as for the vertical stiffness values, E is deduced from the linear regions corresponding to the desired load. The Modulus of Elasticity

is now substituted into the following equation, along with the area, A and the thickness (“length”) of the pad,

$$k_{vert} = \frac{AE}{L} \quad (11)$$

Material property tables for neoprene can be found on a few websites, and this is useful for comparing our E values with the published values. From Figure 37, we can see that the table shows the range of Elastic Modulus for Durometer 30A-95A neoprene. The pads used in this experiment were of Hardness Scale A, so we can use these values to check the ranges of E that we solved for from the material tests. Assuming that the Durometer 30A represents the most flexible neoprene pad that we could have, then E will correspond to a value of 100 psi. Solving equation (11) for a six inch diameter neoprene pad, 0.5” thick, yields the following

$$k_{v30A} = \frac{AE}{L} = \frac{(28.3in^2)(.1ksi)}{0.5in}$$

$$k_{v30A} = 5.66kip / in.$$

If Durometer 95A represents the most rigid pad possible, then E corresponds to 3000 psi. In a similar fashion, we solve for the stiffness of the pad as

$$k_{v95A} = \frac{AE}{L} = \frac{(28.3in^2)(3ksi)}{0.5in}$$

$$k_{v95A} = 169.80kip / in.$$

So now we have our corresponding maximum and minimum nominal stiffness values limits for the neoprene pads we have tested.

COMPARATIVE PHYSICAL PROPERTIES OF RUBBER

TYPE	NATURAL RUBBER	STYRENE BUTADIENE	BUTYL	NITRILE	NEOPRENE
ASTM Designation	NR	SBR	IIR	NBR	CR
PHYSICAL PROPERTIES					
Specific Gravity	0.92-0.93	0.94	0.92	0.98	1.23-1.25
Thermal Conductivity	0.082	0.143	0.053	0.143	0.11
Btu/ft ² /hr/sq ft/F	37	37	32	39	34
Coef of Ther Exp(cubical), 10 ⁻⁵ per F Gum					
MECHANICAL PROPERTIES					
Hardness, Durometer	30A-90A	30A-90A	30A-95A	30A-95A	30A-95A
Tensile Strength 1000 psi	3.5-4.5	2.5-3.0	2.0	1.0-3.5	0.5-3.5
Modulus (100%), psi	150-3000	300-1500	50-500	100-1500	100-3000
Elongation, %	500-700	450-500	300-800	400-600	100-800
Compression Set, Method B, %	10-30	5-30	25	5-20	20-60
Resilience (ASTM 945) %	80	20-90	30	-	50-80
Rebound (Bashore)	-	10-60	-	-	50-80
Hysteresis Resistance	Excellent	Fair-Good	-	-	Very Good
Flex Cracking Resistance	Excellent	Good	-	Fair-Good	Very Good
Tear Resistance	Excellent	Fair	Good	Good	Good
Abrasion Resistance	Excellent	Excellent	Good	Excellent	Excellent
Impact Resistance	Excellent	Excellent	Good	Good	Excellent

← Elastic modulus range

Figure 37: Mechanical Properties for Neoprene (Courtesy of Moldeddimensions.com)

A sample Table, Table 4 shows the difference in stiffness and elastic modulus for the different pads of the same material (varying stiffness). Once the data for all the pads is finalized, averaged stiffness values are compared with the nominal values and will be used for initial guesses of the unknown stiffness parameters during parameter estimation analysis (Table 5).

Table 4: Sample Material Test Results for Duro50 Pads

Pad Setup	Pad # (s)	100 lb (k/in)			200 lb (k/in)			400 lb (k/in)			600 lb (k/in)		
		Exp.	Nominal	E (psi)	Exp.	Nominal	E (psi)	Exp.	Nominal	E (psi)	Exp.	Nominal	E (psi)
1 Duro50	1	34.1	35.2	621.6	58.4	61.1	1081.1	58.4	61.1	1081.1	70.1	72.3	1279.1
	2	46.9	50.0	884.2	65.4	65.3	1155.3	65.4	65.3	1155.3	76.1	75.7	1338.9
	3	42.9	44.0	778.1	53.2	55.9	989.2	60.3	69.1	1221.8	64.1	66.7	1178.9
	4	35.1	37.6	664.9	40.5	42.4	749.0	51.8	53.6	947.9	60.9	68.0	1202.5
	5	31.5	35.2	622.8	43.2	43.5	769.8	68.8	72.2	1276.1	75.0	81.8	1445.9
	6	26.2	26.8	473.9	42.2	43.7	772.9	59.6	61.3	1083.1	65.8	67.8	1199.4
	7	33.5	35.5	627.8	44.9	47.8	845.8	62.1	66.0	1167.1	72.0	73.3	1296.8
	8	33.0	39.2	692.6	49.2	52.7	932.4	63.8	80.0	1414.7	71.4	72.4	1280.3
	10	30.2	33.0	582.9	49.7	50.3	888.7	59.2	63.0	1114.9	70.8	70.4	1244.9
	Average	34.8	37.4	661.0	49.6	51.4	909.4	61.0	65.7	1162.5	69.6	72.0	1274.1

Table 5: Averaged Stiffness Values for Different Load Levels

Pad Type	100 lb range (k/in.)		200 lb range (k/in.)		400 lb range (k/in.)		600 lb range (k/in.)	
Test	Mat. Test	Nominal	Mat. Test	Nominal	Mat. Test	Nominal	Mat. Test	Nominal
1 Duro50	34.8	37.4	49.6	51.4	61.0	65.7	69.6	72.0
1 Duro 70	52.5	59.1	79.4	88.3	94.2	109.5	113.6	128.7
5 Duro50	4.6	4.6	6.5	6.5	8.8	8.7	9.2	9.2
5 Duro 70	19.3	19.9	27.9	26.9	32.7	32.0	32.7	32.0

The same procedure is repeated for all of the required boundary condition setups, including: 1 Duro70, 5 Duro50, 5 Duro70, and the steel pin supports.

Table 5 also shows the behavior of stacking neoprene pads, if we solved the following equation (12) using individual pad stiffness results

$$\left(\frac{1}{k_T} \right) = \sum_{n=1}^N \frac{1}{k_n} \quad (12)$$

we will see that the total stiffness, k_T for the stack of individual pads, is the same as a stack of pad being tested at once on the UTM. We can also conclude that the 5 Duro50 scenario will yield the highest deflections for the experimental load tests due to having the lowest stiffness value. An interesting side note is that the material test for the steel angle shows a non-linear curve for the force versus displacement data (Figure 38).

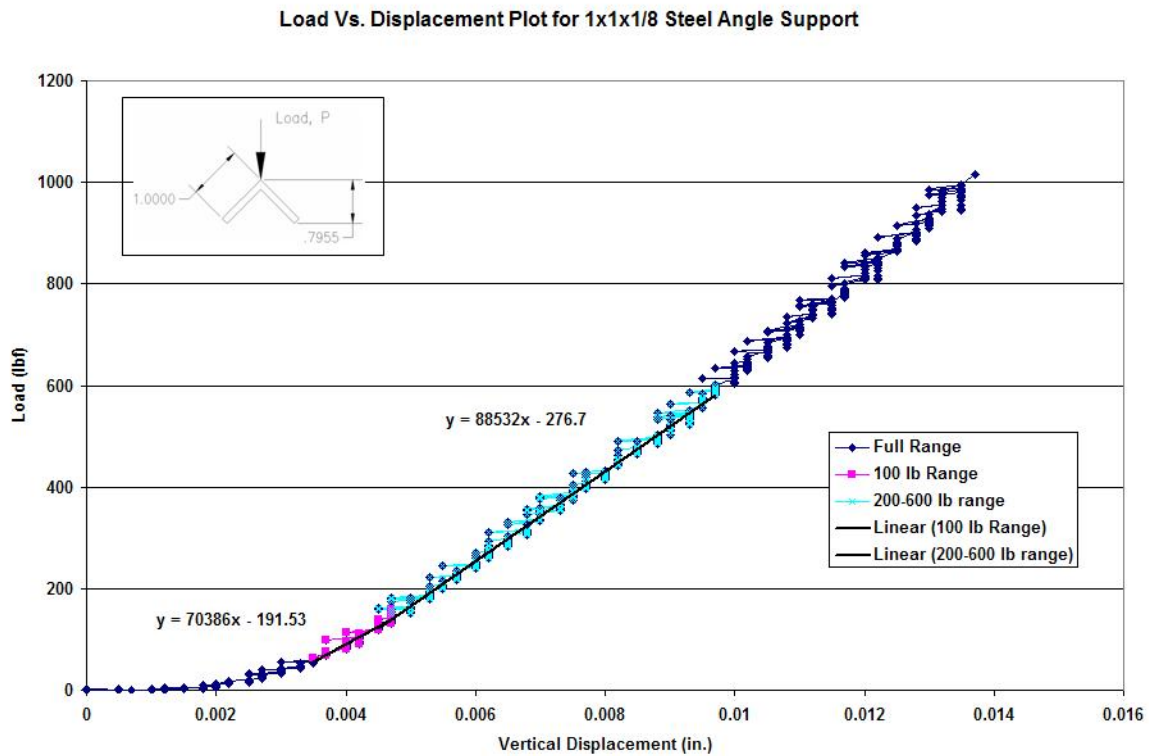


Figure 38: Sample Material Test Plot for Steel Angle Support

The most likely explanation for these results is that as the angle is being loaded, the legs were actually “kicking” outwards and causing the support to deflect small amounts. This behavior only appears to happen within the first couple hundred pounds of loading, before remaining constant for the rest of the load test.

Boundary Condition (BC) Selection

In order to measure the structural response of the test beam under various boundary conditions, the following support conditions were initially looked at:

Table 6: Initial Boundary Condition Cases

BC Name	Left Support	Right Support
BC1	pin	pin
BC2	4 Duro50 pads	4 shim plates + pin
BC3a	1 Duro50	1 Duro50
BC3b	5 Duro50	5 Duro50
BC4a	1 Duro70	1 Duro70
BC4b	5 Duro70	5 Duro70
BC5a	1 Duro50	1 Duro70
BC5b	5 Duro50	5 Duro70

Initially, all of the BC cases (8 total) were utilized in the experimental tests, and the results were analyzed. It was assumed that these cases represented a wide spectrum of support conditions, and after preliminary analysis of the data, four cases stood out more than the others. For the experimental test cases, four out of the eight total BC setups would be used. The four BC's represent a good range of varying support conditions and are listed as follows:

1. **BC1** – Serves as the “baseline” case for the experimental tests. Steel 1x1x1/8 angles were used for the supports, representing a hypothetical pin connection. It is assumed that this setup is behaving closely to that of a truly pinned support (no moment capacity).



Figure 39: Pin Supports (BC1)

2. **BC3a** – This case represents boundary conditions with increased flexibility. For a real-life scenario this would represent a structure whose supports have suffered from minor settlement or damage.



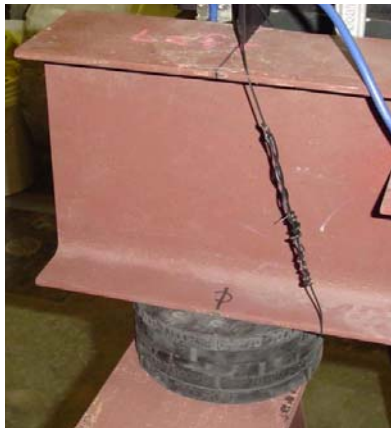
Figure 40: 1 Duro50 Pad Support (BC3a)

3. **BC3b** – The third BC setup represents a structure whose supports have undergone significant amounts of settlement (possibly due to severe damage). Out of the four BC used in the experiments, this case has the most flexibility at the supports.

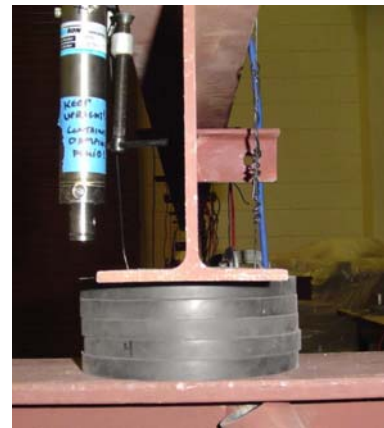


Figure 41: 5 Duro50 Pad Support (BC3b)

4. **BC5b** – By using two different pad types at the supports, this case represents a structure which may have varying degrees of flexibility at both supports. At one support, the 5 Duro50 pads were extremely flexible, while the 5 Duro70 pads offer more flexibility than the pin case (BC1), but were not as severe as the 5 Duro50 pads.



(a)



(b)

Figure 42: (a) 5 Duro70 Pad Support, L-Side (b) 5 Duro50 Pad Support, R-Side

Experimental Setup

The structure used for the experimental tests was a simply supported steel W8x13 I-beam. The overall length of the beam was 156 in, while the clear span was 144 inches (Figure 43). For ease of access to sensors and datalogging equipment, the beam rested on two steel sawhorses each measuring 3 feet in height. The boundary conditions were modified by changing the material that sits on the support, whether it was a neoprene pad (different types and numbers of pads) or a steel angle. Because the length-to-depth ratio is greater than 10, only bending

deformations were considered (Kassimali, 1999). The section properties were verified by using a precise instrument such as a digital caliper, to verify published values for the flange/web widths and thicknesses. It was discovered that the actual dimensions of the beam varied slightly than their published values as defined in the American Institute of Steel Construction Manual (AISC, 2003) Load and Resistance Factored Design (LRFD), 3rd edition. The following table compares the actual versus published AISC dimensions for the W8x13 beam (Table 7).

Table 7: W8x13 Beam Dimension Comparison

W8x13	Area	Web	Flange		Axis X-X
		Thickness, t_w	Width, b_f	Thickness, t_f	I
	in. ²	in.	in.	in.	in. ⁴
Actual	3.96	0.255	4.06	0.255	39.3
AISC	3.84	0.230	4.00	0.255	39.6

For this study, the author assumed that the modulus of elasticity (E), cross-sectional area (A) and moment of inertia (I) were their true values (AISC). Even though there were small differences between the actual and published dimensions of the I-beam, the boundary conditions were still considered the primary source of error between the FEM data and experimental data. The beam properties (E, I, A) were not considered unknown, such that they needed to be updated using the experimental data. This approach can also be considered analogous to a real life case where minor variations may exist between the published material and geometry values and the actual values where boundary conditions may impact the structural behavior considerably more than these variations.



Figure 43: Experimental Test Beam Setup

Only vertical loads were carried out during experiments and were manually applied by stacking 38 lb steel plates at the designated load points. The experimental force locations were also dictated by where they could be applied freely, without interfering with the existing sensors. A very important aspect of this study is that, the beam was instrumented very densely. Displacement measurements were made by using seven cable transducers with a resolution of ± 0.0004 in and a total working range of 1 in. Changes in rotation were measured using seven vibrating wire tiltmeters with resolutions of ± 10 arc-seconds and a range of ± 15 degrees. Seven piezoelectric seismic accelerometers were used to record time-history data. The acceleration data was used to validate the experimental natural frequencies and mode shapes against those of the updated finite element model, for each boundary condition case.

CHAPTER FIVE: TEST RESULTS AND DISCUSSION

Optimization Load Selection

After completing many load case simulations, it was evident that PARIS had difficulty using just one load case to update the unknown stiffness parameters (Figure 44). Results from SPE were obtained and will be commented on later in the section. Due to the measurement and modeling error some of the load cases proposed failed to update to the correct assumed parameters.

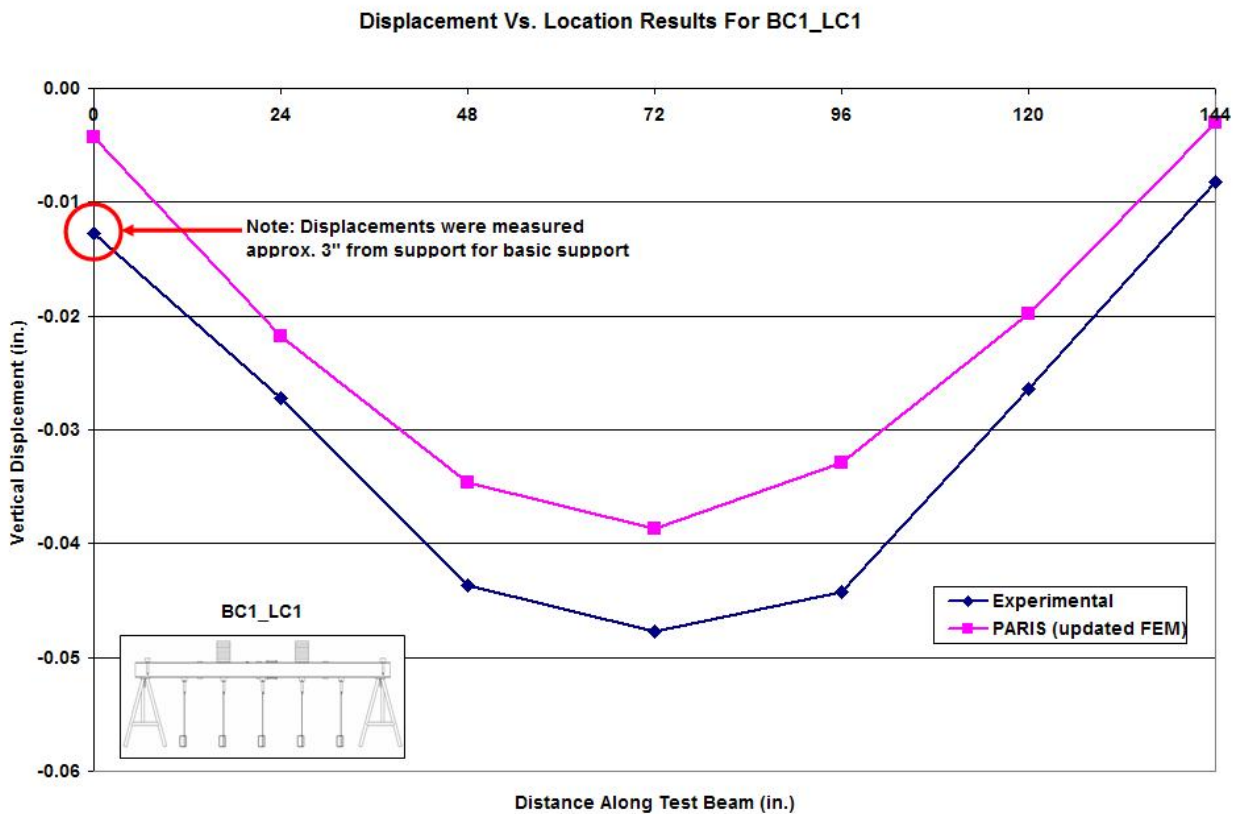


Figure 44: Experimental Vs. FEM (PARIS Updated) Displacement Values

Although the objective function plot showed the algorithm converging to a minimum, physically, the updated stiffness parameter values did not make sense. When assigned to the springs in the FEM and a different load analysis was conducted, the resulting displacements indicated that the support conditions were much stiffer than the experimental setup. There was an average percent difference between the two data sets of around 20-25%; still too high to be considered successful for parameter estimation. As a result, combining multiple load sets into new load combinations for parameter estimation was considered.

In order to obtain a better representation of the overall behavior of the beam, multiple load cases were used for the final optimization process. By combining different load sets, there are more measurements to work with, which is akin to providing more data regarding the beam.

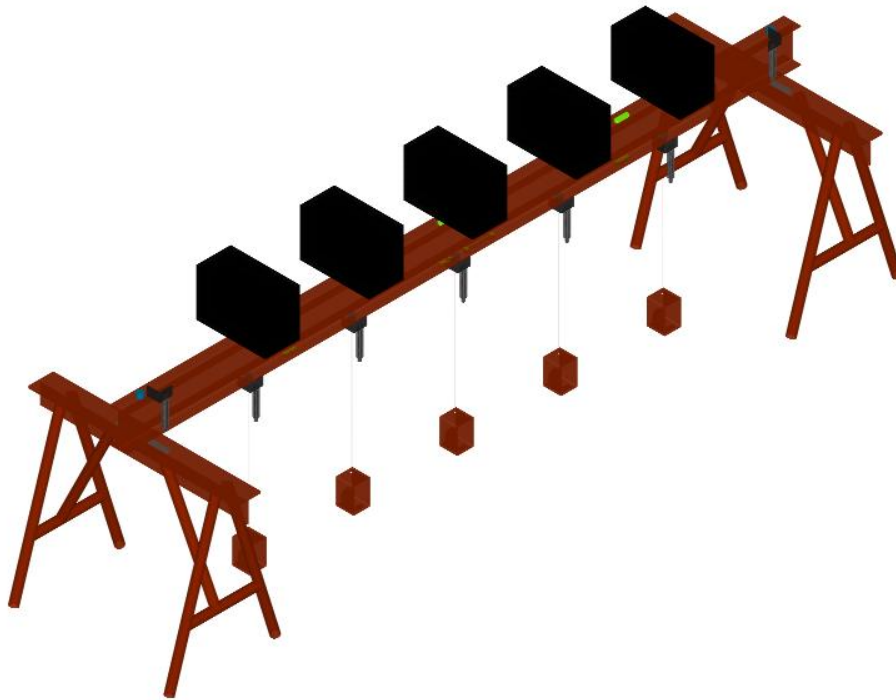


Figure 45: Load Combination LC2_A1A2A3AA5

The load case shown in Figure 45 represents the maximum number of applied loads to the test beam that we can have. The data incorporates measurement responses from all of the single point load cases we measured. Enough information should be provided to have good parameter estimation results for the unknown stiffness parameters. The next load combination that was used is shown in Figure 46 as three point loads on the left hand side of the beam. This load case is a combination of single point loads placed at A1, A2 and A3 load locations. The configuration shown here allowed us to see if the unknown parameters could be updated if only results from loads on half of the structure were measured.

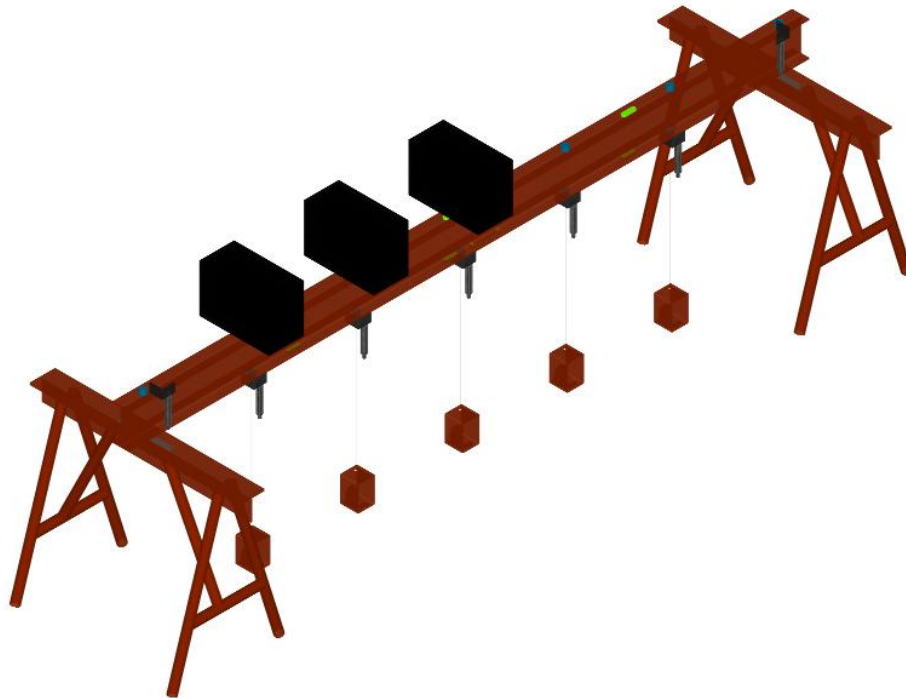


Figure 46: Load Combination LC2_A1A2A3

The load case illustrated by Figure 47 is the opposite of load combination LC2_A1A2A3 in that only the results from point loads on the right side of the beam (at A3, A4 and A5) were known.

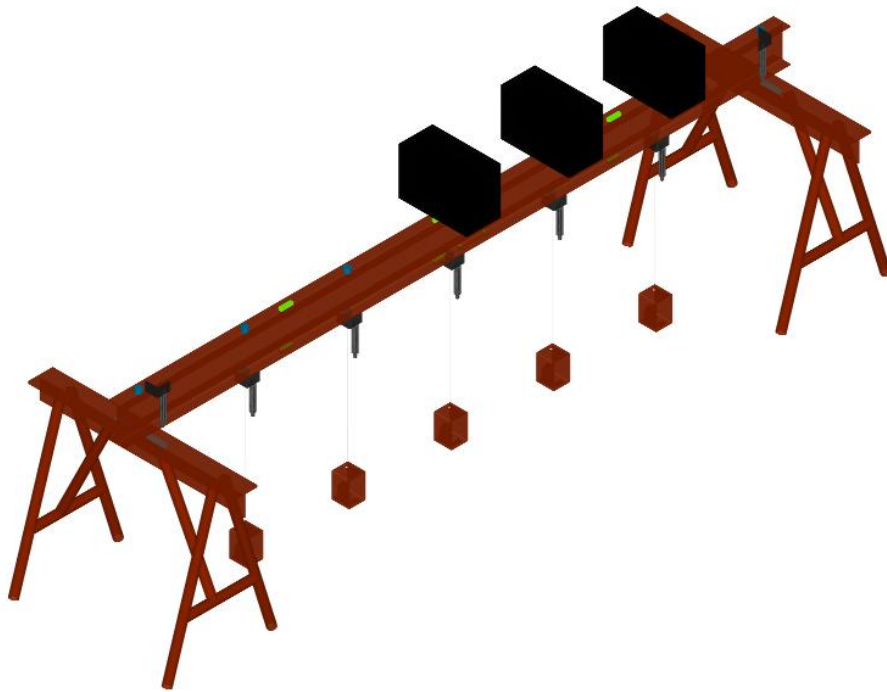


Figure 47: Load Combination LC2_A3A4A5

The final load case combination selected for parameter estimation was a combination of single point load cases at A1, A3, and A5 (Figure 48). The author wanted to see if using load case data from the 1/3 points of the beam was sufficient enough to characterize the entire beam and supports. This combination also use two fewer point load data sets than found in the LC2_A1A2A3A4A5. Using few data sets means fewer load cases were needed, possibly saving testing money for projects in the real-world.

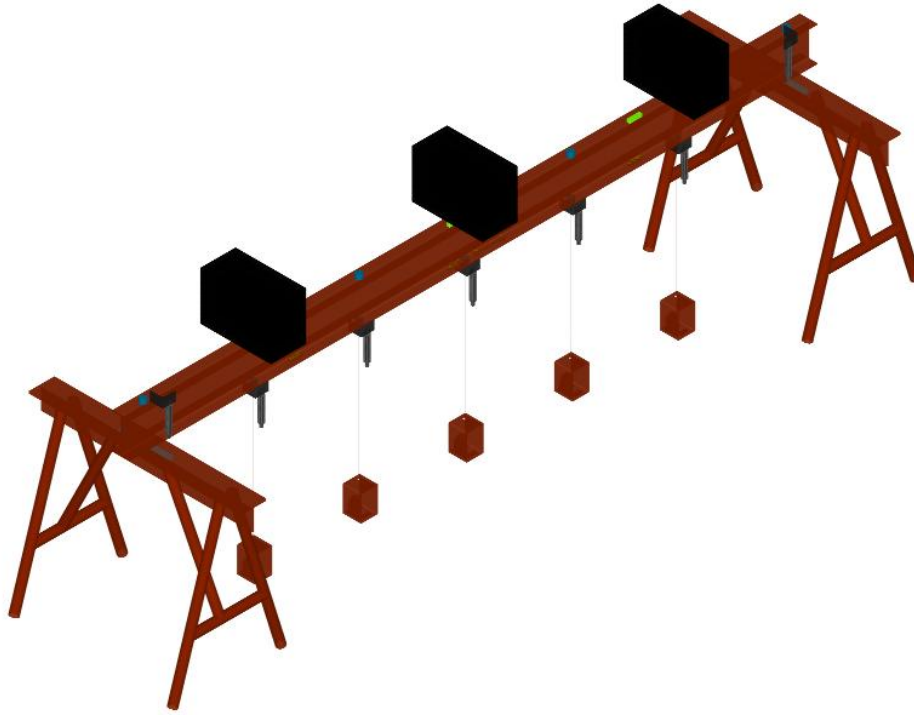


Figure 48: Load Combination LC2_A1A3A5

Measured DOF Selection

After deciding which load cases and combinations we will use for the parameter estimation studies, the author would like to analyze the impact of using different combinations and numbers of measurements. By analyzing the parameter estimation results for these different cases, we can conclude which combinations of sensors will yield the best results. Measurement error also plays a role in the sensor selection process, since there is the possibility that some DOF will overshadow others or are more prone to measurement error. In real-life scenarios, there is a direct relationship between cost and the number of sensors used. Finding the minimum number of sensors required will usually be the most cost-effective solution to the problem. The following sensor combinations will be run for each load combination mentioned in the previous section.

The first scenario we will analyze is one where all available measurements were used for updating the unknown parameters (Figure 49).

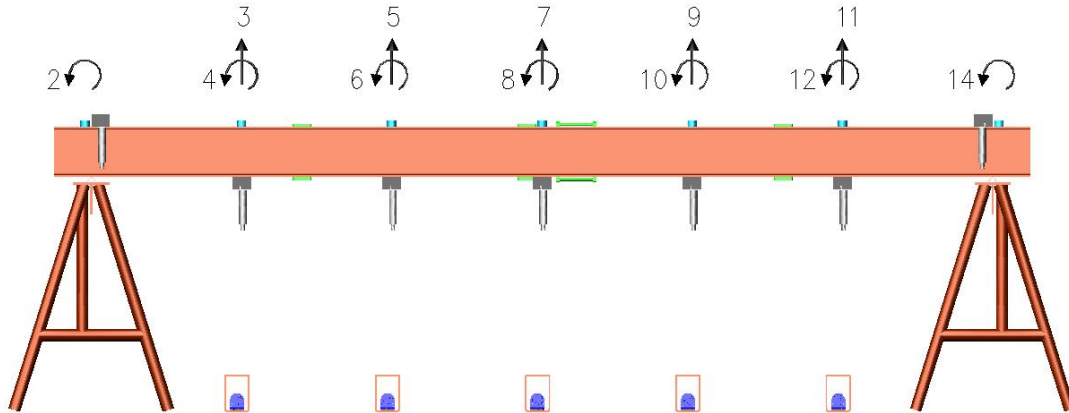


Figure 49: 12 Measured DOF Setup

Of the 14 total global DOF, only two were not equipped with sensors to record measurements. Deflections at the supports (DOF 1 and 13) were unable to be measured due to the setup of the test beam and interference with the supports. This case represents a heavily instrumented structure, but due to support constraints, displacements cannot be made at the supports (i.e. bridges). Once the results for the full 12 MDOF cases were collected, a measurement case utilizing 7 total sensors will be analyzed (Figure 50).

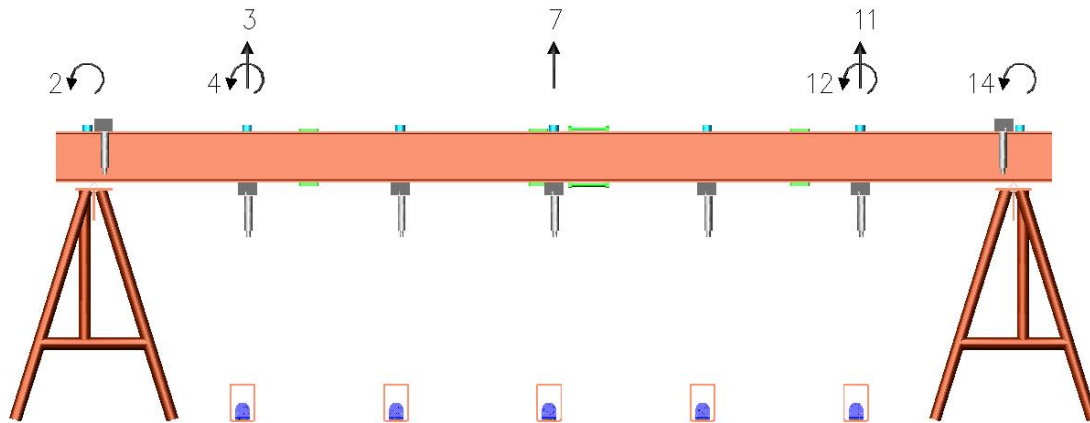


Figure 50: 7 Measured DOF Setup

The reason for selecting 7 measured DOF is that it first lowers the total number of sensors required and secondly represents a good mix of measurements, symmetric about the centerline of the test beam. It is also here where we will start to look at the affect of reducing the number of measurements and the impact it has of the “clarity” of the objective function plot, $J(k)$. For our final sensor combination, we will analyze the results of using only 4 measurements on the test beam (Figure 51). This case represents the minimum number of sensors that will be used to accurately characterize the beam. The rotations at the supports (DOF 2 and 14) as well as displacements at DOF 3 and 11 were used to update the unknown stiffness parameters. Again, all of the sensor and load combinations will be run for each case giving us the number of total cases, $(NTC) = 4 \text{ boundary conditions} \times 4 \text{ load combinations} \times 3 \text{ sensor combinations}$, for a grand total of 48 parameter estimation analysis. This process will also be replicated using SPE in order to compare the accuracy of the two programs, giving us a total of 96 analysis cases.

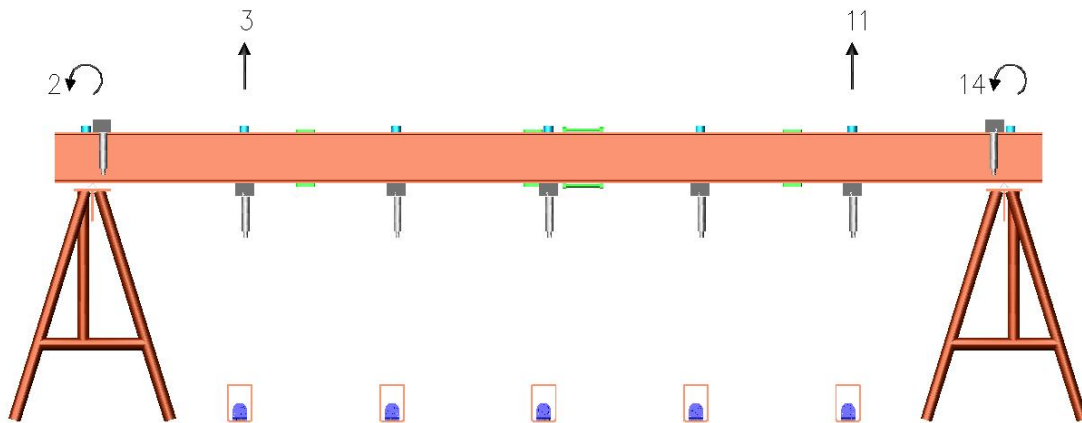


Figure 51: 4 Measured DOF Setup

SPE Statistical Analysis

The author first used single force load sets to test whether or not SPE worksheet would be able to update the unknown stiffness parameters. As mentioned previously, PARIS had trouble using single force load sets to update the parameters, so load combinations were used. SPE was able to use single force load sets because the spreadsheet is setup strictly for this specific problem and the error functions were easily defined. All of the original load cases, including LC1_Full, LC2_A1, etc. as mentioned before were used to update for the unknown spring stiffness parameters using SPE. All 12 measurements were used for each individual load case parameter estimation study. Once all of the spring values were identified, the mean and standard deviation were calculated along with plus/minus two standard deviations, which will form the probability bounds for an example load case. The statistical bounds provide a range in which the plotted displacements from the updated FEM should fall between. Updated stiffness parameters from LC1 will be input into the SAP2000 FEM and then LC3_A2 will be applied to the model.

The displacements from the updated FEM will then be plotted on the same chart as the confidence intervals (Figure 52).

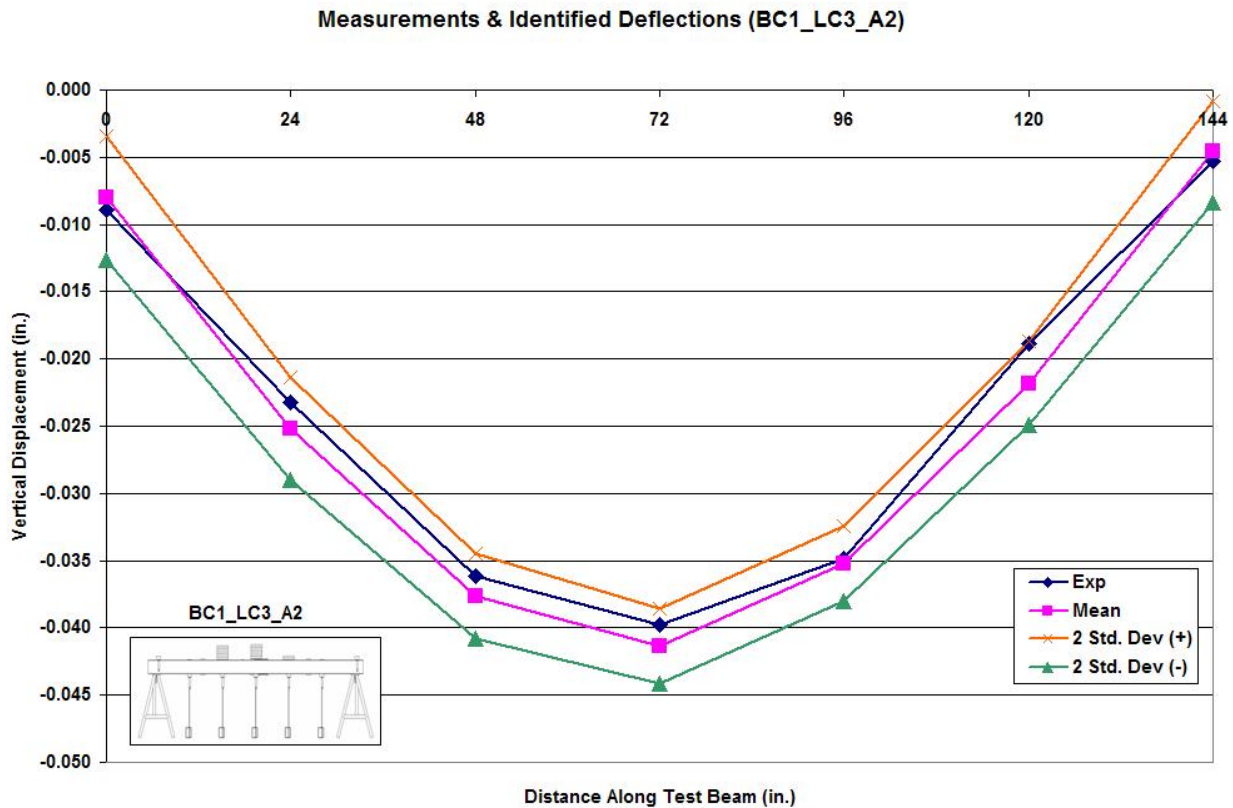


Figure 52: Measurements & Identified Deflections with Statistical Bounds (BC1_LC3_A2)

From the figure we can see that when updated spring values from LC1 were used to update the FEM with a different load case (LC3_A2), the displacement profile falls well within the ± 2 standard deviation bounds.

The same process is then repeated for two other cases, namely BC3a and BC3b. SPE was unable to update the parameters for BC5b (the most flexible) using the load cases specified. We

will revisit this particular BC later on and use multiple load combinations along with PARIS to try and update the spring parameters. Figure 53 shows the confidence intervals for BC3a (1 Duro50 at each support).

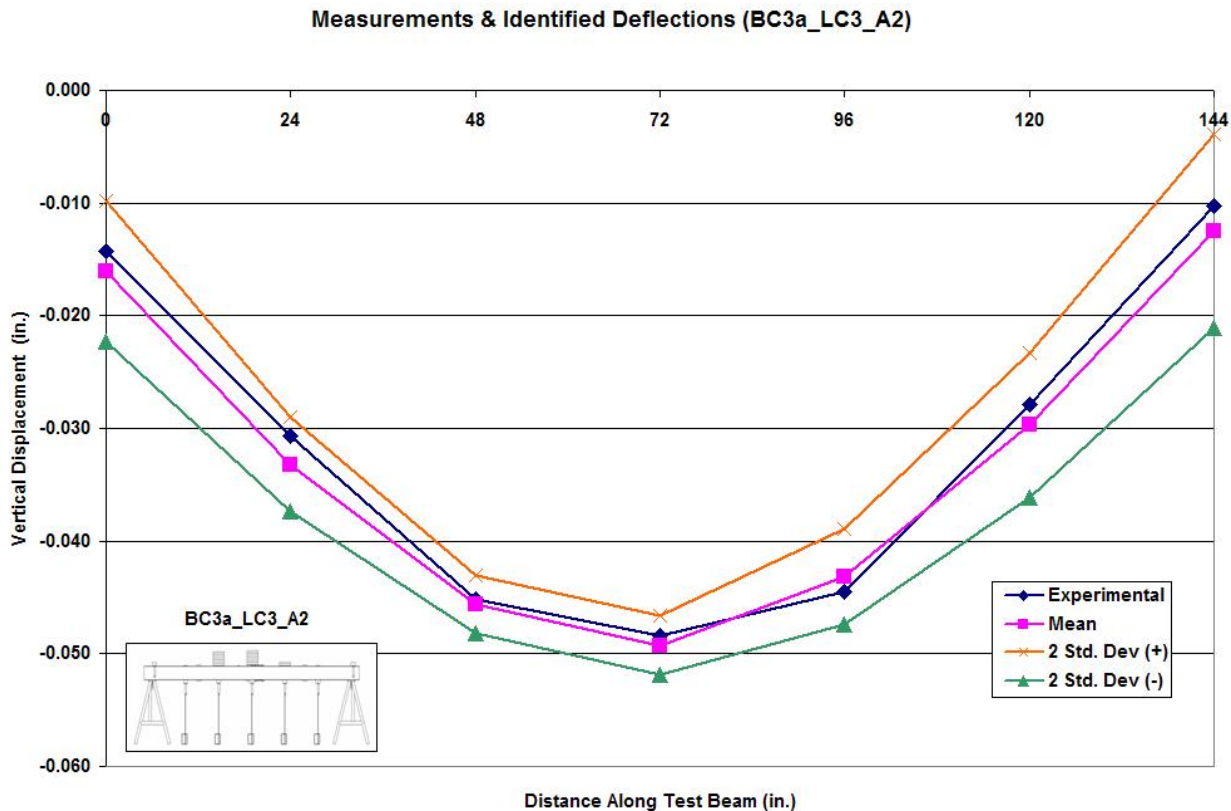


Figure 53: Measurements & Identified Deflections with Statistical Bounds (BC3a_LC3_A2)

Again, after selecting a different load case to obtain the updated FEM displacements, the results fit well within the bounds. The same can also be said for the BC3b results and statistical bounds shown in Figure 54 below. There is a slight bit of discrepancy between a few of the data

points but that is to be expected since this BC is the most flexible of them all and we were modeling the supports as linear-elastic, rather than the non-linear material that they were.

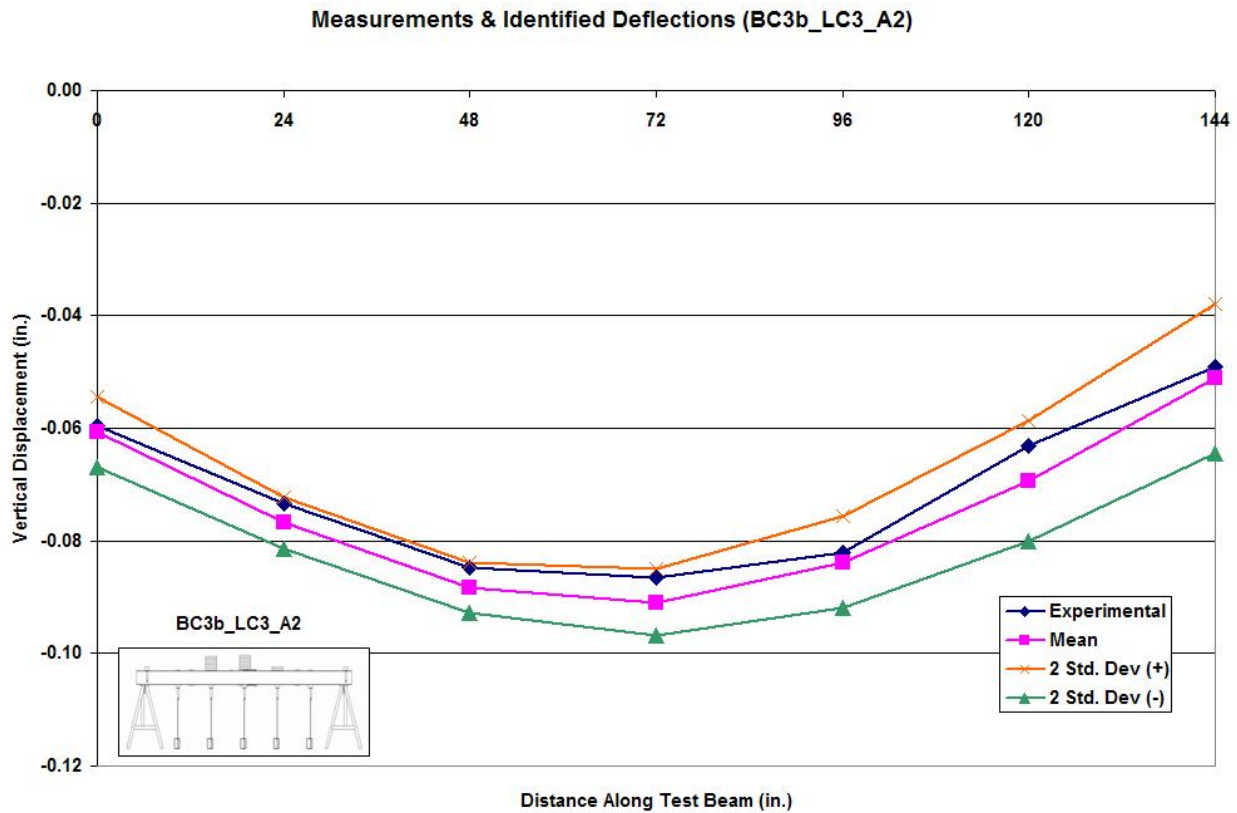


Figure 54: Measurements & Identified Deflections with Statistical Bounds (BC3a_LC3_A2)

For each BC that is analyzed, updated stiffness values were entered into tables that can provide comparisons between the left (K_1) and right (K_2) supports. Table 8 lists the updated values for BC1, and using MATLAB, we can plot a histogram of each support (K_1 and K_2) and use the distribution fitting tool to fit the best curve to the data and determine the mean value for each case.

Table 8: SPE Updated Spring Stiffness Values for BC1 Using Single Force Load Sets

BC #	LC #	K ₁ (k/in.) SPE	K ₂ (k/in.) SPE
BC1	LC1	42.97	46.03
	LC2_A1	88.99	43.34
	LC2_A2	54.83	45.65
	LC2_A3	45.00	81.48
	LC2_A4	39.79	92.11
	LC2_A5	32.48	63.42
	LC3_A1	68.18	124.56
	LC3_A2	58.15	108.51
	LC3_A3	45.70	104.92

Table 9: SPE Updated Spring Stiffness Values for BC3a Using Single Force Load Sets

BC #	LC #	K ₁ (k/in.) SPE	K ₂ (k/in.) SPE
BC3a	LC1	31.20	27.50
	LC2_A1	32.91	14.82
	LC2_A2	22.30	26.16
	LC2_A3	24.61	23.00
	LC2_A4	22.37	36.44
	LC2_A5	20.61	35.70
	LC3_A1	28.18	18.66
	LC3_A2	26.86	24.37
	LC3_A3	18.28	40.78

Table 10: SPE Updated Spring Stiffness Values for BC3b Using Single Force Load Sets

BC #	LC #	K ₁ (k/in.) SPE	K ₂ (k/in.) SPE
BC3b	LC1	6.22	6.32
	LC2_A1	6.74	5.00
	LC2_A2	6.83	5.30
	LC2_A3	6.33	6.08
	LC2_A4	5.99	6.60
	LC2_A5	6.03	6.70
	LC3_A1	6.75	6.43
	LC3_A2	6.59	6.55
	LC3_A3	6.75	7.01

From the data we can see that for the most part (with the exception of BC1 to a certain degree), that the stiffness value generally update to around the same value. The axis of the histograms reference the stiffness values (“Data” on x-axis) and the frequency at which they appear (“Density” on y-axis). Histograms of the stiffness data are shown in the following figures:

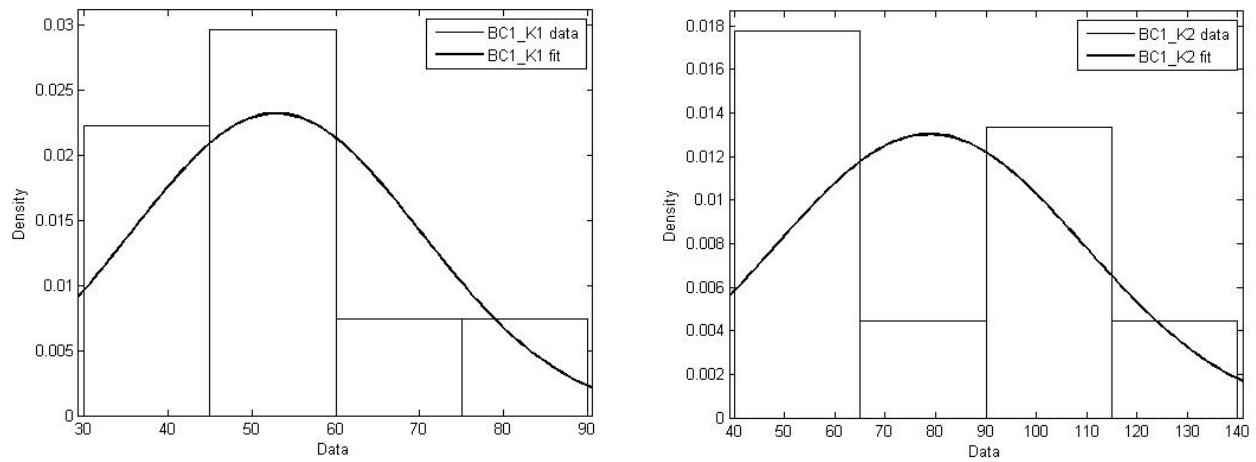


Figure 55: Histograms for BC1 Supports K_1 and K_2

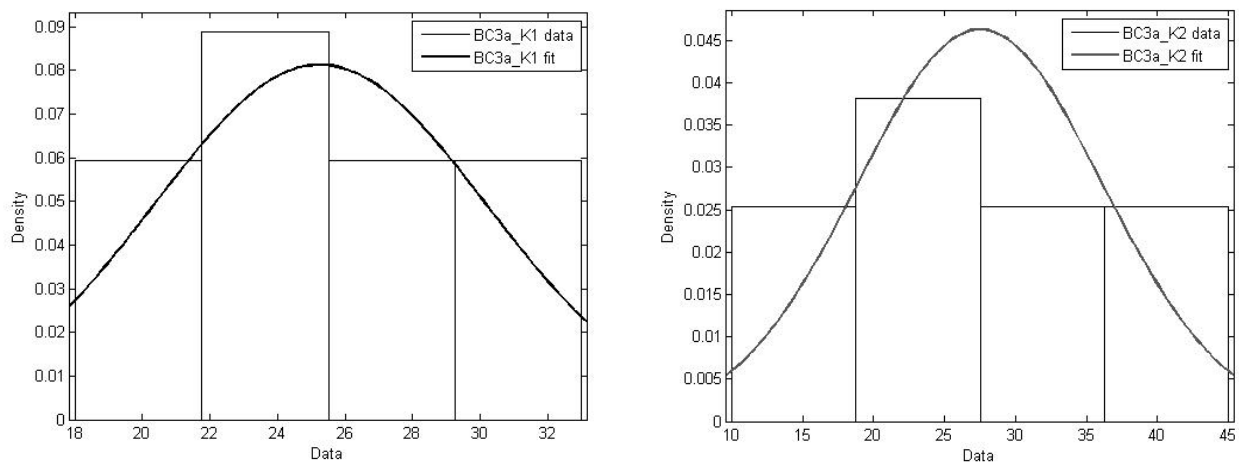


Figure 56: Histograms for BC3a Supports K_1 and K_2

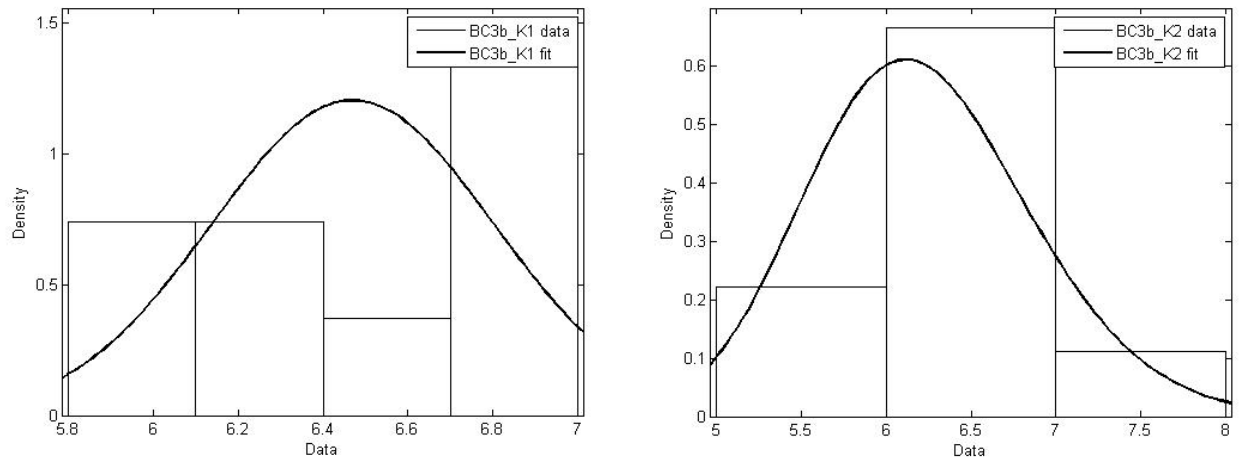


Figure 57: Histograms for BC3a Supports K_1 and K_2

The histograms serve as a visually aid to let use see the frequency and distribution of the updated stiffness terms. The histograms for both BC3a and BC3b show good correlation for both supports, and in fact, we can check the updated values against those that were predicted from the material tests (Table 11).

Table 11: Comparison of Mean Stiffness Values vs. Material Test Data

BC #	K_1 (k/in.) Mean	K_2 (k/in.) Mean	Mat. Test (k/in.)
BC1	52.89	78.89	81.30
BC3a	25.26	27.49	34.80
BC3b	6.47	6.22	6.50

Values from Table 11 represent the stiffness values of the supports based on the experimental data from all of the single load force sets. The mean stiffness values listed in Table 11 were close to the stiffness values from the material tests (corresponding to the 100-200 lb.

load level). There appears to be some discrepancy between K_1 of BC1 and the actual test data, which is probably due to the limitations of SPE during optimization and the non-linear behavior of the pads at different load levels.

BC1 Parameter Estimation Results

A total of four load combinations and three different sensors combinations were used to update the stiffness parameters for the baseline case BC1. We considered this case the baseline condition because it represented the BC with the stiffest support conditions, or a real-life scenario of a beam with no damage at the supports. A total of 12 analysis cases were performed and the results appear in Table 12.

Table 12: Updated Spring Stiffness Values for BC1 w/ Multiple Load & Sensor Cases

BC #	LC #	MDOF	Load Combination	K_1 (k/in.) SPE	K_2 (k/in.) SPE	K_1 (k/in.) PARIS	K_2 (k/in.) PARIS
BC1	LCP1	12	A1A2A3A4A5	61.38	60.70	62.10	61.49
	LCP2	12	A1A2A3	65.40	53.33	61.90	71.01
	LCP3	12	A3A4A5	43.68	71.97	50.75	61.60
	LCP4	12	A1A3A5	71.24	56.67	64.33	66.30
	LCP5	7	A1A2A3A4A5	67.97	70.73	63.92	64.33
	LCP6	7	A1A2A3	67.30	80.73	61.65	66.30
	LCP7	7	A3A4A5	47.32	78.02	63.90	61.47
	LCP8	7	A1A3A5	67.97	70.73	61.90	61.48
	LCP9	4	A1A2A3A4A5	71.23	77.00	59.70	61.40
	LCP10	4	A1A2A3	75.75	43.10	61.46	60.79
	LCP11	4	A3A4A5	59.12	80.42	62.59	61.50
	LCP12	4	A1A3A5	71.23	77.00	62.40	60.19

From the table we can see that there is consistency between the values for each MDOF subgroup, as well as the entire data set. We may not fully expect the stiffness parameters to update to the same values regardless of the load combination use because of the pads non-linear behavior. In

addition, small deflections were taking place at the supports and this may also be contributing to the error from updating the support conditions. Using the data from Table 12, mean values for each MDOF case were used to update the initial FEM (Table 13).

Table 13: Mean Updated Spring Stiffness Values for BC1

BC #	MDOF	$K_{1\mu}$ (k/in.) SPE	$K_{2\mu}$ (k/in.) SPE	$K_{1\mu}$ (k/in.) PARIS	$K_{2\mu}$ (k/in.) PARIS
BC1	12	60.42	60.67	62.61	61.21
	7	62.64	75.05	62.84	63.39
	4	69.33	69.38	62.40	60.19

As can be seen, there is not a large difference between the SPE and PARIS updated stiffness values, and this can be further verified by looking at plot comparing the experimental and updated displacements for a typical LC (Figure 58).

minor differences in the stiffness values, which were not significant enough to change the structural behavior of the beam.

Dynamic test data is also used to validate the updated finite element models. Using the updated model, dynamic results were extracted and then compared to the experimental data (Table 14).

Table 14: BC1 Model Validation Using Dynamic Data

BC #	Mode #	Exp. (Hz)	SPE (12MDOF) Hz	SPE (7MDOF) Hz	SPE (4MDOF) Hz	PARIS (12MDOF) Hz	PARIS (7MDOF) Hz	PARIS (4MDOF) Hz
BC1	1	38.24	37.73	38.18	38.23	37.82	37.89	37.78
			1.34%	0.17%	0.03%	1.12%	0.92%	1.22%
	2	99.25	109.31	113.62	114.28	110.12	110.84	109.75
			10.13%	14.48%	15.14%	10.95%	11.67%	10.57%
	3	143.65	168.10	176.06	176.64	169.46	170.66	168.85
			17.02%	22.56%	22.97%	17.97%	18.80%	17.54%

Table 15: BC1 MAC Value Comparison

BC #	LC	SPE 12MDOF	PARIS 12MDOF	SPE 7MDOF	PARIS 7MDOF	SPE 4MDOF	PARIS 4MDOF
BC1	Mode 1	0.997	0.997	0.997	0.997	0.997	0.997
	Mode 2	0.989	0.987	0.994	0.989	0.987	0.986
	Mode 3	0.960	0.957	0.973	0.960	0.960	0.956

The frequencies for the first mode shape do not differ that much from models using different combinations of sensors (Table 15). The first mode is the critical mode and if we fail to capture

it, then we will miss all other behavior. Again, using 4MDOF versus using all 12MDOF does not appear to have a great impact on the updated finite element models.

Further visualization is facilitated in order to show the updated mode shape 1 versus the experimental data (Figure 59).

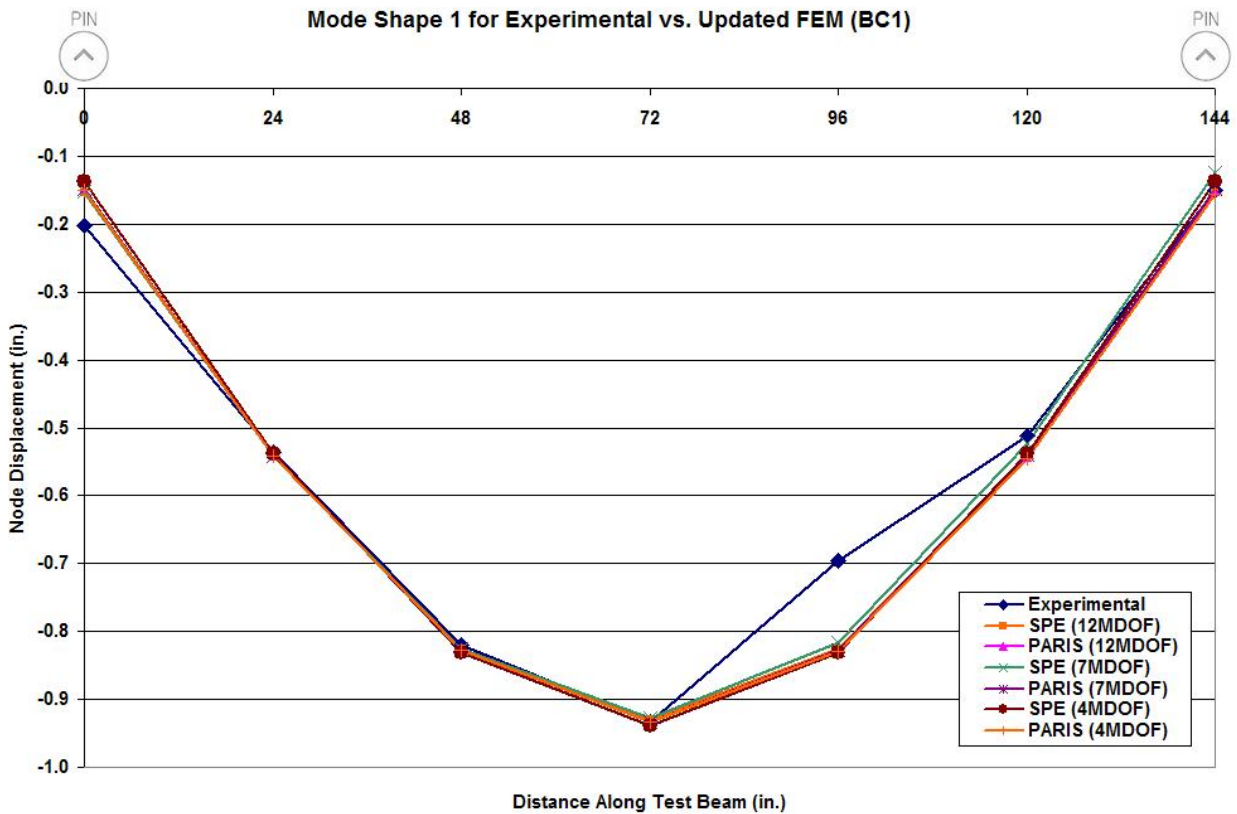


Figure 59: Mode Shape 1 Comparison for Experimental & Updated FEM Data (BC1)

A slight discrepancy in the mode shape is most likely attributed to experimental measurement error, although the SPE and PARIS values were in agreement with one another.

BC3a Parameter Estimation Results

The same load and MDOF combinations were used to update the pad stiffness parameters for BC3a. The results of the parameter estimation studies are shown in Table 16.

Table 16: Updated Spring Stiffness Values for BC3a w/ Multiple Load & Sensor Cases

BC #	LC #	MDOF	Load Combination	K ₁ (k/in.) SPE	K ₂ (k/in.) SPE	K ₁ (k/in.) PARIS	K ₂ (k/in.) PARIS
BC3a	LCP1	12	A1A2A3A4A5	24.56	30.65	31.99	56.32
	LCP2	12	A1A2A3	27.06	21.03	34.66	53.49
	LCP3	12	A3A4A5	20.99	33.50	33.94	55.36
	LCP4	12	A1A3A5	26.45	29.24	34.74	62.16
	LCP5	7	A1A2A3A4A5	32.01	28.25	35.22	61.61
	LCP6	7	A1A2A3	34.50	21.34	22.02	27.00
	LCP7	7	A3A4A5	26.28	30.22	19.67	28.28
	LCP8	7	A1A3A5	32.01	28.25	21.98	20.40
	LCP9	4	A1A2A3A4A5	34.43	28.37	23.45	20.45
	LCP10	4	A1A2A3	40.14	11.44	27.43	27.65
	LCP11	4	A3A4A5	24.61	30.60	28.46	26.15
	LCP12	4	A1A3A5	34.43	28.37	27.98	28.82

From the data, it is evident that the uncertainties in the neoprene pads, specifically the non-linearity, play an important role in capturing the stiffness parameters correctly. Load combination selection also contributes to some of the error in the estimated parameters. Again, we use mean values for each MDOF case and use them to update the initial FEM (Table 17).

Table 17: Mean Updated Spring Stiffness Values for BC3a

BC #	MDOF	K _{1μ} (k/in.) SPE	K _{2μ} (k/in.) SPE	K _{1μ} (k/in.) PARIS	K _{2μ} (k/in.) PARIS
BC3a	12	24.77	28.60	33.72	56.83
	7	31.20	27.01	24.72	34.32
	4	33.40	24.69	27.98	28.82

Using all 12 MDOF for PARIS analysis indicates that measurement or modeling error is causing the parameters to update to very stiff values. This goes back to the idea that having more sensor data may make the objective function “foggy”, whereas less MDOF, 4MDOF in this case, appear to update the parameters to their correct values. This becomes evident if we plot the updated FEM displacements versus the experimental data (Figure 60).

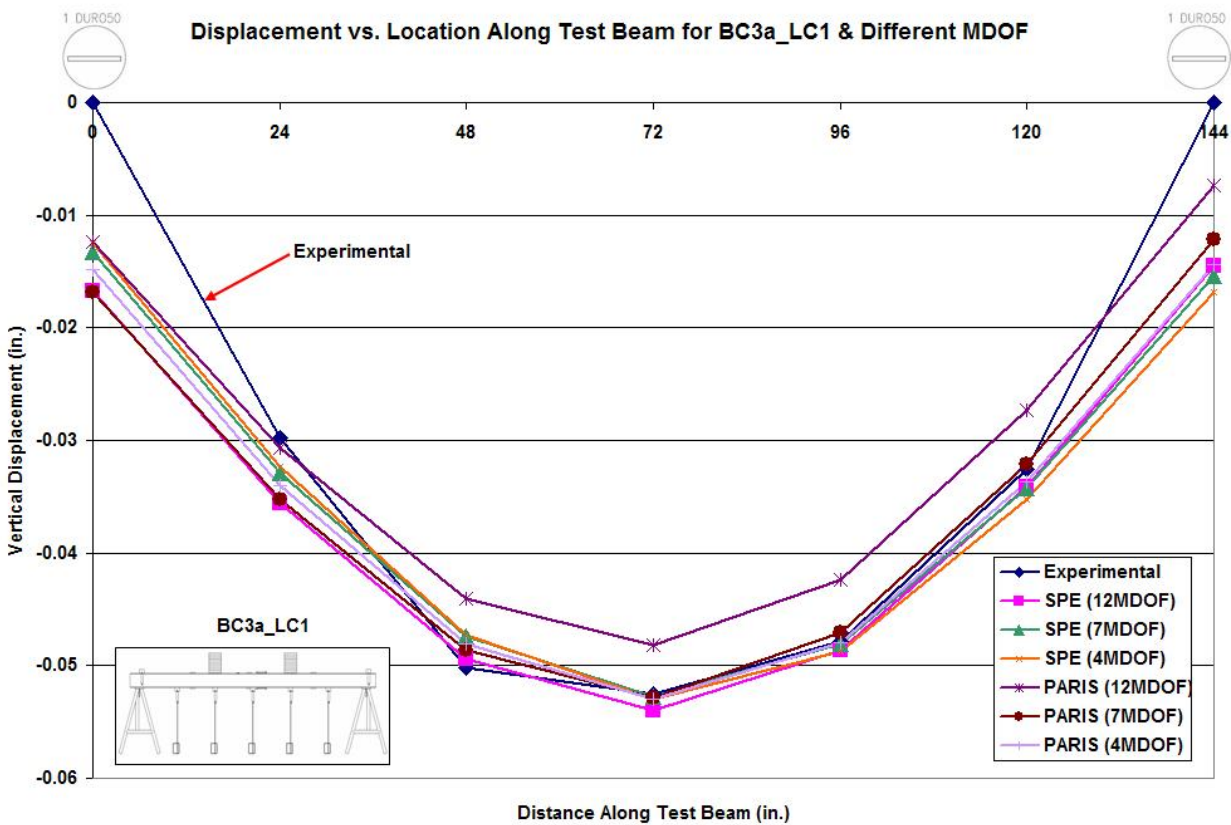


Figure 60: Comparison of Updated FEM and Experimental Displacements for BC3a_LC1

From Figure 60, we can see that the PARIS case using 12 MDOF incorrectly updates the parameters to stiffer values, hence the less displacement. The other combination of MDOF and

loads were in agreement with one another along with the experimental data. Dynamic test data in Table 18 and MAC value comparisons in Table 19 indicate that the updated models were stiffer than the actual test structure, but a plot of the first mode shape (Figure 61) shows that there was generally good correlation between the models.

Table 18: BC3a Model Validation Using Dynamic Data

BC #	Mode #	Exp. (Hz)	SPE (7MDOF) Hz	PARIS (7MDOF) Hz
BC3a	1	37.32	33.98	33.90
	2	100.96	82.20	81.99
	3	152.20	131.56	132.40

Table 19: BC3a MAC Value Comparison

BC #	LC	SPE 7MDOF	PARIS 7MDOF
BC3a	Mode 1	0.990	0.988
	Mode 2	0.976	0.990
	Mode 3	0.943	0.893

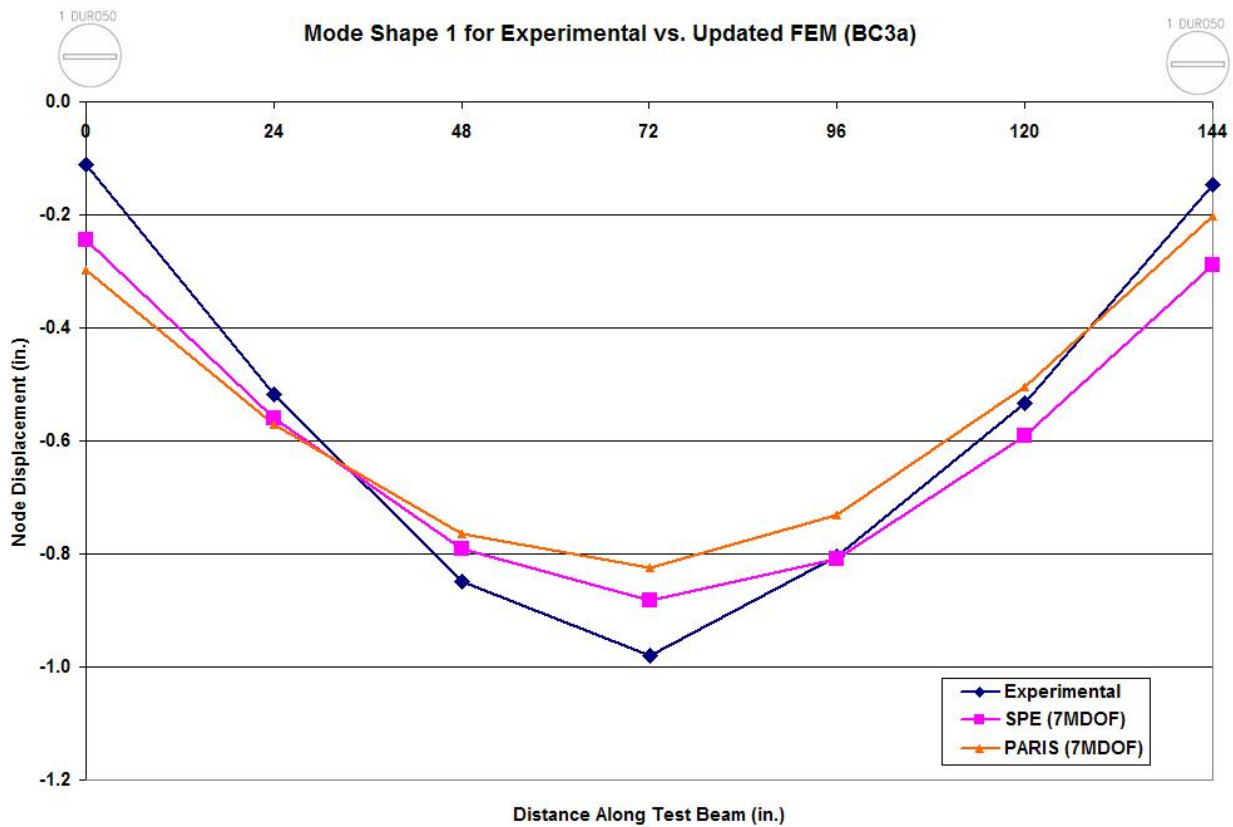


Figure 61: Mode Shape 1 Comparison for Experimental & Updated FEM Data (BC3a)

BC3b Parameter Estimation Results

The author expected this BC test to have the most trouble and error associated with it due to the fact that the stack of 5 Duro50 pads represented very flexible support conditions. Although this BC was initially thought to have high non-linearity, material test plots showed the opposite (Figure 62).

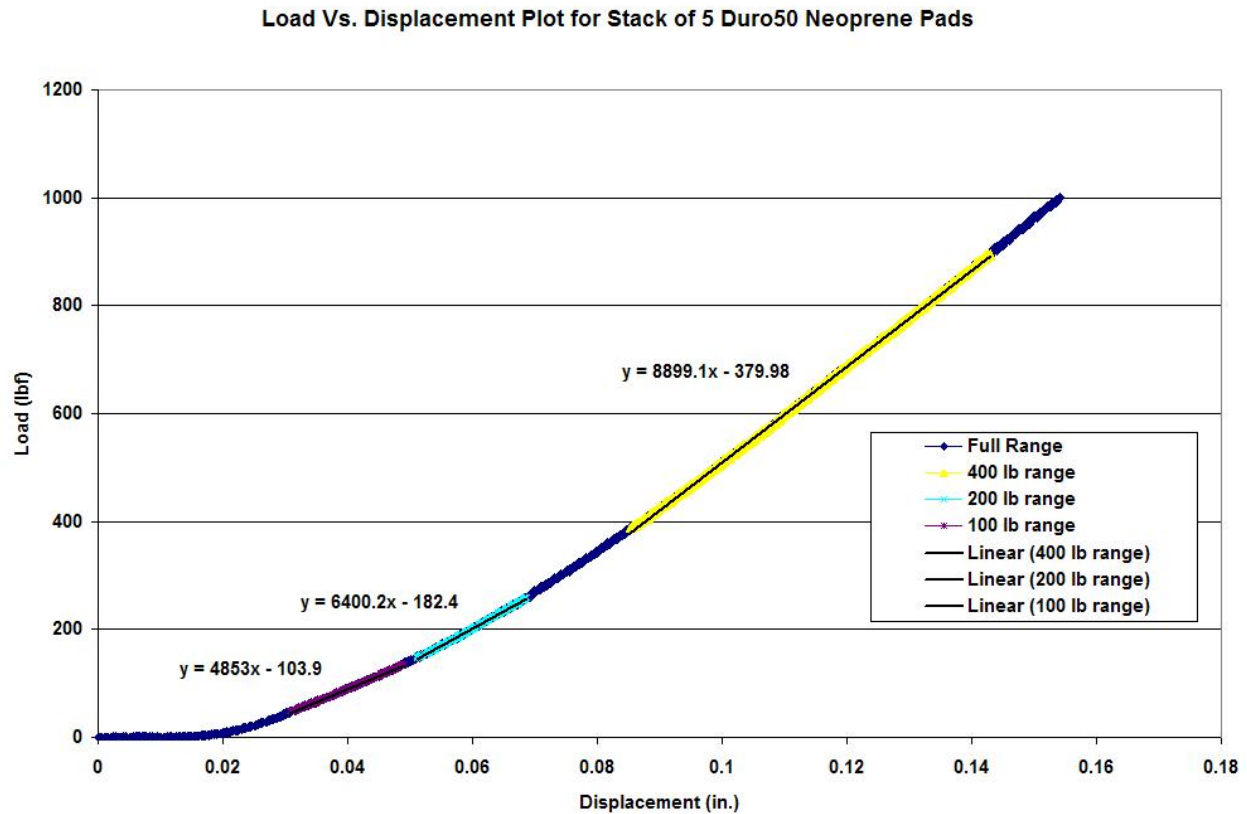


Figure 62: Material Test Plot for 5 Duro50 Neoprene Pads Stacked Together

The stiffness of the pads is non-linear only under low loads and once it reaches 300 pounds, for the most part remains linear. When compared to other material test plots such as those from individual pad Duro50 pad tests (Figure 36), the degree of non-linearity is significantly different. Single Duro50 pads show large increases in vertical stiffness under low applied loads. It is possible that the parameter estimation studies for the BC and LC combinations were successful because the material (when stacked) exhibits linear behavior. Table 20 illustrates the success of both SPE and PARIS in updating the unknown stiffness parameters. When compared with other results from different BC's, the fluctuation in updated values is small.

Table 20: Updated Spring Stiffness Values for BC3b w/ Multiple Load & Sensor Cases

BC #	LC #	MDOF	Load Combination	K ₁ (k/in.) SPE	K ₂ (k/in.) SPE	K ₁ (k/in.) PARIS	K ₂ (k/in.) PARIS
BC3b	LCP1	12	A1A2A3A4A5	6.40	6.39	6.47	5.81
	LCP2	12	A1A2A3	6.61	5.75	8.33	5.22
	LCP3	12	A3A4A5	6.05	6.57	8.21	5.71
	LCP4	12	A1A3A5	6.41	6.45	7.52	5.81
	LCP5	7	A1A2A3A4A5	6.42	6.40	6.13	5.96
	LCP6	7	A1A2A3	6.51	6.02	6.14	5.97
	LCP7	7	A3A4A5	6.16	6.48	6.34	6.18
	LCP8	7	A1A3A5	6.42	6.40	6.19	5.93
	LCP9	4	A1A2A3A4A5	6.56	6.48	6.01	6.01
	LCP10	4	A1A2A3	6.70	5.23	5.88	5.98
	LCP11	4	A3A4A5	5.78	6.59	6.11	6.58
	LCP12	4	A1A3A5	6.56	6.48	5.94	6.01

Table 21 shows the mean values calculated for this boundary condition setup and the good correlation between PARIS and SPE analysis as well as varying MDOF setups.

Table 21: Mean Updated Spring Stiffness Values for BC3b

BC #	MDOF	K _{1μ} (k/in.) SPE	K _{2μ} (k/in.) SPE	K _{1μ} (k/in.) PARIS	K _{2μ} (k/in.) PARIS
BC3b	12	6.37	6.29	7.63	5.64
	7	6.38	6.32	6.20	6.01
	4	6.40	6.19	5.98	6.14

A plot of the displacements from the updated FEM is shown below (Figure 63). For having highly flexible supports, the results of the different studies correlate well with one another. The discrepancy between the case where PARIS uses 12MDOF and the other results is related to measurement error affecting the objective function (as mentioned previously).

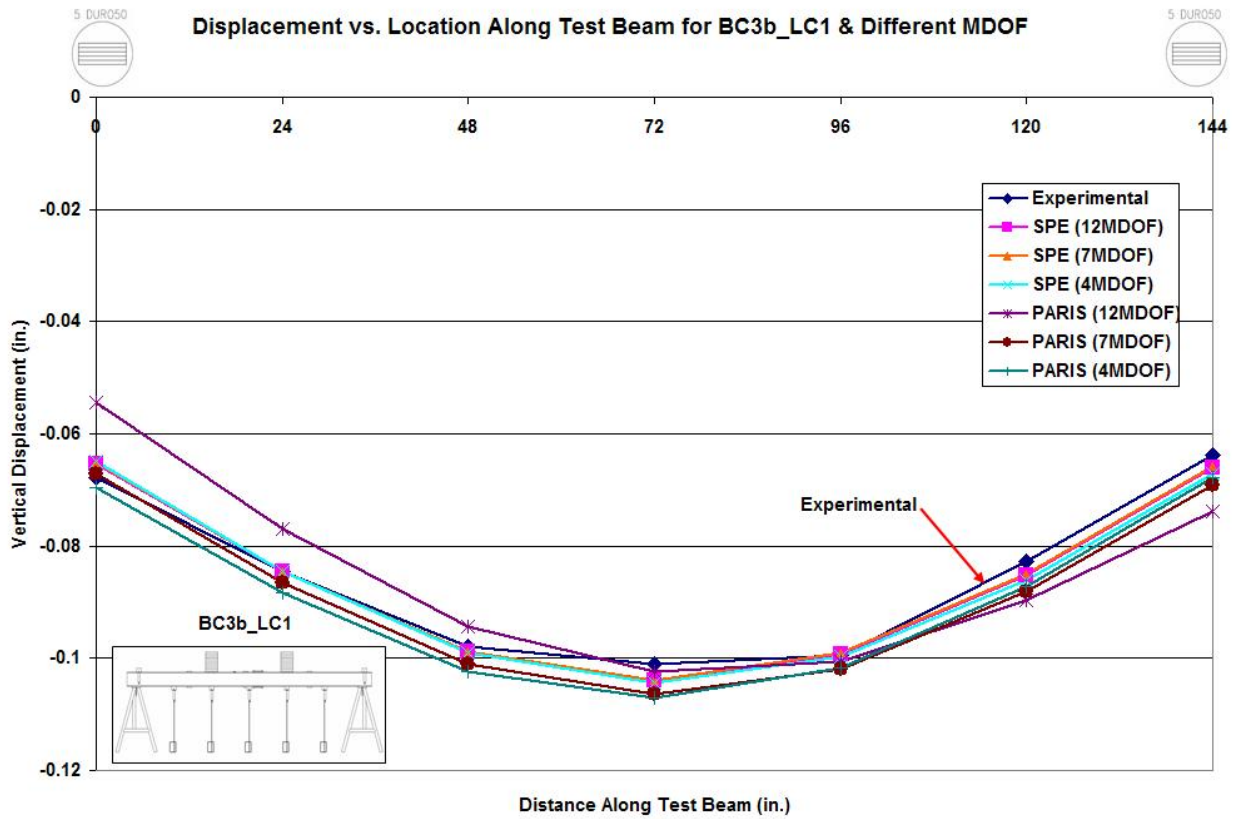


Figure 63: Comparison of Updated FEM and Experimental Displacements for BC3b_LC1

Validation of the updated FEM's using dynamic measurements also proves reliable. For the most part the measured frequencies (Table 22) agree with the results of the experimental tests. MAC value comparisons illustrate the good correlation of the experimental and updated FEM mode shapes (Table 23). Like all previous studies involving neoprene pads, some of the differences in the values may be related to our assumptions that the pads were treated as being linear-elastic.

Table 22: BC3b Model Validation Using Dynamic Data

BC #	Mode #	Exp. (Hz)	SPE (7MDOF) Hz	PARIS (7MDOF) Hz
BC3b	1	25.50	21.88	21.55
	2	52.83	40.70	39.93
	3	95.51	96.52	96.10

Table 23: BC3b MAC Value Comparison

BC #	LC	SPE 7MDOF	PARIS 7MDOF
BC3b	Mode 1	0.998	0.997
	Mode 2	0.999	0.999
	Mode 3	0.991	0.991

A plot of the first mode shape (Figure 64) using experimental data and the updated FEM is shown below. The experimental model is assuming the model is stiffer than what the updated FEM updated to. SPE and PARIS both perform well when optimizing the objective function for this highly flexible case.

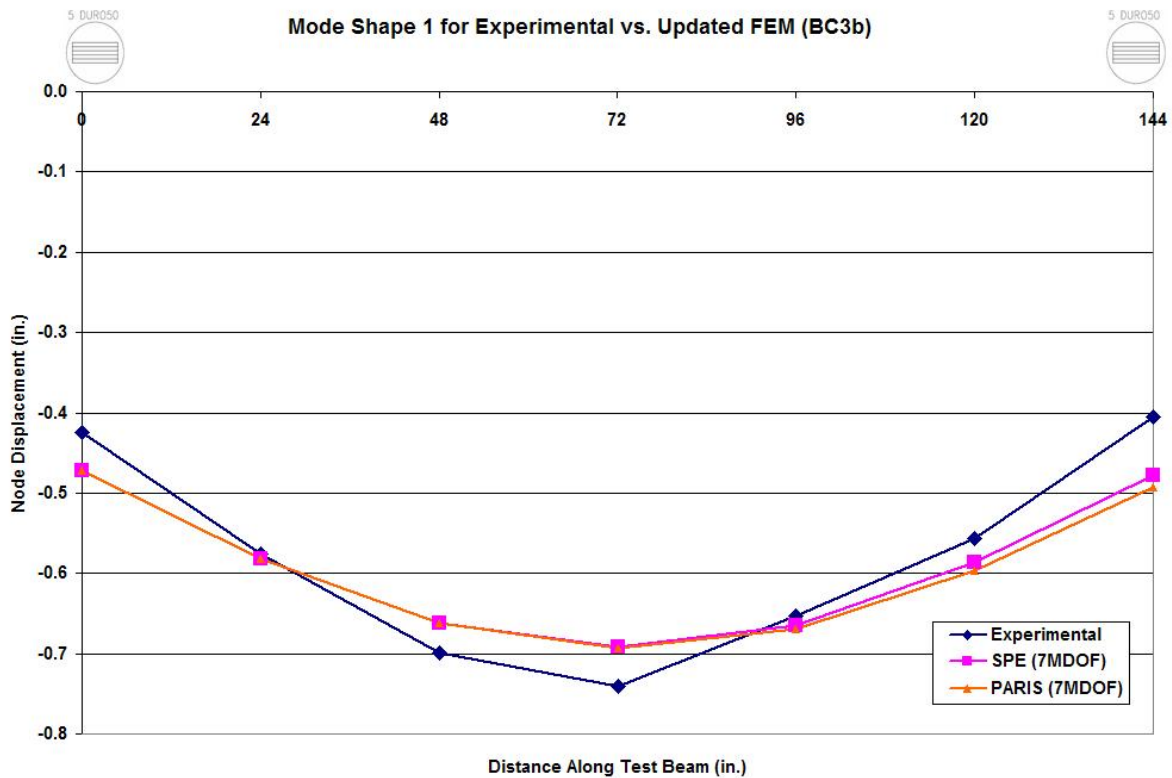


Figure 64: Mode Shape 1 Comparison for Experimental & Updated FEM Data (BC3b)

BC5b Parameter Estimation Results

This was the only BC that SPE failed to update the stiffness parameter on. In Table 24, the SPE program was not able to converge to the correct parameter on the left side of the beam. This issue might be due to the complexity of this particular boundary support case, in that there is an extremely flexible support on the left side, and a rather stiff support at the right side. It appears that PARIS had an easier time updating for both parameters successfully and the difference between the SPE results may be due to the algorithm driving the optimization method.

Table 24: Updated Spring Stiffness Values for BC5b w/ Multiple Load & Sensor Cases

BC #	LC #	MDOF	Load Combination	K ₁ (k/in.) SPE	K ₂ (k/in.) SPE	K ₁ (k/in.) PARIS	K ₂ (k/in.) PARIS
BC5b	LCP1	12	A1A2A3A4A5	5.91	104.94	5.35	21.69
	LCP2	12	A1A2A3	5.86	5181.39	6.41	17.69
	LCP3	12	A3A4A5	5.62	111.05	7.78	17.73
	LCP4	12	A1A3A5	5.94	94.00	6.50	18.41
	LCP5	7	A1A2A3A4A5	5.95	191.61	5.77	29.90
	LCP6	7	A1A2A3	5.93	6438.20	5.77	27.02
	LCP7	7	A3A4A5	5.75	208.20	6.47	36.75
	LCP8	7	A1A3A5	5.95	191.61	5.32	38.22
	LCP9	4	A1A2A3A4A5	5.85	121.90	6.51	25.16
	LCP10	4	A1A2A3	5.84	6319.22	5.53	25.11
	LCP11	4	A3A4A5	5.84	111.75	6.00	24.94
	LCP12	4	A1A3A5	5.85	121.91	6.20	29.51

Mean stiffness values were obtained for each MDOF case and again it was evident that SPE had problems, especially with updating right support parameter, K₂ correctly (Table 25). Physically these values do not make sense, since they indicate that the right side of the beam is extremely stiff.

Table 25: Mean Updated Spring Stiffness Values for BC5b

BC #	MDOF	K _{1μ} (k/in.) SPE	K _{2μ} (k/in.) SPE	K _{1μ} (k/in.) PARIS	K _{2μ} (k/in.) PARIS
BC5b	12	5.83	1372.85	6.51	18.88
	7	5.89	16243.50	5.83	38.23
	4	5.84	1668.70	6.06	29.51

If we plot the resulting displacements from the updated FEM along with the experimental data, a noticeable difference can be observed (Figure 65). This data indicates that the FEM from the PARIS estimations were much stiffer than the physical test structure.

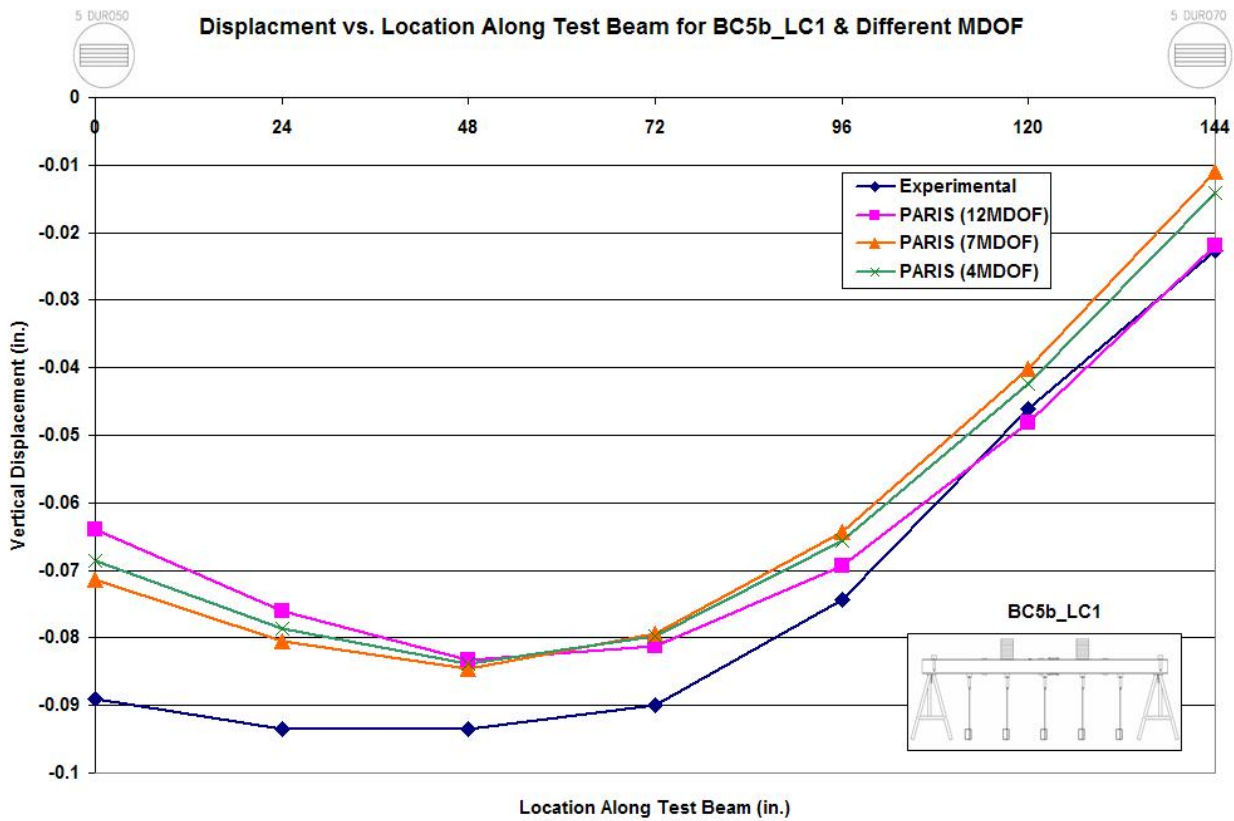


Figure 65: Comparison of Updated FEM and Experimental Displacements for BC5b_LC1

Since all the parameters could not be updated successfully by SPE, validation of the FEM using dynamic data was only carried out for the PARIS case (Table 26).

Table 26: BC5b Model Validation Using Dynamic Data

BC #	Mode #	Exp. (Hz)	SPE (7MDOF) Hz	PARIS (7MDOF) Hz
BC5b	1	27.61	NA	24.61
	2	63.43	NA	61.71
	3	126.16	NA	126.43

Table 27: BC5b MAC Value Comparison

BC #	LC	SPE 7MDOF	PARIS 7MDOF
BC5b	Mode 1	NA	0.995
	Mode 2	NA	0.998
	Mode 3	NA	0.987

Surprisingly, the results of the dynamic studies show that the stiffness parameters used to update the FEM were very good. There is not much error from mode number to mode number which suggests that the experimental data successfully captured the first three modes with high accuracy (Table 27). A plot of the first mode shape (Figure 66) shows that the PARIS model is stiffer at the right support, more so than the experimental data suggests. Both supports appear to differ in their flexibility and a cause for this might be due to the fact that the accelerometers at the ends were not directly in the middle of the supports. After analyzing the experimental data set for the dynamic case, some of the results suggested that the supports themselves were moving or “bouncing” (due to not being properly leveled).

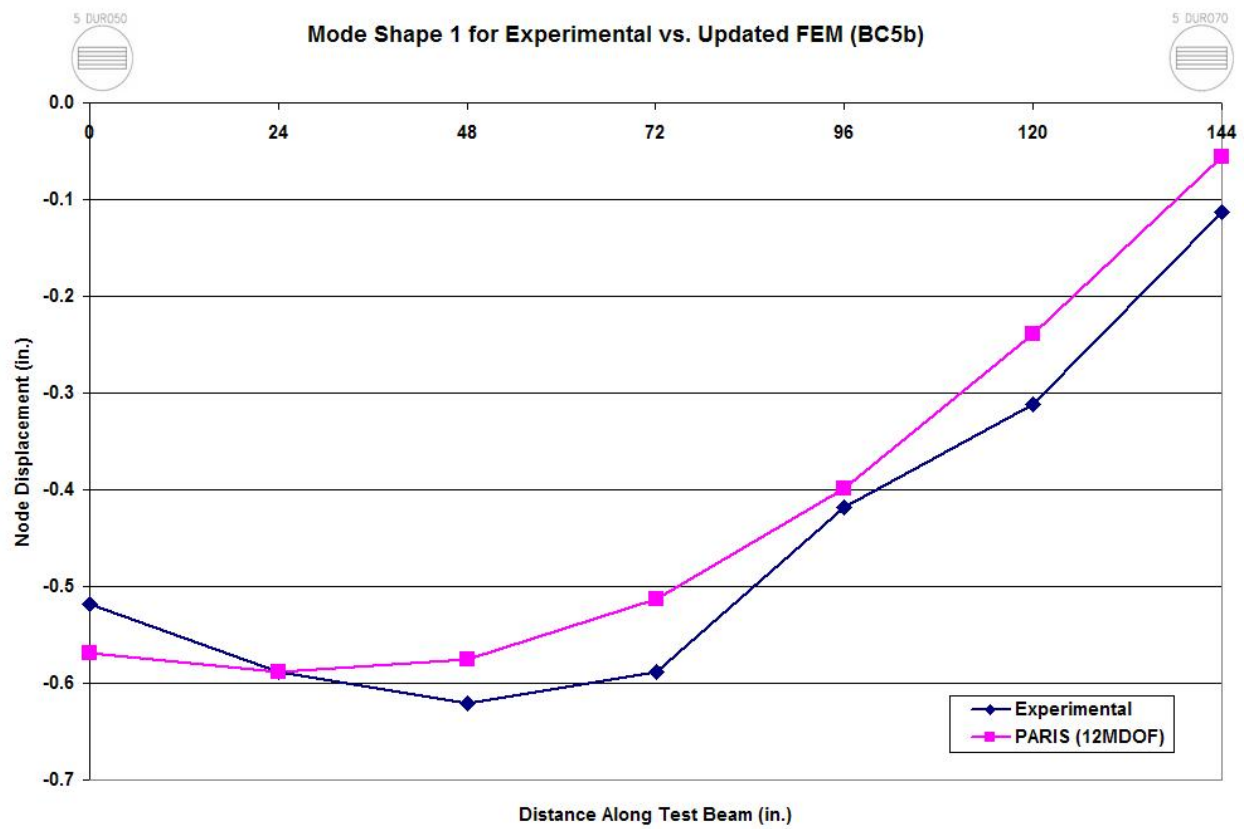


Figure 66: Mode Shape 1 Comparison for Experimental & Updated FEM Data (BC5b)

CHAPTER SIX: CONCLUSIONS AND RECOMMENDATIONS

1) What is the effect of elastomeric pad boundary conditions on the behavior of a particular structure (test beam)?

- *Boundary conditions have major impact on structural behavior in real life applications (even more so than localized damage in many cases):* The analytical and experimental studies showed that boundary conditions of the structures can be identified using static experimental measurements to update a preliminary FEM. This study showed that even a simple “pin-pin” boundary condition is not easy to idealize with an uncalibrated model despite the structure being in a controlled laboratory environment. Therefore, updating the FE models by using experimental data is useful to generate important information such as boundary condition behavior about the structure. It was also observed that changing the boundary conditions affects the structural behavior greatly.
- *Neoprene pads have a great impact on static and dynamic behavior for the particular problem also:* The affect of using flexible supports and their corresponding deflection and modal plots were identified by means of experimental methods. Using different type and number of neoprene pads were employed to simulate change in behavior in a laboratory environment at the boundary conditions due to reasons such as settlement and deterioration of the boundary supports of actual structures.
- *Material tests can be conducted to have good initial estimates for axial stiffness:* Compression tests on the neoprene pads were performed in order to obtain stiffness values for the pads to use as the initial guesses for the case study. Compression tests also

help to identify the behavior or consistency in material properties for individual pads as well as pads stacked together vertically.

2) Can we use a simplified parameter estimation program? How many sensors are necessary (minimum) for successful parameter identification?

- *Use of Spreadsheet Parameter Estimation (SPE) is easier, more suitable for quick analysis in CE design offices:* SPE a straight-forward spreadsheet program which can be setup and utilized by practicing engineers not considered experts in this field. SPE results may be used as a starting point for “quick” analysis checks before carrying out more labor intensive analysis using PARAmeter Identification System (PARIS) software or other automated parameter estimation software. These results may also be used as initial values for PARIS analysis.
- *Is possible to obtain improved and reliable results using SPE:* The unknown stiffness parameters of the test beam boundaries were updated by using a simple optimization spreadsheet as well as a complex and robust parameter estimation program. The FE models were updated using parameters obtained from SPE and PARIS. The updated FE models were analyzed to get deflections under various load conditions. The results were compared with experimental counterparts. When comparing the results of parameter estimation with PARIS and SPE results, the differences in the structural behavior due to updated parameters are not significantly different from each other as well as from the experimental results. However, there are also cases such as one end is extremely flexible (BC5b - mixed pads), SPE did not perform well while PARIS was successful.

- *Based on the structure and parameters to be updated, less sensors may be used but more loading conditions may be helpful:* A total of 12 measurements including deflection and rotations are employed for cases entitled as 12 MDOF. However, it is seen that the number of measurements can be reduced up to 4 MDOF to approximate the 12 MDOF results. The important issue is that more load combinations are needed to better capture and represent the actual behavior of the structure. The FE models that were updated using different sensor configurations (12, 7 and 4 MDOF) are compared against the static load test results as well as the dynamic frequency and mode shapes. Generally good correlation was observed validating the SPE and PARIS results.

Recommendations

- *Use other boundary condition data (Pin + shims, Duro70 pads):* There are many other data sets of different boundary conditions, utilizing stiffer pads and a combination of mixed pads, as well as additional load cases. A comparative analysis of these data sets, as well as optimizing the number and locations of required sensors should be addressed in future studies.
- *Use strain data for parameter estimation:* Static strain measurement data should be used in conjunction with the static strain error function. Strain data was recorded for each of the load cases carried out in this analysis. Studies involving the impact of multiple types of strain sensors, such as foil-bonded strain gages, and vibrating wire gages for parameter estimation should be carried out. These types of sensors are common tools used by many engineering working in the field of structural engineering today. They are cost-effective

and unlike displacement transducers, require no frame of reference, so they can be placed just about anywhere on a structure.

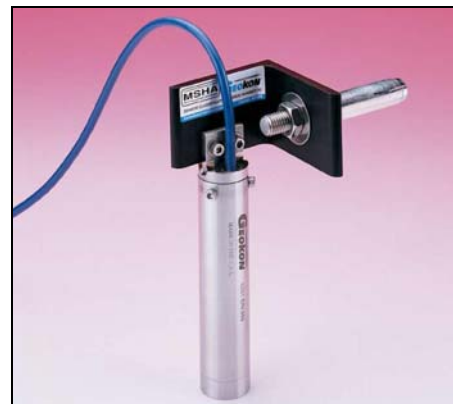
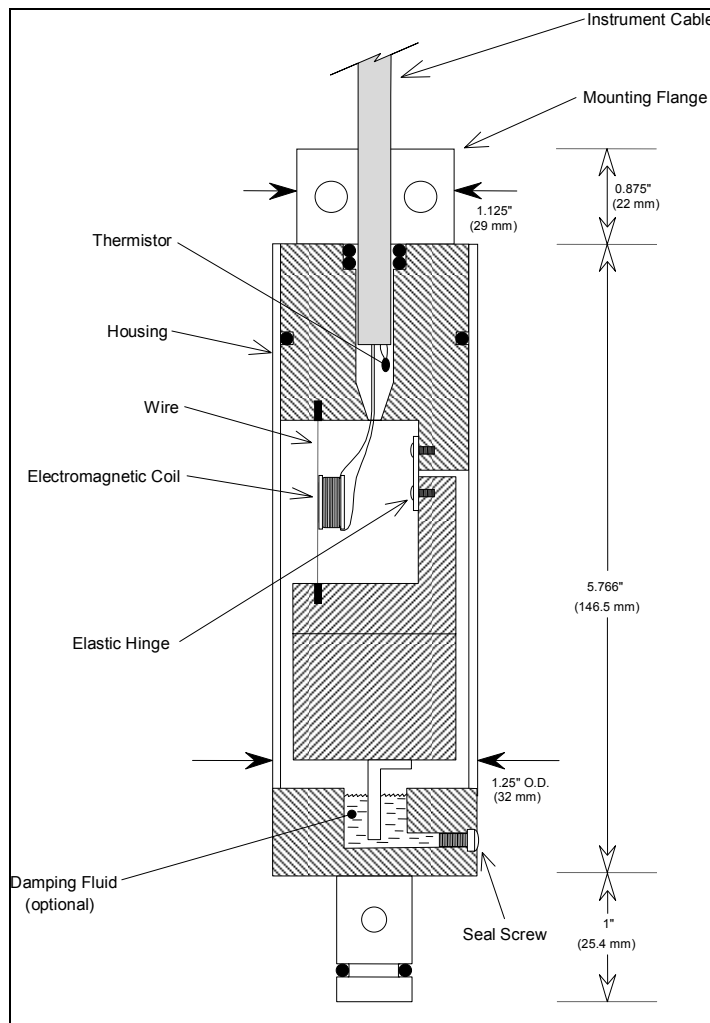
- *Update moment of inertia values, I_{xx} :* In this study, the moment of inertia for the section was assumed to be the true value (even though field measurements indicated minute differences in the values). Future studies should involve updating for this unknown parameter in order to reduce some of the error which may be contributing to the estimation process.
- *Dynamic data for parameter estimation:* Dynamic data such as experimental frequencies and modes can be used as input for the parameter estimation process in order to update the mass of the structure. Updated mass parameters can then be used to update the FEM's element mass properties, such that the error between the original and updated dynamic model is minimized. Again, independent dynamic tests can be used to correlate the experimental versus than updated dynamic model frequencies and mode shapes.
- *Restrain boundary supports (clamping, bolting, to provide rotational stiffness):* A variation of the same study can take place by clamping or fixing the beam and pads to the supports. By providing some rotational restraint at the boundaries, studies involving semi-rigid joints can take place as well as further analysis of the influence of neoprene pads.
- *Expand the spreadsheet optimization (SPE) concept and other parameter estimation approaches to UCF Grid structure and real life structures:* Parameter estimation studies involving the UCF grid structure can be conducted to explore issues when the structure is multi-dimensional and redundant. While the theory and procedures were proven successfully on a laboratory beam, the goal of future studies should be to implement

these ideas on real-life structures such as buildings or bridges. The use of practical optimization approach may be useful for condition assessment and load rating of actual structures by design engineers.

APPENDIX A: INSTRUMENTATION

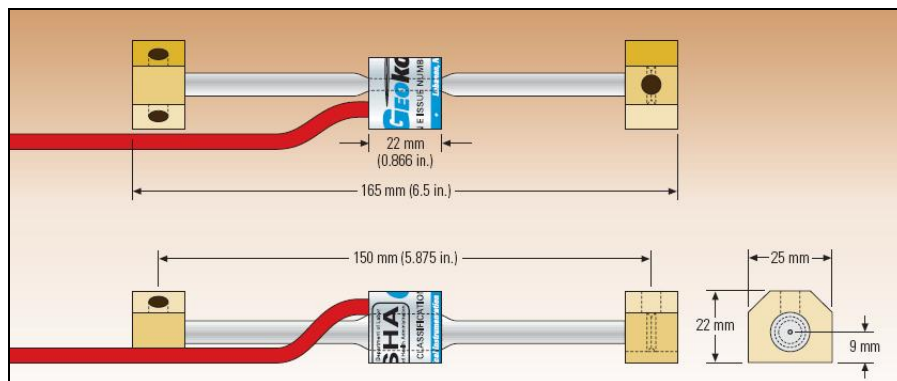
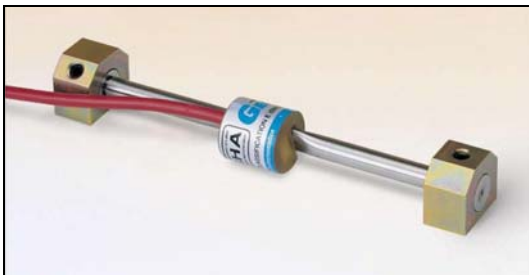
Geokon Model 6350 Vibrating Wire Tiltmeter

Geokon Model 6350 Technical Specifications	
Range:	$\pm 15^\circ$
Resolution:	8 arc seconds
Accuracy:	$\pm 0.1\%$ FSR
Linearity:	1.5% FSR
Frequency Range:	1400-3500 Hz
Diameter:	1.250"
Length:	7.375"
Temperature Range:	-40 to +175° F
Material:	304 Stainless Steel



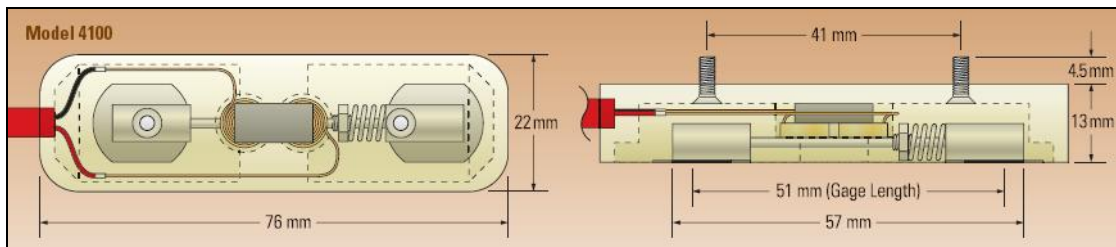
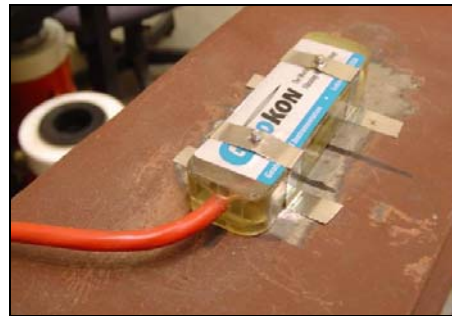
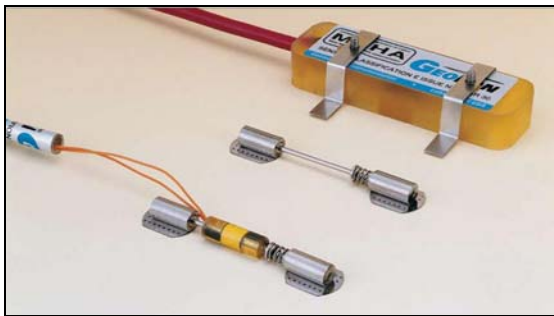
Geokon Model 4000 Vibrating Wire Tiltmeter

Geokon Model 4000 Technical Specifications	
Range (nominal):	3000 $\mu\epsilon$
Resolution:	0.1 $\mu\epsilon$
Accuracy:	$\pm 0.5\%$ FS
Linearity:	0.5% FS
Frequency Range:	450-1200 Hz
Dimensions (gage):	6.125" x 0.750"
Temperature Range:	-20 to +80° C
Active Gage Length:	5.875 in.



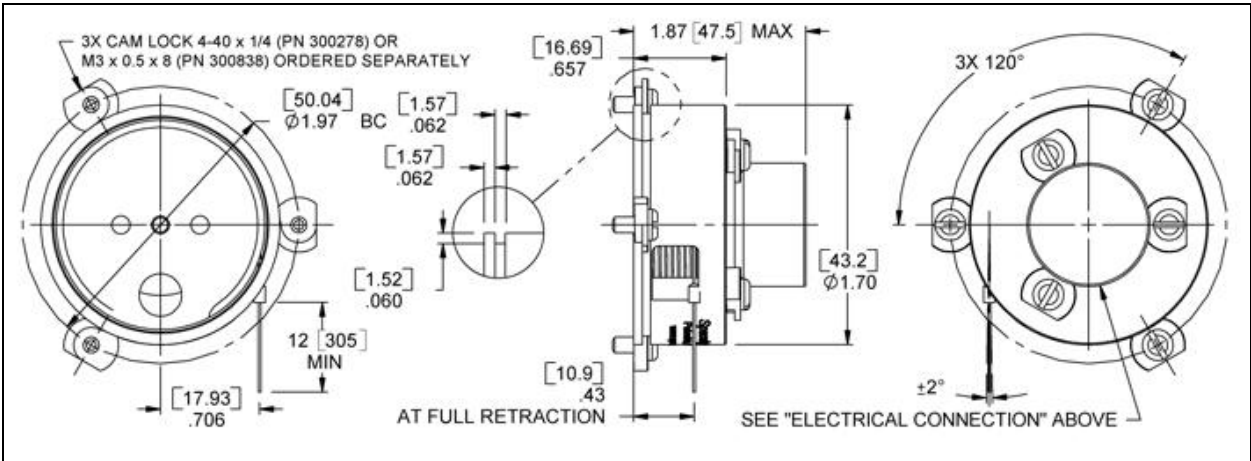
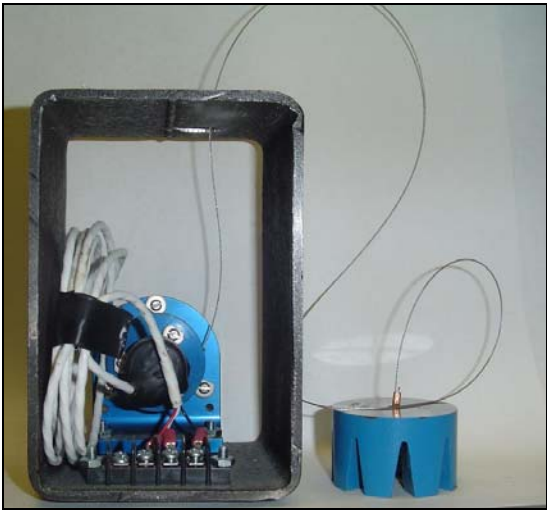
Geokon Model 4100 Vibrating Wire Tiltmeter

Geokon Model 4100 Technical Specifications	
Range (nominal):	2500 $\mu\epsilon$
Resolution:	0.1 $\mu\epsilon$
Accuracy:	$\pm 0.5\%$ FS
Linearity:	2.0% FS
Frequency Range:	1400-3500 Hz
Dimensions (gage):	2.250" x 0.250"
Temperature Range:	-20 to +80° C
Active Gage Length:	2.008 in.



SpaceAge Control Displacement Transducer

Spaceage Control Position Transducer Technical Specifications	
Range:	13.2 in.
Resolution:	infinite signal
Electrical Output:	Analog
Linearity:	±0.25%
Nominal Mass:	3 oz
Outline Dimensions:	1.7" dia. X 1.87"
Nominal Cable Tension:	5 to 25 oz
Temperature Range:	-40 to +185° F
max. cable accel:	20 g's



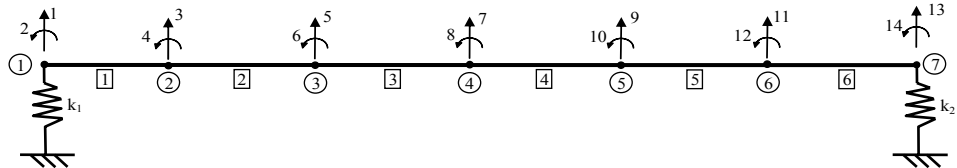
APPENDIX B: SPREADSHEET PARAMETER ESTIMATION (SPE)

Spreadsheet Parameter Estimation (SPE)

Developed by Kevin Francoforte M.S.C.E. 2007
Revision Date: 3/07

PURPOSE:	The purpose of this spreadsheet is to perform Parameter Estimation of a test structure using Excel's built-in SOLVER tool to minimize a given objective function for a non-linear optimization problem, described below. Experimental measurement data will be
----------	--

PROBLEM:	An experimental test structure consisting of a 12 foot steel I-beam (W8x13 section) is simply supported by two steel sawhorses. A variety of boundary conditions were tested using steel angles and Neoprene pads to compare stiff and reduced stiffness support
----------	--



PROCEDURE:	The following steps serve as a guide for performing Parameter Estimation on a test beam structure, utilizing experimental measurements:
------------	---

STEP 1	Experimental Measurement Data (Listed according to boundary condition (BC) and load case (LC):
--------	--

BC1	LC1	BC1_LC1_A1 0.00000 0.00086 -0.02718 -0.00065 -0.04162 -0.00040 -0.04553 0.00000 -0.04121 0.00043 -0.02636 0.00067 0.00000 0.00087	LC2	BC1_LC2_A1 0.00000 -0.00027 -0.01099 -0.00019 -0.01321 -0.00003 -0.01279 0.00009 -0.01139 0.00014 -0.00078 0.00018 0.00000 0.00000 0.00024	BC1_LC2_A2 0.00000 -0.01980 -0.00037 -0.02142 -0.00003 -0.02312 0.00009 -0.01958 0.00019 -0.01177 0.00031 0.00000 0.00037	BC1_LC2_A3 0.00000 -0.01524 -0.00031 -0.02284 -0.00017 -0.02525 -0.00002 -0.01992 0.00020 -0.01320 0.00034 0.00000 0.00049	BC1_LC2_A4 0.00000 -0.00038 -0.00019 -0.01785 -0.00024 -0.02243 -0.00006 -0.01992 0.00017 -0.01387 0.00040 0.00000 0.00044	BC1_LC2_A5 0.00000 -0.00023 -0.00038 -0.00019 -0.01250 -0.00015 -0.01494 -0.00005 -0.01584 0.00007 -0.01070 0.00021 0.00000 0.00028	LC3	BC1_LC3_A1 -0.01111 -0.00894 -0.00751 -0.00065 -0.02200 -0.00047 -0.00063 -0.03427 -0.00019 -0.02848 0.00014 -0.02708 0.00035 -0.01429 0.00049 -0.00319 0.00058	BC1_LC3_A2 -0.00068 -0.02322 -0.00063 -0.03427 -0.00019 -0.03977 0.00003 -0.03489 0.00037 -0.01891 0.00063 -0.00530 0.00077	BC1_LC3_A3 -0.00038 -0.02038 -0.00064 -0.03427 -0.00038 -0.03735 -0.00005 -0.03560 0.00031 -0.02105 0.00063 -0.00638 0.00080
BC3a	LC1	BC3a_LC1_A1 -0.01780 -0.00082 -0.02983 -0.00077 -0.05024 -0.00040 -0.05258 0.00007 -0.04780 0.00042 -0.02254 0.00079 -0.01428 0.00084	LC2	BC3a_LC2_A1 -0.01177 -0.00045 -0.01985 -0.00016 -0.02195 0.00000 -0.01725 0.00012 -0.01371 0.00019 -0.01168 0.00023 -0.00316 0.00045	BC3a_LC2_A2 -0.01197 -0.00045 -0.01985 -0.00040 -0.02195 0.00000 -0.02738 0.00010 -0.02100 0.00024 -0.01588 0.00038 -0.00532 0.00045	BC3a_LC2_A3 -0.00084 -0.00038 -0.01701 -0.00040 -0.02988 -0.00024 -0.03248 0.00007 -0.02906 0.00025 -0.01791 0.00042 -0.00708 0.00056	BC3a_LC2_A4 -0.00822 -0.00038 -0.01312 -0.00037 -0.02361 -0.00024 -0.02713 -0.00008 -0.02492 0.00016 -0.01673 0.00042 -0.00709 0.00051	BC3a_LC2_A5 -0.00429 -0.00023 -0.00886 -0.00021 -0.01531 -0.00016 -0.01636 -0.00007 -0.01652 0.00005 -0.01677 0.00017 -0.00779 0.00051	LC3	BC3a_LC3_A1 -0.01644 -0.00058 -0.02712 -0.00058 -0.04569 -0.00021 -0.04221 0.00016 -0.03346 0.00031 -0.02212 0.00051 -0.00735 0.00065	BC3a_LC3_A2 -0.01430 -0.00073 -0.03071 -0.00070 -0.04519 -0.00037 -0.04839 0.00009 -0.04448 0.00042 -0.02783 0.00066 -0.01027 0.00077	BC3a_LC3_A3 -0.01181 -0.00063 -0.03119 -0.00063 -0.04105 -0.00042 -0.04126 0.00005 -0.04414 0.00035 -0.02890 0.00065 -0.01133 0.00075
BC3b	LC1	BC3b_LC1_A1 -0.06770 -0.00080 -0.08443 -0.00075 -0.00786 -0.00043 0.00039 -0.08283 0.00078 -0.05368 0.00083	LC2	BC3b_LC2_A1 -0.04867 -0.00009 -0.05157 0.00002 -0.04783 0.00019 -0.10108 0.00033 -0.08940 0.00040 -0.02354 0.00047 -0.01254 0.00049	BC3b_LC2_A2 -0.04165 -0.00040 -0.04785 -0.00028 -0.05283 0.00019 -0.05104 0.00003 -0.04584 0.00031 -0.04334 0.00047 -0.02367 0.00049	BC3b_LC2_A3 -0.03332 -0.00056 -0.04289 -0.00044 -0.05140 -0.00019 -0.04603 0.00003 -0.05269 0.00031 -0.04334 0.00040 -0.02367 0.00042	BC3b_LC2_A4 -0.01918 -0.00052 -0.03445 -0.00051 -0.04355 -0.00037 -0.04802 -0.00019 -0.05376 0.00003 -0.04923 0.00028 -0.02367 0.00038	BC3b_LC2_A5 -0.01323 -0.00049 -0.02269 -0.00049 -0.03213 -0.00037 -0.04197 -0.00033 -0.04899 -0.00019 -0.05209 0.00003 -0.04274 0.00003	LC3	BC3b_LC3_A1 -0.07127 -0.00033 -0.07905 -0.00030 -0.08888 0.00002 -0.07683 0.00012 -0.06444 0.00052 -0.04888 0.00075 -0.04874 0.00089	BC3b_LC3_A2 -0.05966 -0.00091 -0.07338 -0.00058 -0.08467 0.00002 -0.07683 0.00012 -0.06210 0.00052 -0.06314 0.00063 -0.04874 0.00066	BC3b_LC3_A3 -0.04237 -0.00086 -0.05965 -0.00075 -0.07353 -0.00042 -0.07631 0.00019 -0.08598 0.00028 -0.07349 0.00045 -0.06090 0.00052

BC5b	LC1	BC5b_LC1	LC2	BC5b_LC2_A1	BC5b_LC2_A2	BC5b_LC2_A3	BC5b_LC2_A4	BC5b_LC2_A5	LC3	BC5b_LC3_A1	BC5b_LC3_A2	BC5b_LC3_A3
		-0.0899		-0.0504	-0.0492	-0.03816	-0.02952	-0.01072		-0.0899	-0.0877	-0.04705
		-0.0028		-0.0017	-0.0012	-0.00019	-0.00021	-0.00021		-0.0017	-0.00037	-0.00040
		-0.0937		-0.05601	-0.05033	-0.04254	-0.03013	-0.01489		-0.08295	-0.07160	-0.05317
		-0.0019		-0.00024	-0.00005	-0.00016	-0.00012	-0.00012		0.00000	-0.00021	-0.00031
		-0.09352		-0.04819	-0.04962	-0.04390	-0.03320	-0.01547		-0.07639	-0.07282	-0.05961
		0.00009		0.00045	0.00017	-0.00003	-0.00009	-0.00010		0.00033	0.00009	-0.00009
		-0.08998		-0.03663	-0.03824	-0.03735	-0.03098	-0.01856		-0.06242	-0.06544	-0.05762
		0.00054		0.00051	0.00042	0.00007	0.00002	0.00002		0.00051	0.00038	0.00017
		-0.07440		-0.02937	-0.03329	-0.03489	-0.03023	-0.01922		-0.05038	-0.05625	-0.05340
		0.00063		0.00051	0.00058	0.00045	0.00033	0.00012		0.00094	0.00084	0.00063
		-0.04602		-0.01356	-0.01356	-0.01605	-0.01499	-0.01142		-0.02212	-0.02890	-0.02961
		0.00110		0.00052	0.00062	0.00054	0.00054	0.00023		0.00101	0.00106	0.00091
		-0.02271		-0.00035	-0.00200	-0.00381	-0.00480	-0.00577		-0.00311	-0.00791	-0.01164
		0.00152		0.00070	0.00072	0.00075	0.00066	0.00033		0.00105	0.00112	0.00096

STEP 3 Experimental Load Case Data (Load cases used to collect measurement data):

Exp. LCs	LC1	LC1	LC2	LC2_A1	LC2_A2	LC2_A3	LC2_A4	LC2_A5	LC3	LC3_A1	LC3_A2	LC3_A3
		0		0	0	0	0	0		0	0	0
		0		0	0	0	0	0		0	0	0
		0		-0.416	0	0	0	0		-0.314	0	0
		0		0	0	0	0	0		0	0	0
		-0.41554		0	-0.416	0	0	0		-0.314	-0.314	0
		0		0	0	0	0	0		0	0	0
		0		0	0	-0.416	0	0		-0.076	-0.314	-0.314
		-0.41593		0	0	0	0	0		0	-0.076	-0.314
		0		0	0	0	-0.416	0		0	0	0
		0		0	0	0	0	-0.416		0	0	-0.076
		0		0	0	0	0	0		0	0	0
		0		0	0	0	0	0		0	0	0
		0		0	0	0	0	0		0	0	0

STEP 3 Enter (copy, paste) the experimental MEASUREMENT (U^e) & FORCE (F^e) vector you want to use in the following spaces:

{U} ^e	BC5b_LC1	Global DOF	{F} ^e	LC1	Global DOF
	-0.01780	1		0	1
	-0.00082	2		0	2
	-0.02983	3		0	3
	-0.00077	4		0	4
	-0.05024	5		-0.41554	5
	-0.00040	6		0	6
	-0.05258	7		0	7
	0.00007	8		0	8
	-0.04780	9		-0.41593	9
	0.00042	10		0	10
	-0.03254	11		0	11
	0.00079	12		0	12
	-0.01428	13		0	13
	0.00084	14		0	14

STEP 4 Input the initial or best "guess" values for the unknown boundary condition springs (These are the "adjustable" cells for Solver):

Spring #	Stiffness	Units
K ₁	505050.00	kip/in
K ₂	100000.00	kip/in

Note: Once Solver optimizes the "TARGET CELL" (or objective function), these cells will represent the UPDATED stiffness variables

STEP 5 This is the global stiffness matrix for the test beam structure. Cells K₂₂ and K₁₃₁₃ will be updated to reflect the change in the boundary condition vertical stiffness:

[K] ⁱ	1	2	3	4	5	6	7	8	9	10	11	12	13	14	DOF
	506046.875	11963	-996.88	11963	0	0	0	0	0	0	0	0	0	0	1
	11963	191400	-11963	95700	0	0	0	0	0	0	0	0	0	0	2
	-996.88	-11963	1993.8	0	-996.88	11963	0	0	0	0	0	0	0	0	3
	11963	95700	0	382800	-11963	95700	0	0	0	0	0	0	0	0	4
	0	0	-996.88	-11963	1993.8	0	-996.88	11963	0	0	0	0	0	0	5
	0	0	11963	95700	0	382800	-11963	95700	0	0	0	0	0	0	6
	0	0	0	0	-996.88	-11963	1993.8	0	-996.88	11963	0	0	0	0	7
	0	0	0	0	11963	95700	0	382800	-11963	95700	0	0	0	0	8
	0	0	0	0	0	0	-996.88	-11963	1993.8	0	-996.88	11963	0	0	9
	0	0	0	0	0	0	11963	95700	0	382800	-11963	95700	0	0	10
	0	0	0	0	0	0	0	0	-996.88	-11963	1993.8	0	-996.88	11963	11
	0	0	0	0	0	0	0	0	11963	95700	0	382800	-11963	95700	12
	0	0	0	0	0	0	0	0	0	0	-996.88	-11963	100996.875	-11963	13
	0	0	0	0	0	0	0	0	0	0	11963	95700	-11963	191400	14

STEP 6 The following transform [T] matrix partitions ("rearrange") [K] according to "known" & "unknown" DOF (i.e. "measured" and "unmeasured" DOF):

[T]	1	2	3	4	5	6	7	8	9	10	11	12	13	14	Old	New
	0	0	0	0	0	0	0	0	0	0	0	0	1	0		
	1	0	0	0	0	0	0	0	0	0	0	0	0	0		
	0	1	0	0	0	0	0	0	0	0	0	0	0	0		
	0	0	1	0	0	0	0	0	0	0	0	0	0	0		
	0	0	0	1	0	0	0	0	0	0	0	0	0	0		
	0	0	0	0	1	0	0	0	0	0	0	0	0	0		
	0	0	0	0	0	1	0	0	0	0	0	0	0	0		
	0	0	0	0	0	0	1	0	0	0	0	0	0	0		
	0	0	0	0	0	0	0	1	0	0	0	0	0	0		
	0	0	0	0	0	0	0	0	1	0	0	0	0	0		
	0	0	0	0	0	0	0	0	0	1	0	0	0	0		
	0	0	0	0	0	0	0	0	0	0	1	0	0	0		
	0	0	0	0	0	0	0	0	0	0	0	1	0	0		
	0	0	0	0	0	0	0	0	0	0	0	0	1	0		

STEP 7 Rearrange the EXPERIMENTAL displacement and force vectors as well:

{U _p } ^e	-0.0008203	2	radians
	-0.02983	3	in
	-0.0007679	4	radians
	-0.05024	5	in
	-0.0004014	6	radians
	-0.06258	7	in
	0.0000698	8	radians
	-0.0478	9	in
	0.0004189	10	radians
	-0.03254	11	in
	0.0007854	12	radians
	0.0008403	14	radians
	0	1	
	0	13	

{F _p } ^e	0	2	
	0	3	kip
	0	4	
	-0.41554	5	kip
	0	6	
	0	7	kip
	0	8	
	-0.41593	9	kip
	0	10	
	0	11	kip
	0	12	
	0	14	
	0	1	
	0	13	

STEP 8 The following matrix is used as part of the calculation to determine the INITIAL transformed matrix:

11963	191400.00	-11963.00	95700	0.00	0	0.00	0.00	0.00	0	0	0	0.00	0	0.00
-997	-11963.00	1993.80	0	-997	11963.00	0	0.00	0.00	0	0	0	0.00	0	0.00
11963	95700	0	382800	-11963.00	95700.00	0	0.00	0.00	0	0.00	0.00	0	0.00	0.00
0	0	-997	-11963	1994	-997	11963.00	0.00	0.00	0	0.00	0	0.00	0	0.00
0	0	11963	95700	0	382800	-11963	95700	0	0.00	0.00	0	0.00	0	0.00
0	0	0	0	-997	-11963	1994	-997	11963	0.00	0.00	0	0.00	0	0.00
0.00	0	0	0.00	0.00	11963	95700	0	-11963	95700	0	0	0.00	0	0.00
0	0.00	0.00	0	0.00	0.00	0.00	-997	1994	0	-997	11963	0	0.00	0.00
0.00	0	0	0.00	0	0.00	0	0	-997	-11963	1994	0	-997	11963.00	0.00
0	0	0	0	0.00	0	0	0.00	0	11963	95700.00	0	-11963	95700.00	0.00
0	0	0	0	0.00	0	0.00	0	0.00	0	0	11963.00	95700.00	-11963	191400.00
506047	11963	-997	11963	0	0	0.00	0	0.00	0	0.00	0	0.00	0.00	0.00
0	0	0	0	0	0	0	0.00	0.00	0	-997	-11963.00	100997	-11963.00	0.00

STEP 9 The following matrix is the "INITIAL" transformed matrix as calculated by Excel:

[K _T] ⁱ =		K _{aa}		K _{ab}											
		K _{ba}		K _{bb}											
[K _T] ⁱ	2	3	4	5	6	7	8	9	10	11	12	14	1	13	DOF
	191400	-11963	95700	0	0	0	0	0	0	0	0	0	11963	0	2
	-11963	1993.8	0	-996.88	11963	0	0	0	0	0	0	0	-996.88	0	3
	95700	0	382800	-11963	95700	0	0	0	0	0	0	0	11963	0	4
	0	-996.88	-11963	1993.8	0	-996.88	11963	0	0	0	0	0	0	0	5
	0	11963	95700	0	382800	-11963	95700	0	0	0	0	0	0	0	6
	0	0	0	-996.88	-11963	1993.8	0	-996.88	11963	0	0	0	0	0	7
	0	0	0	11963	95700	0	382800.0	-11963	95700	0.0	0	0	0	0	8
	0	0	0	0	0	-996.88	-11963	1993.8	0.0	-996.88	11963	0	0	0	9
	0	0	0	0	0	11963	95700	0.0	382800.0	-11963	95700	0	0	0	10
	0	0	0	0	0	0	0	-996.88	-11963	1993.8	0.0	11963	0	-996.88	11
	0	0	0	0	0	0	0	11963	95700	0.0	382800.0	95700	0.0	-11963	12
	0	0	0	0	0	0	0	0	0	-11963	95700	191400.0	0	-11963.0	14
	11963	-996.88	11963	0	0	0	0	0	0	0	0	0	506046.9	0	1
	0	0	0	0	0	0	0	0	-996.88	-11963	-11963.0	0	0	100996.9	13

STEP 10 Using Excel's matrix calculations, the global INITIAL stiffness matrix will be condensed to the "KNOWN" DOF:

STEP 10A Excel will now calculate the inverse of sub-matrix [K_{aa}]:

[K _{aa}] ⁻¹	1.9761E-06	0
	0	9.9013E-06

STEP 10B Excel will now multiply sub-matrix $[K_{aa}]^{-1}$ with sub-matrix $[K_{ab}]^T$:

$[K_{ab}]^T [K_{bb}]^{-1}$	0.023640103	0.0000
	-0.001969636	0.0000
	0.023640103	0.0000
	0	0.0000
	0	0.0000
	0	0.0000
	0	0.0000
	0	0.0000
	0	0.0000
	0	-0.0099
	0	-0.1184
	0	-0.118449209

STEP 10C Excel will now multiply sub-matrices $[K_{aa}]^{-1}$ and $[K_{ab}]^T$ with sub-matrix $[K_{aa}]^T$:

$[K_{ab}]^T [K_{bb}]^{-1} [K_{ba}]^T$	282.81	-23.57	282.81	0.00	0.00	0	0.00	0	0	0	0	0	0	0
	-23.57	1.96	-23.57	0.00	0.00	0	0.00	0	0	0	0	0	0	0
	282.81	-23.57	282.81	0.00	0.00	0	0.00	0	0	0	0	0	0	0
	0.00	0.00	0.00	0.00	0.00	0	0.00	0	0	0	0	0	0	0
	0.00	0.00	0.00	0.00	0.00	0	0.00	0	0	0	0	0	0	0
	0.00	0.00	0.00	0.00	0.00	0	0.00	0	0	0	0	0	0	0
	0.00	0.00	0.00	0.00	0.00	0	0.00	0	0	0	0	0	0	0
	0.00	0.00	0.00	0.00	0.00	0	0.00	0	0	0	0	0	0	0
	0.00	0.00	0.00	0.00	0.00	0	0.00	0	0	0	0	0	0	0
	0.00	0.00	0.00	0.00	0.00	0	0.00	0	0	0	0	0	0	0
	0.00	0.00	0.00	0.00	0.00	0	0.00	0	0	0	0	0	0	0
	0.00	0.00	0.00	0.00	0.00	0	0.00	0	0	0	0	0	0	0

STEP 10D Excel will now subtract the result of $[K_{aa}]^{-1} \times [K_{ab}]^T \times [K_{ba}]^T$ from sub matrix $[K_{aa}]^T$:

$[K_{aa}]^T - [K_{ab}]^T [K_{bb}]^{-1} [K_{ba}]^T$	191117.19	-11939.43	95417.19	0.00	0.00	0	0.00	0	0	0	0	0	0	0
	-11939.43	1991.84	23.57	-996.88	11963.00	0	0.00	0	0	0	0	0	0	0
	95417.19	23.57	382517.19	-11963.00	95700.00	0	0.00	0	0	0	0	0	0	0
	0.00	-996.88	0.00	11963.00	1993.80	0.00	-996.88	11963.00	0	0	0	0	0	0
	0.00	11963.00	95700.00	0.00	382800.00	-11963	95700.00	0	0	0	0	0	0	0
	0.00	0.00	0.00	-996.88	-11963.00	1993.8	0.00	-996.88	11963	0	0	0	0	0
	0.00	0.00	0.00	11963.00	95700.00	0	382800.00	-11963	95700	0	0	0	0	0
	0.00	0.00	0.00	0.00	0.00	-996.88	-11963.00	1993.8	0	-996.88	11963	0	0	0
	0.00	0.00	0.00	0.00	0.00	11963	95700.00	0	382800	-11963	95700	0	0	0
	0.00	0.00	0.00	0.00	0.00	0	0.00	-996.88	-11963	95700.00	-118.0796479	11844.92035	11844.92035	11844.92035
	0.00	0.00	0.00	0.00	0.00	0	0.00	11963	95700	-118.0796479	381382.9921	94282.9921	94282.9921	94282.9921
	0	0	0	0.0000	0.0000	0	0	0	0	11844.92035	94282.9921	189982.9921	189982.9921	189982.9921

STEP 10E Excel will now calculate the inverse of $[K_{aa}]^T - [K_{ab}]^T \times [K_{bb}]^{-1} \times [K_{ba}]^T$:

$([K_{aa}]^T - [K_{ab}]^T [K_{bb}]^{-1} [K_{ba}]^T)^{-1}$	0.0000	0.0008	0.0000	0.0011	0.0000	0.0011	0.0000	0.0009	0.0000	0.0005	0.0000	0.0000	0.0000	0.0000
	0.0008	0.0167	0.0006	0.0253	0.0002	0.0260	-0.0001	0.0207	-0.0003	0.0113	-0.0004	-0.0004	-0.0005	-0.0005
	0.0000	0.0006	0.0000	0.0009	0.0000	0.0010	0.0000	0.0008	0.0000	0.0004	0.0000	0.0000	0.0000	0.0000
	0.0011	0.0253	0.0009	0.0427	0.0004	0.0460	-0.0001	0.0373	-0.0006	0.0207	-0.0008	-0.0008	-0.0009	-0.0009
	0.0000	0.0002	0.0000	0.0004	0.0000	0.0006	0.0000	0.0006	0.0000	0.0003	0.0000	0.0000	0.0000	0.0000
	0.0011	0.0260	0.0010	0.0460	0.0006	0.0540	0.0000	0.0460	-0.0006	0.0280	-0.0010	-0.0010	-0.0011	-0.0011
	0.0000	-0.0001	0.0000	-0.0001	0.0000	0.0000	0.0000	0.0001	0.0000	0.0001	0.0000	0.0000	0.0000	0.0000
	0.0009	0.0207	0.0008	0.0373	0.0006	0.0460	0.0001	0.0427	-0.0004	0.0253	-0.0009	-0.0009	-0.0011	-0.0011
	0.0000	-0.0003	0.0000	-0.0006	0.0000	-0.0006	0.0000	-0.0004	0.0000	-0.0002	0.0000	0.0000	0.0000	0.0000
	0.0005	0.0113	0.0004	0.0207	0.0003	0.0280	0.0001	0.0253	-0.0002	0.0167	-0.0006	-0.0006	-0.0008	-0.0008
	0.0000	-0.0004	0.0000	-0.0008	0.0000	-0.0010	0.0000	-0.0009	0.0000	-0.0006	0.0000	0.0000	0.0000	0.0000
	0.0000	-0.0005	0.0000	-0.0009	0.0000	-0.0011	0.0000	-0.0011	0.0000	-0.0008	0.0000	0.0000	0.0000	0.0000

STEP 11 Excel will now solve for the ANALYTICALLY determined measurements by multiplying the previous matrix (STEP 10E) by $\{F_p\}^0$:

$\{U_p\}^1 = ([K_{aa}]^T - [K_{ab}]^T [K_{bb}]^{-1} [K_{ba}]^T) \{F_p\}^0$	-0.000831476
	-0.019124254
	-0.000727578
	-0.03326008
	-0.000415793
	-0.038250068
	-7.73389E-08
	-0.03326327
	0.000415703
	-0.019128287
	0.000727587
	0.000831516

STEP 12 Use the SOLVER tool to minimize the objective function:

Error Function Equation	Analytically determined measurements {U _n } ⁱ	-	Experimentally determined measurements {U _n } ^e	=	Difference (error) {E}
	-0.00083		-0.00082		0.00001
	-0.01012		-0.02083		0.010705746
	-0.00073		-0.00077		4.03217E-05
	-0.03326		-0.05024		0.01697992
	-0.00042		-0.00040		-1.43628E-05
	-0.03825		-0.05258		0.014329932
	0.00000		0.00007		-6.98773E-05
	-0.03326		-0.04780		0.01453673
	0.00042		0.00042		-3.19872E-06
	-0.01913		-0.03254		0.013411713
	0.00073		0.00079		-5.78133E-05
	0.00083		0.00084		-8.78351E-06

KNOWN DOF	Units
2	radians
3	in
4	radians
5	in
6	radians
7	in
8	radians
9	in
10	radians
11	in
12	radians
14	radians

Set the "TARGET CELL", which is the square root of the sum of the squares, from {E}:

Minimize this cell: ("Target Cell") 0.00059948

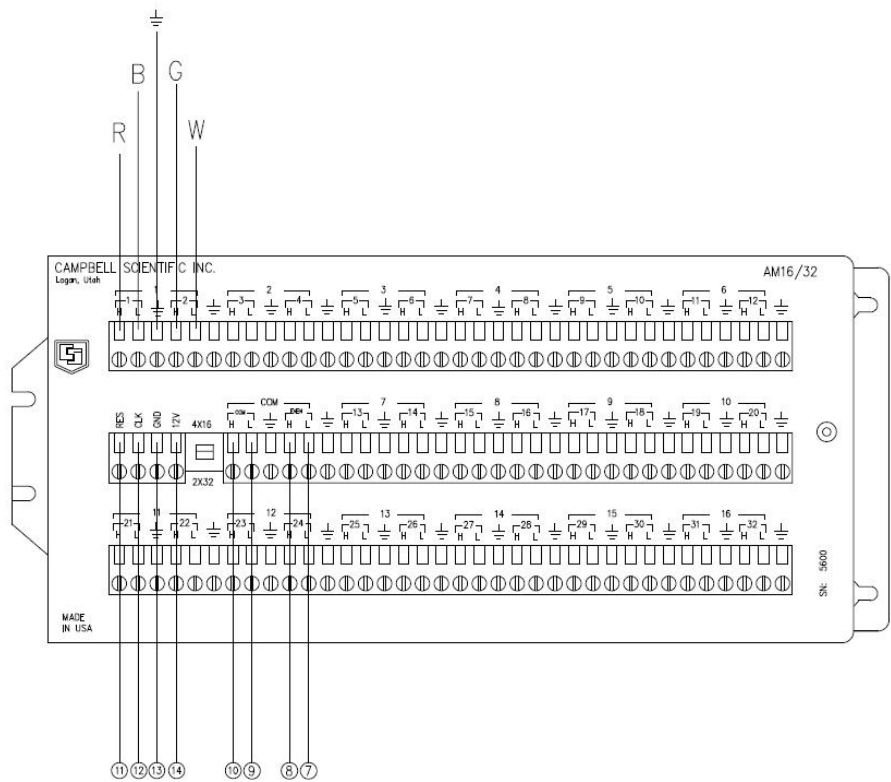
STEP 13 Record the "INITIAL" and "UPDATED" values for the unknown springs in the following tables (according to BC, LC):

		Spring #	BC1 LC1	BC1 LC2 A1	BC1 LC2 A2	BC1 LC2 A3	BC1 LC2 A4	BC1 LC2 A5	BC1 LC3 A1	BC1 LC3 A2	BC1 LC3 A3
BC1	UPDATED	K ₁ ^u	42.97	88.90	64.83	45.00	36.79	32.48	88.15	88.15	45.70
		K ₂ ^u	46.03	43.34	45.85	81.48	92.11	83.42	124.56	108.51	104.92
		Spring #	BC3a LC1	BC3a LC2 A1	BC3a LC2 A2	BC3a LC2 A3	BC3a LC2 A4	BC3a LC2 A5	BC3a LC3 A1	BC3a LC3 A2	BC3a LC3 A3
BC3a	UPDATED	K ₁ ^u	31.20	32.91	22.30	24.51	22.37	20.61	28.18	28.86	18.26
		K ₂ ^u	27.50	14.82	26.16	23.00	36.44	35.70	18.86	24.37	40.78
		Spring #	BC3b LC1	BC3b LC2 A1	BC3b LC2 A2	BC3b LC2 A3	BC3b LC2 A4	BC3b LC2 A5	BC3b LC3 A1	BC3b LC3 A2	BC3b LC3 A3
BC3b	UPDATED	K ₁ ^u	6.22	6.74	6.83	6.33	6.99	6.03	6.75	6.99	6.75
		K ₂ ^u	6.32	5.00	5.30	6.08	6.60	6.70	6.43	6.55	7.01
		Spring #	BC5b LC1	BC5b LC2 A1	BC5b LC2 A2	BC5b LC2 A3	BC5b LC2 A4	BC5b LC2 A5	BC5b LC3 A1	BC5b LC3 A2	BC5b LC3 A3
BC5b	UPDATED	K ₁ ^u	4.78				5.34	6.45		6.14	6.15
		K ₂ ^u	24.11				147.55	72.50		80.67	50.93

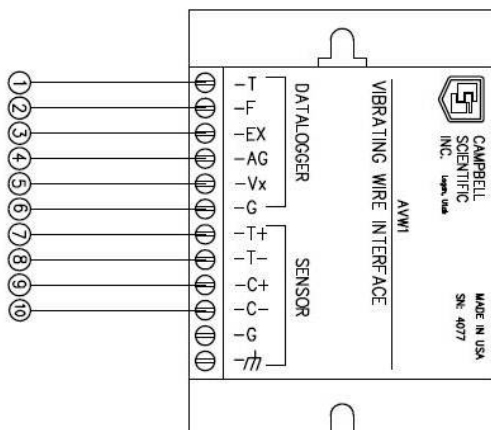
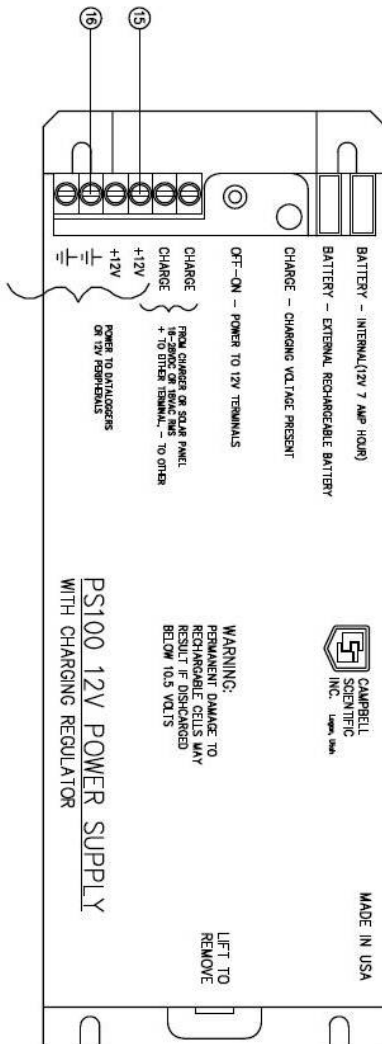
APPENDIX C: DATALOGGER SETUP

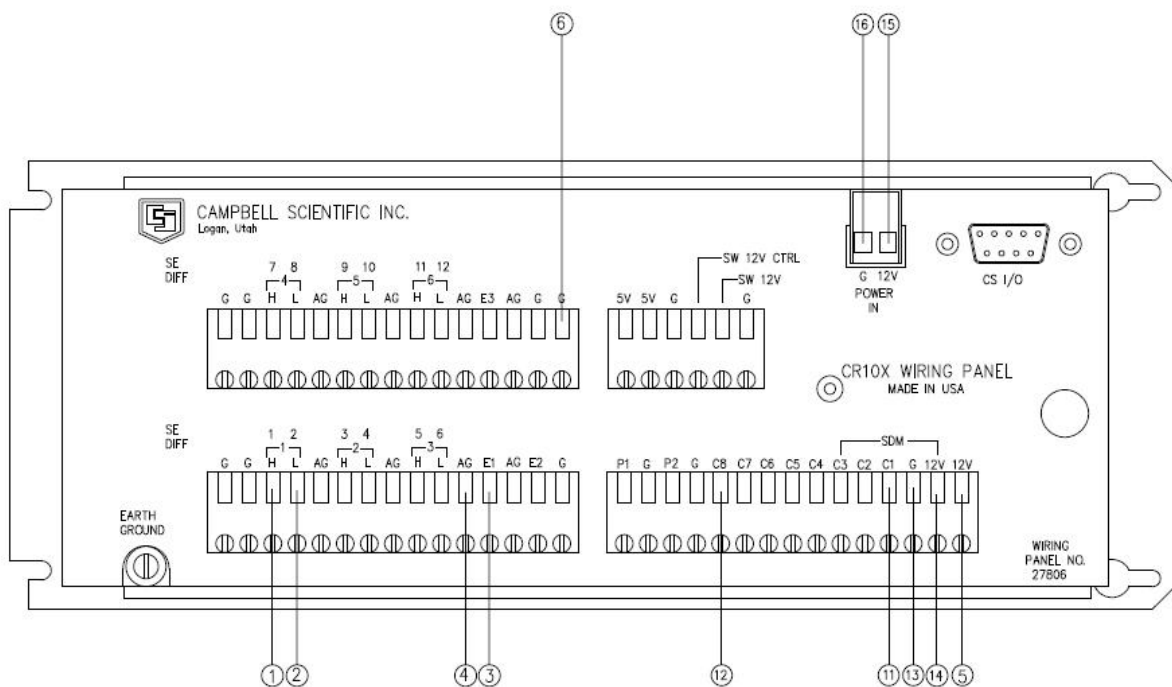
DATA ACQUISITION SETUP				
CONNECTION	CR10X	AVW1	AM16/32	PS100
1	H1	T		
2	L1	F		
3	E1	EX		
4	AG	AG		
5	12V	Vx		
6	G	G		
7		T+	COM L2	
8		T-	COM H2	
9		C+	COM L1	
10		C-	COM H1	
11	C1		RES	
12	C8		CLK	
13	G		GND	
14	12V		12V	
15	12V			12V
16	G		G	

CR10X Master Connection Table



AM16/32 Multiplexer Wiring Diagram





CR10X DATALOGGER

LIST OF REFERENCES

- AASHTO. (2004). *AASHTO LRFD Bridge Design Specifications*, American Association of State Highway and Transportation Officials, Washington, D.C.
- Aktan, E., Catbas, N., Turer, A., and Zhang, Z. (1998). "Structural Identification: Analytical Aspects." *Journal of Structural Engineering*, 124(7), 817-829.
- Bourg, D. M. (2006). *Excel Scientific Engineering Cookbook*, O'Reilly Media.
- Catbas, F. N., Brown, D. L., and Aktan, A. E. (2004) "Parameter Estimation for Multiple-Input Multiple Output Modal Analysis of Large Structures." *Journal of Engineering Mechanics*, 130(8), 921-930.
- Catbas, F. N., Ciloglu, and Aktan, A. E., "Strategies for Condition Assessment of Infrastructure Populations: A Case Study on T-beam Bridges," *Structure and Infrastructure Engineering Journal*, SIE, Vol. 1, No. 3, pp.221-238, 2005.
- Catbas, F.N., Ciloglu, S.K., Hasancebi, O., Grimmelsmann, K. A., Aktan, A. E. (2007) "Limitations in Structural Identification of Large Constructed Structures." ASCE, *Journal of Structural Engineering*, Aug. 2007.
- Ciloglu, K., Catbas, F. N., Pervizpour, M., Wang, A., and Aktan, A. (2001). "Structural Identification of Phenomenological Physical Models with Controlled Mechanisms of Uncertainty." SPIE.
- Computers and Structures, Inc. (2006). "SAP2000 ". Berkeley, CA.
- Felton, L. P., and Nelson, R. B. (1997). *Matrix Structural Analysis*, John Wiley & Sons, Inc.
- Frontline Systems, Inc. (2006). <http://www.solver.com>
- Fylstra, D., Lasdon, L., Watson, J. and Waren, A. (1998) "Design and Use of the Microsoft Excel Solver", *Interfaces*, INFORMS, 28, 29-55.
- Jaishi, B., and Ren, W.-X. (2005). "Structural Finite Element Model Updating Using Ambient Vibration Test Results." *Journal of Structural Engineering*, 131(4), 617-628.
- Jang, J.-H., Yeo, I., Shin, S., and Chang, S.-P. (2002). "Experimental Investigation of System-Identification-Based Damage Assessment on Structures." *Journal of Structural Engineering*, 128(5), 673-682.
- Kassimali, A., (1999) *Matrix Analysis of Structures*, Pacific Grove: Brooks/Cole Publishing Company. 1st Ed.

- Liu, P.-L., and Chian, C.-C. (1997). "Parametric Identification of Truss Structures Using Static Strains." *Journal of Structural Engineering*, 123(7), 927-933.
- Oh, B. H., and Jung, B. S. (1998). "Structural Damage Assessment with Combined Data of Static and Modal Tests." *Journal of Structural Engineering*, 124(8), 956-965.
- Sanayei, M., Doebling, S. W., Farrar, C. R., Wadia-Fascetti, S., and Arya, B. "Challenges in Parameter Estimation for Condition Assessment of Structures." 8.
- Sanayei, M., Imbaro, G. R., McClain, J. A. S., and Brown, L. C. (1997). "Structural Model Updating Using Experimental Static Measurements." *Journal of Structural Engineering*, 123(6), 792-798.
- Sanayei, M., McClain, J. A. S., Wadia-Fascetti, S., and Santini, E. M. (1999). "Parameter Estimation Incorporating Modal Data and Boundary Conditions." *Journal of Structural Engineering*, 125(9), 1048-1055.
- Sanayei, M., and Saletnik, M. J. (1996a). "Parameter Estimation of Structures from Static Strain Measurements. I: Formulation." *Journal of Structural Engineering*, 122(5), 555-562.
- Sanayei, M., and Saletnik, M. J. (1996b). "Parameter Estimation of Structures from Static Strain Measurements. II: Error Sensitivity Analysis." *Journal of Structural Engineering*, 122(5), 563-572.
- Sanayei, M., Santini-Bell, E., Javdekar, C., Edelmann, J., and Slavsky, E. (2006). "Damage Localization and Finite-Element Model Updating Using Multiresponse NDT Data." *Journal of Bridge Engineering*, 11(6), 688-698.
- Sanayei, M., Wadia-Fascetti, S., Santini, E. M., and Arya, B. "Significance of Modeling Error in Structural Parameter Estimation." *Computer-Aided Civil and Infrastructure Engineering*, 16.
- Sanayei, M., *PARIS, PARAmeter Identification System*. V.9.2.2. Department of Civil and Environmental Engineering, Tufts University, Medford, MA, 2004.
- Sanayei, M. (2007). "Phone Interview." Medford, Massachusetts.
- Ventura, C.E., Lord, J-F., Dascotte, E., Brincker, R., and Anderson, P. (2003). "FEM Updating Using Ambient Vibration Data from a 48-storey Building in Vancouver, British Columbia, Canada." *The 32nd International Congress and Exposition on Noise Control Engineering*, August 25-28.